

Air Force Institute of Technology

**AFIT Scholar**

---

Theses and Dissertations

Student Graduate Works

---

3-26-2002

## GPS-Derived Precipitable Water Compared with the Air Force Weather Agency's MM5 Model Output

Patricia A. Vollmer

Follow this and additional works at: <https://scholar.afit.edu/etd>



Part of the [Meteorology Commons](#)

---

### Recommended Citation

Vollmer, Patricia A., "GPS-Derived Precipitable Water Compared with the Air Force Weather Agency's MM5 Model Output" (2002). *Theses and Dissertations*. 4502.

<https://scholar.afit.edu/etd/4502>

This Thesis is brought to you for free and open access by the Student Graduate Works at AFIT Scholar. It has been accepted for inclusion in Theses and Dissertations by an authorized administrator of AFIT Scholar. For more information, please contact [richard.mansfield@afit.edu](mailto:richard.mansfield@afit.edu).



**GPS-DERIVED PRECIPITABLE WATER  
COMPARED WITH THE AIR FORCE  
WEATHER AGENCY'S MM5 MODEL  
OUTPUT**

THESIS

Patricia A. Vollmer, Captain, USAF

AFIT/GM/ENP/02M-11

**DEPARTMENT OF THE AIR FORCE  
AIR UNIVERSITY**

***AIR FORCE INSTITUTE OF TECHNOLOGY***

---

---

**Wright-Patterson Air Force Base, Ohio**

APPROVED FOR PUBLIC RELEASE; DISTRIBUTION UNLIMITED.

## Report Documentation Page

|   |   |  |
|---|---|--|
| <b>Report Date</b><br>26 Mar 02   | <b>Report Type</b><br>Final   | <b>Dates Covered (from... to)</b><br>Jun 2001 - Mar 2002 |
| <b>Title and Subtitle</b><br>GPS-Derived Precipitable Water Copared with the Air Force Weather Agency's MM5 Model Output  | <b>Contract Number</b>  |  |
|   | <b>Grant Number</b>   |  |
|   | <b>Program Element Number</b>   |  |
| <b>Author(s)</b><br>Capt Patricia A. Vollmer, USAF  | <b>Project Number</b>   |  |
|   | <b>Task Number</b>  |  |
|   | <b>Work Unit Number</b>   |  |
| <b>Performing Organization Name(s) and Address(es)</b><br>Air Force Institute of Technology Graduate School of Engineering and Management (AFIT/EN) 2950 P Street, Bldg 640 WPAFB OH 45433-7765 | <b>Performing Organization Report Number</b><br>AFIT/GM/ENP/02M-11  |  |
|   | <b>Sponsoring/Monitoring Agency Name(s) and Address(es)</b><br>AFWA/DNXT Attn: Bruce Telfeyan 301 Peacekeeper Dr. Offutt AFB NE |  |
|   |   | <b>Sponsor/Monitor's Acronym(s)</b>                      |
|   |   | <b>Sponsor/Monitor's Report Number(s)</b>                |
| <b>Distribution/Availability Statement</b><br>Approved for public release, distribution unlimited   |   |  |
| <b>Supplementary Notes</b><br>The original document contains color images.  |   |  |

**Abstract**

Current moisture initialization sources lack the spatial and temporal resolution required for mesoscale moisture forecast accuracy critical for military operations. The Global Positioning System (GPS) satellite constellation provides an opportunity to extract accurate moisture observations based on the refraction of the GPS signal through the troposphere. GPS-derived precipitable water (PW) from two different research areas was independently compared with the Air Force Weather Agency's (AFWAs) MM5 PW model output. Results were concurrent with similar studies comparing GPS-derived PW with numerical weather models. The mean correlation in CONUS was 92.5%, while in Alaska it was 72.8%. Mean model biases were 1.22 mm in CONUS and 0.69 mm in Alaska. Mean RMSEs were 4.36 mm in CONUS and 2.76 mm in Alaska. In addition, comparisons were made between moist and dry locations, showing a 21.5% difference in correlation and a 17.8% difference in RMSE. The GPS networks superior temporal resolution captured the diurnal variations in PW, while the model consistently failed to take such variations into account as its forecast progressed. This seems it could be the largest source of error between the two data sets. A number of non-meteorological error sources exist that could impact use of GPS-derived PW in operational applications, such as terrain differences between the GPS receiver sites and the model interpolated heights. These error sources need to be further addressed prior to operational assimilation of this data into military weather models.

**Subject Terms**

Meteorology, Global Positioning System, Numerical Methods and Procedures, Satellites, Atmospheric Moisture Content

**Report Classification**

unclassified

**Classification of this page**

unclassified

**Classification of Abstract**

unclassified

**Limitation of Abstract**

UU

**Number of Pages**

108

The views expressed in this thesis are those of the author and do not reflect the official policy or position of the United States Air Force, Department of Defense, or the U. S. Government.

AFIT/GM/ENP/02M-11

GPS-DERIVED PRECIPITABLE WATER COMPARED WITH THE AIR FORCE  
WEATHER AGENCY'S MM5 MODEL OUTPUT

THESIS

Presented to the Faculty

Department of Engineering Physics

Graduate School of Engineering and Management

Air Force Institute of Technology

Air University

Air Education and Training Command

In Partial Fulfillment of the Requirements for the

Degree of Master of Science in Meteorology

Patricia A. Vollmer, BS

Captain, USAF

March 2002

APPROVED FOR PUBLIC RELEASE; DISTRIBUTION UNLIMITED.


GPS-DERIVED PRECIPITABLE WATER COMPARED WITH THE AIR FORCE  
WEATHER AGENCY'S MM5 MODEL OUTPUT

Patricia A. Vollmer, BS  
Captain, USAF

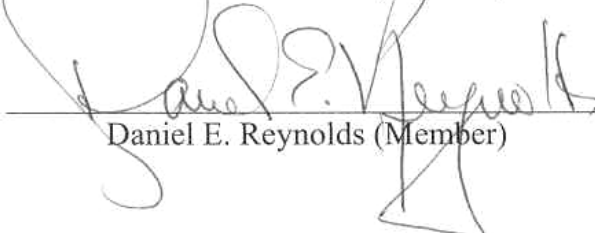
Approved:

  
\_\_\_\_\_  
Gary R. Huffines (Chairperson)

1 March 2002  
date

  
\_\_\_\_\_  
Michael K. Walters (Member)

1 March  
date

  
\_\_\_\_\_  
Daniel E. Reynolds (Member)

1 March  
date

## Acknowledgements

First and foremost, I would like to thank the members of my thesis committee, Major Gary Huffines, Lieutenant Colonel Michael Walters and Professor Dan Reynolds. You allowed me to pursue a new, unusual subject that was seemingly in left field. You deserve my thanks for your patience and understanding in my excitement over the many iterations of results, as well as for your continuing to challenge me throughout the thesis process. In addition, Major John Raquet and 2d Lieutenant David Garay from the Electrical Engineering Department receive my gratitude for their expertise in GPS navigation.

My appreciation goes out to the many members of the GPS meteorology community who spent hours educating me on GPS meteorology and then provided me valuable feedback on my results. Seth Gutman, Kirk Holub, and Sher Wagoner at the NOAA Forecast Systems Laboratory provided me with acres of information and access to their American data sets. Also, Jennifer Haase and Eric Calais from the Department of Atmospheric Sciences at Purdue University deserve thanks for courteously providing me feedback and insight into how to interpret my results.

Thanks go to those at the Air Force Weather Agency who took time from their busy real-world obligations to assist me with MM5-related issues. Of note are Captain Rob Swanson, Dr. Scott Applequist and Matthew Sittel.

The members of AFIT ENP GM-02M, especially those colleagues who were also doing MM5-related research, are in my debt for contributing to the free exchange of ideas, criticisms, and opinions that is an example of science at its best.

And finally, I'm eternally grateful to my wonderful husband who provided me valuable feedback even while working on this own Master's thesis. I'll never forget that Friday night when we sat at home on opposite ends of the couch and read each other's theses. He tolerated my constantly sitting in front of the computer, both in the weather lab and at home...as if a keyboard and mouse had grown out of my hands! Please know that it was only temporary.



## Table of Contents

|  | Page |
|--|------|
| Acknowledgements .....   | iv   |
| List of Figures .....  | vii  |
| List of Tables.....  | ix   |
| List of Tables.....  | ix   |
| Abstract .....   | x    |
| I. Introduction.....   | 1    |
| 1.1 Background .....   | 1    |
| 1.2 Problem Statement .....  | 4    |
| 1.3 Research Impact .....  | 5    |
| 1.4 Research Objective.....  | 6    |
| 1.5 Hypotheses .....   | 7    |
| II. Literature Review .....  | 8    |
| 2.1 The Global Positioning System.....                                 | 8    |
| 2.2 Use of GPS for Meteorological Research .....                       | 11   |
| 2.3 The Fifth-Generation Mesoscale Model .....                         | 14   |
| 2.4 Using GPS Meteorology to Validate and Improve Forecast Models..... | 17   |
| III. Methodology .....   | 25   |
| 3.1 Data Collection.....   | 25   |
| 3.2 Sources of Error .....   | 27   |
| 3.3 Coding of Processing Programs .....                                | 33   |
| IV. Results and Discussion .....                                       | 39   |
| 4.1 CONUS .....  | 39   |
| 4.2 Alaska.....  | 57   |

|  |    |
|--|----|
| V. Conclusions .....                           | 65 |
| 5.1 CONUS Conclusions .....                    | 66 |
| 5.2 Alaska Conclusions .....                   | 67 |
| 5.3 Recommendations for Future Work .....      | 68 |
| Bibliography .....                             | 70 |
| Appendix A: Geodetic Information .....         | 73 |
| Appendix B: RAOB Geodetic Information .....    | 75 |
| Appendix C: Location-Specific Statistics ..... | 76 |
| Vita .....                                     | 95 |

## List of Figures

|  | Page |
|--|------|
| Figure 1. Schematic of the GPS Satellite Vehicle Constellation .....   | 8    |
| Figure 2. Diagram of the Satellite Coverage Transposed on a Global Map Projection... 9   | 9    |
| Figure 3. Visualization of How GPS Determines Precise Location .....   | 10   |
| Figure 4. The American GPS Precipitable Water Receiver Network .....   | 26   |
| Figure 5. Area of Influence of a GPS-Derived Precipitable Water Reading. ....  | 35   |
| Figure 6. Area of Influence in MM5 Grid.....   | 35   |
| Figure 7. NEXRAD Mosaic Image from 15 UTC 8 July 2001.....   | 40   |
| Figure 8. NEXRAD Mosaic Image from 09 UTC 25 July 2001.....  | 41   |
| Figure 9. NEXRAD Mosaic Image from 00 UTC 12 August 2001.....  | 41   |
| Figure 10. NEXRAD Mosaic Image from 08 UTC 14 September 2001 .....   | 42   |
| Figure 11. CONUS Domain-Wide Statistical Summaries. ....   | 43   |
| Figure 12. Mean Correlation of Each GPS Receiver Location: CONUS 06 UTC<br>Initialization, 06-Hour Forecast .....                  | 45   |
| Figure 13. Mean Bias of Each GPS Receiver Location: CONUS 06 UTC Initialization,<br>06-Hour Forecast.....                          | 46   |
| Figure 14. Mean Normalized RMSE of Each GPS Receiver Location: CONUS 06 UTC<br>Initialization, 06 Hour Forecast.....               | 47   |
| Figure 15. Mean Normalized Standard Deviation of Each GPS Receiver Location:<br>CONUS 06 UTC Initialization, 06 Hour Forecast..... | 48   |
| Figure 16. Mean Correlation of Each GPS Receiver Location: CONUS 18 UTC<br>Initialization, 06-Hour Forecast .....                  | 49   |

|  |    |
|--|----|
| Figure 17. Mean Bias of Each GPS Receiver Location: CONUS 18 UTC Initialization,<br>06-Hour Forecast.....                          | 49 |
| Figure 18. Mean Normalized RMSE of Each GPS Receiver Location: CONUS 18 UTC<br>Initialization, 06-Hour Forecast .....              | 50 |
| Figure 19. Mean Normalized Standard Deviation of Each GPS Receiver Location:<br>CONUS 18 UTC Initialization, 06-Hour Forecast..... | 51 |
| Figure 20. Number of Observations Available for Calculating the 06 UTC Initialization,<br>06 Hour Forecast Statistics.....         | 52 |
| Figure 21. Number of Observations Available for Calculating the 18 UTC Initialization,<br>06 Hour Forecast Statistics.....         | 52 |
| Figure 22. Moist Sites vs. Dry Sites Statistical Summaries: CONUS 18 UTC<br>Initialization, 06 Hour Forecast.....                  | 53 |
| Figure 23. Elevation Comparisons: CONUS 06 UTC Initialization, 06 Hour Forecast  | 54 |
| Figure 24. GPS/RAOB Coastal vs. Inland Statistical Summaries .....   | 56 |
| Figure 25. Representative Alaska IR Satellite Imagery from 12 UTC 19 July 2001.....  | 57 |
| Figure 26. Alaska Domain-Wide Statistical Summaries.....   | 59 |
| Figure 27. Alaska By-Location Statistical Summaries: 00 UTC Initialization, 06 Hour<br>Forecast .....                              | 61 |
| Figure 28. Alaska By-Location Statistical Summaries: 12 UTC Initialization, 06 Hour<br>Forecast .....                              | 62 |

## List of Tables

|   | Page |
|---|------|
| Table 1. AFWA MM5 Physics Packages.....   | 16   |
| Table 2. Sample GPS-MET Data from Bartlett, NH for 6 July 2001 .....              | 25   |
| Table 3. Representation of Makes and Models of GPS Receivers .....                | 28   |
| Table 4. Representation of Makes and Models of GPS Antennas .....                 | 28   |
| Table 5. Comparison of GPS Orbit Calculations Available in GPS-MET Processing..   | 30   |
| Table 6. Available GPS Processing Software .....                                  | 31   |
| Table 7. Sample RAOB-Based Precipitable Water for Charleston, SC.....             | 36   |
| Table 8. Sample GPS vs. RAOB Comparison File for Slidell, LA.....                 | 36   |
| Table 9. Sample Output File for a 45-Hour Forecast Valid 8 July 2001 03 UTC ..... | 37   |
| Table 10. Location-specific PW Data for Spokane, WA. ....                         | 37   |
| Table 11. Sample Statistical Summary by DTG .....                                 | 38   |
| Table 12. Sample Statistical Summary File by Location.....                        | 38   |
| Table 13. Summary of GPS-RAOB Comparisons in CONUS .....                          | 55   |
| Table 14. Summary Statistics of Fairbanks GPS-PW and RAOB-PW Comparison. ....     | 64   |

### **Abstract**

Current moisture initialization sources lack the spatial and temporal resolution required for mesoscale moisture forecast accuracy critical for military operations. The Global Positioning System (GPS) satellite constellation provides an opportunity to extract accurate moisture observations based on the refraction of the GPS signal through the troposphere. GPS-derived precipitable water (PW) from two research areas was independently compared with the Air Force Weather Agency's (AFWA's) MM5 PW model output. Results were concurrent with similar studies comparing GPS-derived PW with numerical weather models. The mean correlation between the GPS-derived PW values and MM5 output in CONUS was 92.5%, while in Alaska it was 72.8%. Mean model biases between the two data sets were  $-1.22$  mm in CONUS and  $0.69$  mm in Alaska, where a positive bias signifies the GPS network having higher PW values. Mean root mean square errors were  $4.36$  mm in CONUS and  $2.76$  mm in Alaska. In addition, comparisons were made between moist and dry locations as well as inland and coastal locations, and a special study was done comparing GPS receiver site elevation and standard deviation.

The GPS network's superior temporal resolution captured the diurnal variations in PW, while the model consistently failed to take such variations into account as its forecast progressed. This difference in diurnal patterns seems to be the largest source of error between the GPS and MM5 data sets. A number of non-meteorological error sources exist that could impact use of GPS-derived PW in operational applications, such

as terrain differences between the GPS receiver sites and the model interpolated heights. These error sources need to be further addressed prior to operational assimilation of this data into military weather models.

# GPS-DERIVED PRECIPITABLE WATER COMPARED WITH THE AIR FORCE WEATHER AGENCY'S MM5 MODEL OUTPUT

## I. Introduction

### 1.1 Background

Global Positioning System (GPS)-derived precipitable water (PW) provides unprecedented spatial and temporal resolution of water vapor, a highly variable parameter that is currently very difficult to initialize accurately. By measuring the “wet delay” of a transmission to a GPS receiver, where the delay is proportional to the integrated water vapor, it is possible to remotely sense a line-of-sight precipitable water amount for a given transmission time and receiver location. This parameter can be normalized into an estimate of a vertically integrated precipitable water value. In order to produce the most accurate water vapor measurement, the GPS receiver must have a means to measure temperature and sea level pressure concurrently.

*1.1.1 Delays in the GPS Signal.* The Global Positioning System was established by the U.S. government in the early 1980s as a crucial element in navigation and relative positioning. Today, GPS includes a constellation of 24 low-earth-orbit (LEO) satellite vehicles that transmit signals in the L-band (1.2 and 1.6 GHz) to terrestrial users equipped with receivers. These signals are converted into information to aid in



navigation, timing, and positioning, not only for military assets, but also for many civilian uses (Trimble 1996).

Due to the requirement for highly accurate GPS readouts in every transmission, post-processing procedures have been developed to factor out the signal delays from each of these transmissions. These delays are excess path lengths due to the phase shifting between the standing signal and the transmission signal and are factored out of the signal through post-processing at the receiver end of the transmission. There are two major components of the GPS signal delay: the hydrostatic delay and the wet delay.

Hydrostatic delay arises from the nondipole moment of the total atmosphere. This part of the delay factors in all constituents of the neutral atmosphere (to include nitrogen, oxygen, argon, and other trace gases) including a component of water vapor. These constituents have relatively uniform composition in the troposphere. Using a surface pressure measurement, the hydrostatic delay is calculated. With surface pressure measurements, the hydrostatic delay can be measured to better than 1 mm (Businger 1996).

The wet delay arises from the refractivity of the water vapor in the neutral atmosphere. Due to the variability of water vapor in the tropopause, the wet delay can vary from 10 mm in desert regions to more than 400 mm in more humid regions. Not only is there an excellent spatial variability in wet delay, but there also exists a significant temporal variability. When the wet delay is measured in the zenith direction, a simple relationship exists from which precipitable water can be measured.

**1.1.2 Research Efforts in GPS Meteorology.** Exploiting the GPS signal delay for meteorological applications is a relatively young endeavor, with the GPS network only having been in operation since the mid-1980s. GPS meteorology shows considerable promise for both short- and long-term meteorological applications, including climatology. In addition, research is ongoing for the assimilation of GPS water vapor data into larger-scale forecast models, the mapping of global water vapor patterns in a manner similar to computerized axial tomography (CAT scanning), and the measurements of atmospheric refractivity soundings via radio occultation to gather global information about temperature, humidity and ionospheric structures (Ware 2000).

**1.1.3 Precipitable Water in the AFWA MM5.** The Fifth Generation Mesoscale Model (MM5) is a three-dimensional, non-hydrostatic, primitive-equation, nest-grid model with a terrain following sigma ( $\sigma$ ) vertical coordinate system (Grell 1995). It is the Air Force Weather Agency's (AFWA's) weather forecast model of choice. As of this writing, AFWA runs MM5 windows over 29 worldwide mission critical theaters of operations. AFWA maintains 18 parent domains, from which 11 inner nest windows are derived (Applequist 2001).

Kuo (1993) has already shown that precipitable water, despite being a two-dimensional variable, can be aptly assimilated into the MM5. Therefore, it is plausible that with its exceptional temporal and spatial resolution, GPS-derived precipitable water can be a valuable input for modeling tenuous water vapor variables.

Gutman (2001) has offered theories on how GPS PW can be integrated into mesoscale models by using a vertical aliasing technique, similar to the one mentioned by

Kuo (1993). Gutman shows a case study in which GPS PW was assimilated into the National Center for Environmental Prediction's (NCEP's) Rapid Update Cycle 2 (RUC-2) mesoscale forecast model. In addition, he cites previous studies in which it has been shown that the most vertical variability in the integrated vertical moisture profile is in the lower 4000 m.

Currently, AFWA uses the Multivariate Optimal Interpolation (MVOI) scheme to assimilate its data for use by the MM5. MVOI uses point analyses in the vertical to derive vertical profiles of temperature, winds, and moisture. GPS-derived moisture products are currently not assimilated into the MM5 (partly due to the form of assimilation technique). By summer 2002, AFWA's analysis scheme will transition from MVOI to the 3-Dimensional Variational Analysis (3DVAR) system. This method is designed to employ more data sources along with parallelization techniques to compile more information in a comparable amount of time (Ritz et al. 2001). This future transition provides more validity to this research, for 3DVAR will be able to ingest the GPS-derived products for initialization.

## **1.2 Problem Statement**

Currently, GPS-derived PW is not assimilated into any operational weather model, due to a number of factors. Less than 100 sensors are available in the continental United States (CONUS), and less than 100 sensors are available throughout Europe. While the receiver density is currently comparable to the upper-air sounding network, inconsistencies with the GPS receivers and the delay-processing software result in the meteorology community's hesitation to fully implement the network.

AFWA traditionally has been at the leading edge of taking advantage of new data sources for operational use. For example, AFWA was at the forefront of using GOES sounder data as a legitimate data source, long before other operational centers considered such a source as valid. The results of this comparison should demonstrate the utility of GPS-derived PW in numerical weather prediction applications, however, its temporal resolution would make it of best use in a variational assimilation system. Through this research, AFWA may make the decision to assimilate the GPS-derived PW not long after their 3DVAR assimilation scheme becomes operational in 2002.

### **1.3 Research Impact**

For an NWP user to have confidence in a numerical model, it is important for the data being used to initialize the model to be as accurate as possible. Today's numerical models are able to use advanced methods to aptly blend real-world observation data with previously obtained model output. This way, the model is less likely to react to contaminated data.

AFWA is at the forefront of incorporating the best technology to optimize model initialization. It uses the most accurate observation data with the highest temporal and spatial resolution that is computationally possible.

This research will compare GPS-derived precipitable water with the output from AFWA's MM5. GPS-derived precipitable water overcomes the challenges that exist in other moisture observations. For example, radiosonde balloons are only launched every 12 hours from a network of sites that average 500 km between each launch site. Also,

GOES sounder data is only valid in clear-air areas. The presence of cloud water contaminates the data.

Should AFWA begin to ingest GPS-derived PW, the model's moisture output will be nudged towards truer values and will improve the overall quality of the model's output: more valuable forecast data for our nations' warfighters.

#### **1.4 Research Objective**

This research will compare GPS-derived precipitable water (PW) against an operational numerical weather prediction (NWP) forecast model. By doing an independent data comparison in two of AFWA's MM5 theaters of operation, a first-look analysis will be performed that can transition to the next step: experimentally assimilating the new data into the model initialization itself. Studies have already demonstrated the excellent value GPS-derived PW can provide to other forecast models, both by independent data comparisons as well as by legitimate assimilations into the model. This will be the first study involving AFWA's operational MM5 output in GPS-derived PW research.

The objective will be to assess whether GPS-derived PW is a value-added data source, in particular, a recommendation of whether the AFWA MM5 might produce more accurate output should GPS-derived PW be included. With the advent of their 3DVAR initialization scheme in mid-2002, AFWA will be able to ingest the PW values for operational use. Through various statistical analyses, quantitative comparisons will provide the reader with evidence supporting the accomplishment of this objective. Statistics that will make these comparisons include correlation, bias, RMSE, and standard

deviation. These statistics can be partitioned into various categories, such as model initialization time, forecast integration time, and location.

### **1.5 Hypotheses**

Based on other studies that will be detailed in Chapter II, this research is expected to show a reasonable correlation between the GPS-derived PW and the MM5 output. However, the errors that will evolve between the two parameters will concur with errors that already exist between radiosonde-derived PW and MM5 output: the MM5 has a persistent moist bias.

Variations in these results will exist in the different theaters. For example, the data in CONUS will have a continental influence, while the values in Alaska will have a body of water possibly impacting the model results. In addition, the differences in GPS receivers and processing software will cause varying results. Such differences will prevent accurate comparisons between the two theaters.

Finally, the comparisons between the GPS-derived PW and the radiosonde values will show a slight bias, but this bias is expected to be well within the error tolerances of both measurement sensors. This will further substantiate AFWA using these data for model initialization.

## II. Literature Review

### 2.1 The Global Positioning System

**2.1.1 Historical Perspective.** The Global Positioning System was established by the U.S. government in the early 1980s as a crucial element in navigation and relative positioning. Today's GPS network consists of 24 or more low-earth orbit satellite vehicles that transmit signals in the L1 (1228 MHz) and L2 (1575 MHz) bands to terrestrial users that are equipped with receivers (Leick 1990). Until May 2000, the military had the capability to exercise Selective Availability, which would have intentionally degraded the signal for national security purposes. The Clinton administration ended the feature, thus giving the civilian community reliable enhanced capabilities (Leopold 2000). Figures 1 and 2 show diagrams of how the GPS satellite vehicle constellation is arranged and how their ground tracks ensure global coverage.

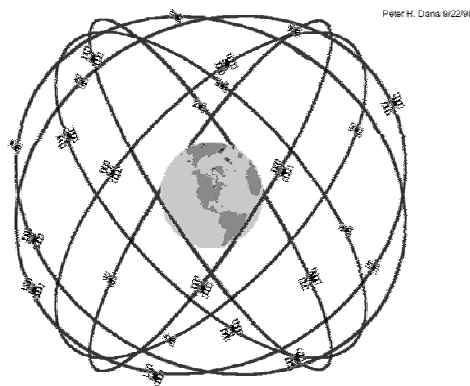


Figure 1. Schematic of the GPS Satellite Vehicle Constellation. The nominal constellation has 24 satellite vehicles distributed among 6 orbital planes. Altitude: 20,200 km. Inclination Angle: 55 degrees. Courtesy of Dana (1999).

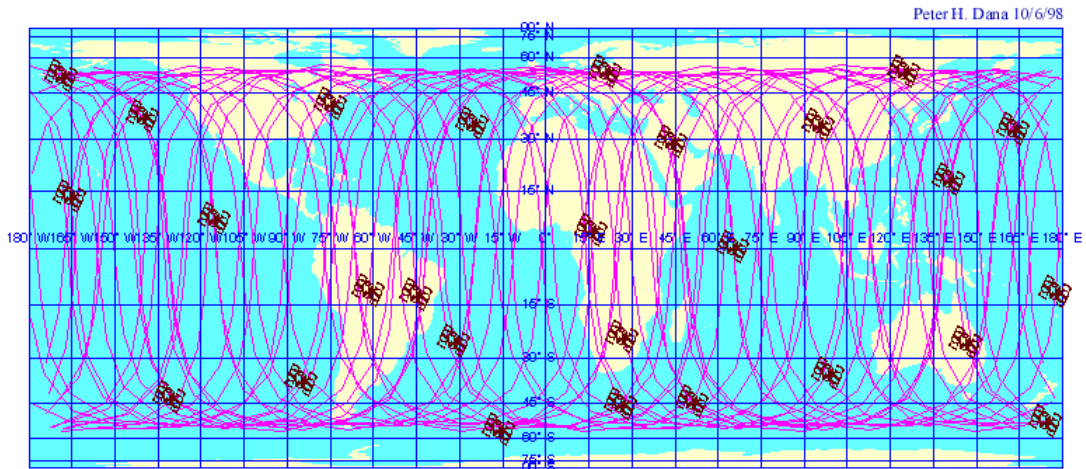


Figure 2. Diagram of the Satellite Coverage Transposed on a Global Map Projection. Ground tracks are shown over a 24-hour period from 29-30 September 1998. Courtesy of Dana (1999).

**2.1.2 Determining Location with GPS.** The signals disseminated from the satellite vehicles are converted into time and distance information. For a GPS location calculation two steps are required: phase shifting of the pseudorandom codes and trilateration.

Phase shifting of the pseudorandom code is the first step in determining ground position. Each satellite vehicle transmits a signal of binary code (ones and zeroes). The ground receiver intercepts this code, and then times its own code to match the satellite vehicle's transmission. The time it takes for the receiver to match up its code, multiplied by the speed of light, gives the ground the receiver the distance it is from the satellite vehicle (Leick 1990).

Trilateration is the process of determining distance from sighting at least four satellite vehicles from any ground positioned receiver on earth. The fourth satellite vehicle is required to resolve receiver clock errors. When a ground receiver is able to determine its distance from the satellite vehicles, the receiver can then use trilateration to



determine its precise location on the earth's geoid (Figure 3). By imagining each satellite's range as a sphere, the intersection of the spheres will constitute the location (Trimble 1996).

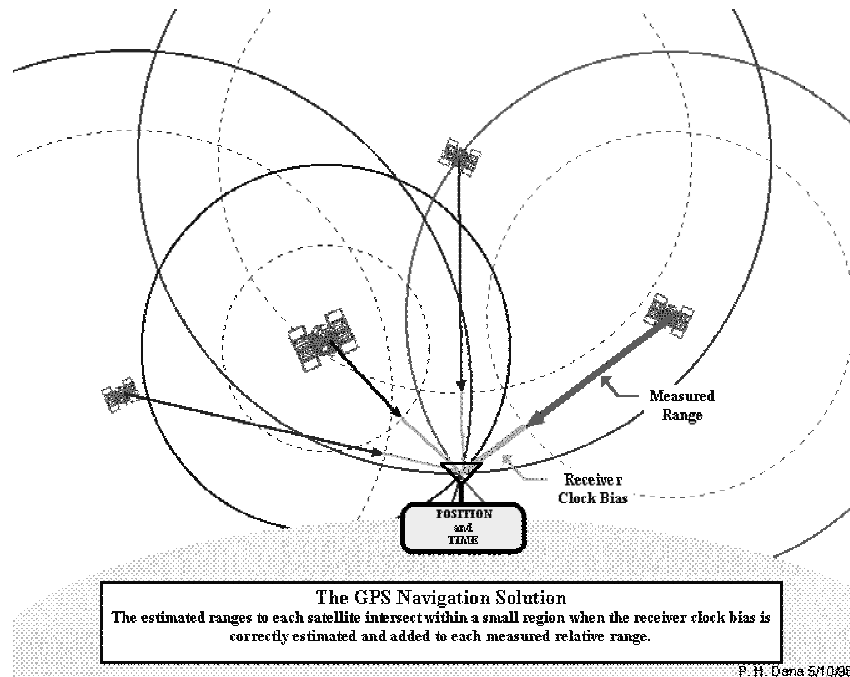


Figure 3. Visualization of How GPS Determines Precise Location. Courtesy of Dana (1999).

**2.1.3 The Current Status and Future of GPS.** Currently, the GPS network satellite vehicles are on the Block IIR build, manufactured by Lockheed-Martin. This constellation was emplaced in 1995, and each satellite is anticipated to have a 10-year design life (Hofmann-Wellenhof 1993). In anticipation of the expiration of the Block IIR systems, Boeing Satellite Systems is expected to begin GPS Block IIF production by the end of 2002, with the first satellite scheduled for a 2005 delivery. In addition, the Department of Defense was expected to request proposals for the Block III design in Fall 2001 (Smith 2001). These plans will ensure reliable coverage.

## 2.2 Use of GPS for Meteorological Research

It has only been in the past decade that geodesists and meteorologists have discovered the relationship between GPS receiver transmissions and the water vapor in the troposphere overlying the receiver site. Meteorologists are interested in taking advantage of this relationship due to its high temporal and spatial resolution, as well as the portability and economy of the measurement devices. Military meteorologists are particularly interested in the passive nature of this remote sensing capability.

Each GPS transmission between a satellite vehicle and ground receiver contains a total delay that must be processed out of the navigation reading. This delay has two parts: the ionospheric delay and the neutral atmosphere delay. Using both the L1 and L2 signals factors the ionospheric delay out, via a dispersion relation relating the two carrier signals. The neutral atmosphere delay (also known as the tropospheric delay) is on the order of 2 m and consists of the hydrostatic delay and the wet delay (Bevis 1992).

Saastamoinen (1972) was among the first to discover the relationship between the refractivity of the atmosphere and the satellite signal delays. The total tropospheric delay consists of the sum of the hydrostatic delay and the wet delay. The hydrostatic delay arises from the dry constituents of the atmosphere. This part of the delay factors in all constituents of the neutral atmosphere (to include nitrogen, oxygen, argon, and other trace gases) *except* the dipole component of water vapor. These constituents have relatively uniform composition in the troposphere. Using a surface pressure measurement, the hydrostatic delay is calculated (Bevis 1992):

$$ZHD = \frac{(2.2779 + 0.0024) \cdot P_s}{(1 - 0.00266 \cdot \cos(2\phi) - 0.00028 \cdot H)} \quad (1)$$

In Equation (1),  $P_s$  is the surface pressure, and the term in the denominator is the variation of the gravitational constant with latitude ( $\phi$ ) and height ( $H$ ). With accurate surface pressure measurements, the hydrostatic delay can be measured to better than 1 mm (Businger 1996).

The wet delay arises from the refractivity of the water vapor in the neutral atmosphere. Due to the variability of water vapor in the troposphere, the wet delay can vary from 10 mm in arid regions to more than 400 mm in more humid regions, such as the tropics. Not only is there a significant spatial variability in wet delay, but there also exists a significant temporal variability.

A simple relationship exists between the zenith wet delay and precipitable water, as seen in Equation (2):

$$PW = \Pi \cdot ZWD \quad (2)$$

where PW is precipitable water in a vertical column, and the zenith wet delay is typically a slant-wise wet delay measurement that has been normalized with a mapping function that is roughly related to the inverse of the sine of the elevation angle (Neill 1996).

The wet delay through the atmosphere is measured in the zenith direction with a simple integration seen in (3):

$$ZWD = 10^{-6} \left[ k_2 \cdot \int \left( \frac{P_v}{T} \right) dz + k_3 \cdot \int \left( \frac{P_v}{T^2} \right) dz \right] \quad (3)$$

where  $P_v$  is the partial pressure of water vapor,  $T$  is the atmospheric temperature and  $k_2$  and  $k_3$  are empirical refractivity constants.

The proportionality constant  $\Pi$  is another simple calculation as seen in (4):

$$\Pi = \frac{10^6}{\rho \cdot R_v \cdot \left[ \left( \frac{k_3}{T_m} \right) + k_2 \right]} \quad (4)$$

where  $R_v$  is the gas constant for water vapor,  $\rho$  is the density of liquid water,  $T_m$  is the mean temperature through a vertical layer (which is further discussed in the next section), and  $k_2$  and  $k_3$  are constants related to the refractivity of water, obtained empirically (Bevis 1994). Therefore, what one sees is a basic relationship, which only requires knowledge of the elevation angle of the satellite vehicle in relation to the ground receiver, the surface pressure to separate the wet delay from the hydrostatic delay, and the mean temperature through the vertical layer.

**2.2.1 Calculation of Mean Temperature.** The calculation of the mean temperature,  $T_m$  (in Kelvins), through the layer has been simplified even further. Bevis (1992) determined a linear relationship between surface and mean temperatures in the continental United States (CONUS) by comparing the mean temperatures from 8718 radiosonde observations with their respective surface temperatures. He determined that the regression equation  $T_m \approx 70.2 \text{ K} + 0.72 T_s$  would yield a precipitable water value with no more than 2% error due to the regression itself. Note that this regression is only good for CONUS and may not apply in other geographic regions. Liou (2001) employed the same technique in Taiwan, using 586 Taipei radiosondes, and empirically derived the relationship  $T_m \approx 1.07T_s - 31.5 \text{ K}$ .

**2.2.2 Calculation of  $\Pi$ .** Emardson and Derks (2000) have taken the regression a step further, by incorporating latitude and time of year into the formula for  $\Pi$ , resulting in a relationship unique to each GPS receiver site:

$$\Pi = 10^{-8} \rho R_v k_2 + 10^{-8} \rho R_v k_3 \theta + a_1 T_s \sin\left(\frac{2\pi t_d}{365}\right) + a_2 \cos\left(\frac{2\pi t_d}{365}\right) \quad (5)$$

In Equation (5),  $k_2$  and  $k_3$  are the same constants as in (4),  $a_1$  and  $a_2$  are empirical constants relating the surface temperature to a mean temperature,  $\theta$  is the latitude of the receiver site in radians, and  $t_d$  is the Julian day (in decimal form). To obtain this relationship, the authors used over 120,000 radiosonde profiles from 38 upper air sites throughout Europe.

Based on these empirical formulae and simplifications, Bevis (1992) has determined that the error still remains within 4%, which is within the tolerance of other existing moisture measurement sets (such as radiosondes).

## 2.3 The Fifth-Generation Mesoscale Model

The Fifth Generation Pennsylvania State University-National Center for Atmospheric Research Mesoscale Model version 3 (MM5v3) is the Air Force Weather Agency's numerical model of choice for its operational applications.

**2.3.1 Historical Perspective.** The model was first developed by Richard Anthes and T.T. Warner at the Pennsylvania State University (PSU) in 1971, and then was enhanced through cooperation with the National Center for Atmospheric Research (NCAR). Version 3 of the modeling system has been available since July 1999. AFWA has been running the MM5 as its primary operational numerical model since 1997.

**2.3.2 Model Setup.** The MM5 is a limited-area, non-hydrostatic, three-dimensional model that employs primitive equations. The model is in a nested-grid form that calculates output for a parent domain as well as one or more sub-domains. Grell (1995) provides additional information about the model setup.

The MM5 uses a terrain-following sigma ( $\sigma$ ) vertical coordinate, a unitless value defined in Grell (1995) as (6):

$$\sigma = \frac{(p - p_t)}{(p_s - p_t)} \quad (6)$$

where  $p$  is a reference pressure based on user-defined constants and terrain,  $p_s$  is the surface pressure, and  $p_t$  is the specified top pressure. AFWA's MM5 configuration has 41 sigma levels.

The Air Force Weather Agency (AFWA) has taken advantage of the flexibility of this model by allowing variations in nest configurations and physics parameterizations. As of Fall 2001, AFWA runs MM5 windows over 29 worldwide mission critical theaters of operations. They maintain 18 parent domains, from which 11 inner nest windows are derived (Applequist 2001, personal correspondence). In addition, the MM5 has physics packages that AFWA has the option to configure to best take advantage of a particular theater of interest. Theaters that will be addressed in this research all have the same physics packages, as outlined in Table 1 (Craig 2000).

AFWA MM5's parent domains each have 45 km grid resolution, while the inner nest domains have spacings that range from 15 km to 1.67 km. Parent domains are initialized and run twice per day, running 72-hour forecasts in 3-hour intervals. The 15

km inner nest, the domain used for this research, initializes two times per day, 6 hours after the parent domain's run. Inner nests produce 48-hour forecasts, also in 3-hour intervals.

Table 1. AFWA MM5 Physics Packages. Adapted from Craig (2001).

| <b>Parameter</b>         | <b>Scheme</b>                 |
|--------------------------|-------------------------------|
| Atmospheric Radiation    | Dudhia Longwave and Shortwave |
| Cumulus Parameterization | Grell Convective              |
| Explicit Schemes         | Reisner Mixed Phase           |
| Planetary Boundary Layer | MRF PBL                       |
| Soil Model               | Multi-Layer Thermal Diffusion |

**2.3.3 Model Initialization.** Until January 2001, the MM5 used synoptic background fields based on the Aviation Model (AVN) or the Navy Operational Global Atmospheric Prediction System (NOGAPS). AFWA's MM5 now initializes its parent domains using a Mesoscale Data Assimilation System / Multivariate Optimal Interpolation (MDAS/MVOI) scheme. The inner nests are not initialized in this way; instead it uses the parent windows. With MDAS/MVOI, the model can now use its own forecast background fields, combined with global analyses, to generate accurate analysis fields that adapted well to the various 45 km resolution parent domain locations (Ritz et al. 2001). With MDAS/MVOI, GPS-derived PW is unable to be of temporal value to the model. A more temporally dynamic assimilation scheme is required to better take advantage of the temporal variability PW values, such as 3DVAR, explained in the next section.

**2.3.5 3DVAR Assimilation Scheme.** By summer 2002, AFWA is expected to have transitioned all of its parent domain initializations to the 3-Dimensional Variational Analysis (3DVAR) system. 3DVAR will accommodate virtually all of the observation types that MDAS/MVOI currently employs, along with some new types, to include wind profiler data. It is expected that GPS-derived precipitable water will be among the data types accommodated by 3DVAR. Parallelization of the data assimilation and interpolation techniques over several processors will also make incorporating GPS-derived PW easier (Ritz 2001).

## **2.4 Using GPS Meteorology to Validate and Improve Forecast Models**

Studies have already shown how GPS-derived precipitable water observations compare with numerical forecast model output. Some studies assimilated the PW values into the model initialization, while others simply conducted an independent data comparison, similar to this research. For further details on these studies, the reader is directed to the references cited in the text. Summaries of a selection of these studies follow.

**2.4.1 High Resolution Limited Area Model (HIRLAM).** The HIRLAM model is a regional NWP system developed by the weather services of the Nordic countries, along with Ireland, Holland, and Spain.

Yang et al. (1999) compared GPS precipitable water data with a  $0.21^\circ$  resolution HIRLAM configuration similar to the operational version at the Danish Meteorological Institute. Comparisons of the 6, 12, and 30-hour forecasts of precipitable water with the



concurrent GPS precipitable water values at 25 sites in Sweden and Finland were conducted. This study was performed between August and November 1995 and over 11,000 observations were compared.

Results of the comparison between the GPS PW values and the HIRLAM analysis were very optimistic. Correlations ranged from 0.91 to 0.96, averaging 0.94, and RMSE ranged between 1.9 and 3.4 mm, with a mean value of 2.4 mm, approximately 18% of the mean PW value. For the 6, 12, and 30-hour forecasts, the correlations were 0.94, 0.93 and 0.93, respectively, and the RMSEs were 2.4, 2.5, and 2.6 mm, respectively.

In Spain, Cucurull et al. (2000) employed the HIRLAM model to compare analysis and forecast precipitable water values with GPS-derived PW values at five GPS sites in the Madrid Sierra region of central Spain. The case was during 2-15 December 1996 and involved two frontal passages. The HIRLAM analyses, when compared with the GPS-derived PW values, resulted in a model moist bias of 0.2 mm and an RMS difference of 2.1 mm. The 24-hour HIRLAM forecast resulted in a bias of  $-1.2$  mm and an RMSE of 3 mm. The higher values were expected of the longer forecast integration time.

Finally, Lenderink and Meijgaard (2001) compared the performance of a modified HIRLAM model, the HIRHAM4, with the Nordic GPS network. The HIRHAM4 is a high-resolution ( $0.167^\circ$ ) version of HIRLAM with a physics package known as ECHAM4. For comparison, the authors also modified the ECHAM4 package with revised cloud and turbulence schemes. At the same time, both the HIRLAM and European Centre for Medium-Range Weather Forecasting (ECMWF) models' analyses

were used in the HIRHAM4 to assess which would handle the high-frequency variation of GPS-derived integrated water vapor (IWV). This setup was run for three frontal passages from 28 August to 5 September 1995.

The study concluded that, in the first 24 hours of forecast, the HIRLAM analyses produced a more accurate depiction of the high variability of the IWV fields, most likely due to the higher resolution ( $0.4^\circ$ ) of the HIRLAM grid compared to the  $1.5^\circ$  ECMWF. After 24 hours, the ECMWF was superior. Regarding the comparison between the two model physics packages, the revised physics package better captured the maxima and minima of IWV during frontal passages, as well as the timing of these peak values.

**2.4.2 Rapid Update Cycle (RUC).** Wolfe and Gutman (2000) have pioneered American efforts to bring GPS meteorology into operational forecasting. In their 2000 study, they assimilated GPS-derived PW into the Mesoscale Analysis and Prediction System (MAPS), which is NOAA's research version of the RUC model. The RUC is a high frequency, state-of-the-art analysis and forecast system run by the National Centers for Environmental Prediction (NCEP). Most operational RUC forecasts are run on 40-km and 20-km resolution grids and seldom exceed 12-hour integration times. In this study, GPS-IPW values were assimilated into the RUC analyses every three hours from 20-29 June 1997 using optimal interpolation.

Output was assessed for the Purcell, OK GPS-receiver site. The analyses showed a mean bias of 1.8 mm (RUC had more moisture) and an error range of 5.5 to  $-6.9$  mm. Only one 12-hour forecast was evaluated in this study, and the preliminary results showed that GPS-IPW in the model better captured variations in convective precipitation.

Smith et al. (2000) provided more detail in the same ongoing RUC assimilation study. In this case, GPS-IPW observations were assimilated every 3 hours into a 60-km resolution, 25-sigma level RUC window over the central United States. Every three hours, a new analysis was produced, using the previous 3-hour forecast as the background field. Parallel runs of the RUC with and without the GPS-IPW have been ongoing since November 1997.

The GPS data provided valuable information at a temporal and spatial resolution that cannot be obtained through a radiosonde network. Because GPS data is available approximately every half hour in the American GPS-MET network, it was possible to ingest the GPS values at every analysis time, while the radiosonde data is only available every 12 hours. In the case presented in Smith et al. (2000), from 16 to 17 April 1998, a cold front crossed eastern Texas. The GPS data moistened the 3-hour forecast of relative humidity fields by 14% ahead of the front, and dried out the fields by 23% behind. This resulted in a 1% improvement of the 850mb RH and a 2% improvement of the 500 mb RH.

Smith et al. (2000) made two other observations that must be considered for future work on assimilation of GPS data into NWP. First, the GPS observations themselves must maintain an accuracy of at least 1.5 mm to be considered a value-added data source. This value has to include errors that could evolve from inaccuracies in orbit, temperature and pressure measurements, and post-processing. It was also concluded that the high variability of IPW limits the value of the data to making improvements in the short-term, especially in the 12-hour forecast timeframe.

Gutman and Benjamin (2001) provided an update to the same experiment, this time with a more populated CONUS GPS-MET network. When Smith et al. (2000) started their work, there were only 18 stations. By late 1999 the number had jumped to 58, including a number of sites on coastlines, where moisture data are often the most variable. Now forecast RH values at both 850 mb and 700 mb were improved by an average of 4.5%. At one model run, the 3-hour forecast was improved by as much as 40%!

Other conclusions found by Gutman and Benjamin (2001) involve the required accuracy and timeliness of the GPS data. In order for the GPS data to be of value to an NWP model, it must be measured at a higher accuracy than the model's error budget. The current convention is for models to analyze the precipitable water fields to within 3 mm accuracy. The Department of Energy has conducted a number of Water Vapor Intensive Observing Periods (WVIOPs), which compares precipitable water from 6 different sources at a facility near Lamont, OK. The results from this period show that GPS-derived precipitable water has an accuracy of about 1 mm, which is well within the tolerances required for a valuable data source for NWP. Concerning the timeliness, observations for initialization into numerical weather models is considered "real-time" if it can be ingested in the current assimilation cycle. This timeline is unique to each model, and the RUC requires 20-30 minutes before an observation is considered late. Currently, for quick post-processing, a "rapid orbit" calculation is required in the processing software. Scripps Institution of Oceanography has the capability to make such orbit calculations with its processing software in 24 hours (compared to 1-2 weeks),

and has done so to well within 1 mm accuracy, which adheres to the tolerances for assimilation into numerical models.

**2.4.3 PSU/NCAR MM5.** De Pontecca and Zou (2001) reported on an assimilation of GPS total zenith delay observations into the MM5 for a precipitation forecast in southern California during an El Nino event. The data was ingested, using a 4DVAR assimilation scheme, into a 6-km resolution domain with 20 sigma levels. A domain based on the 54-km NCEP reanalysis over the western United States was the parent to a 6-km nested grid that served as an initial condition in the 4-DVAR assimilation scheme. After two hours worth of observation ingest, the scheme required a 12-hour spinup, necessary to acquire the dynamic stability and damping of smaller scale gravity waves.

De Pontecca and Zou (2001) compared total zenith delays from MM5 output that was run both with and without the GPS data. The results were remarkable. First, the bias between the model run and the GPS observations was reduced by more than 90% when the GPS data was assimilated. Secondly, the precipitation forecasts were timelier and more accurate, by an average of 33.15%.

Cucurull et al. (2001) also performed a 4DVAR assimilation of simulated GPS-derived PW into a very fine scale MM5 over Spain. Their grid resolutions were 6 km and 2 km, with 5 minute and 30 second terrain resolution, respectively. In this study, simulated values of PW were assimilated using a 4DVAR scheme. First the MM5 was run over the period of interest and PW values were estimated at each grid point at 30 minute intervals. This created an “idealized” fictitious GPS network. This information was then re-introduced to the model using variational assimilation.

Results of this experiment showed the model's high sensitivity to the PW observations. However, no numeric results were available due to the paper's emphasis on assimilation of ZTD into the model.

**2.4.4 Deutsche Wetterdienst (DWD) Models.** Köpken (2001) employed three models derived from the DWD's limited area forecast and analysis system: the Europa Model ( $1/2^\circ$  horizontal resolution and 20 sigma levels), the Deutschland Model ( $1/8^\circ$  horizontal resolution and 30 sigma levels), and the BALTEX Model ( $1/6^\circ$  horizontal resolution and 31 sigma levels).

Köpken's work was conducted with the same Nordic GPS network as Yang (1999) and Lenderink and Meijgaard (2001). The study was conducted over August – October 1995. The GPS data was taken in 30 minute increments and was not assimilated into the models.

The results of Köpken's study were promising, with correlations between the BALTEX model and the GPS data near 90%, and bias of less than 3 mm. The model positive bias was consistent throughout the experiment period at virtually all GPS receiver sites, and for all three of the models. Such a bias was also seen in the HIRLAM model. To further investigate this bias, comparisons between the GPS data and radiosonde data were also performed. Köpken's results for six stations in Sweden and Finland indicated the GPS possessing a slight dry bias of about 1.3 mm. This could indicate that the DWD models have an overall moist bias of approximately 1.5 mm.

**2.4.5 Swedish Meteorological and Hydrological Institute Model.** A Central European GPS meteorology network of 15 sites was analyzed in Borbas (1998). A

numerical model developed by the Swedish Meteorological and Hydrological Institute was used for comparison. This model was a primitive equation model with a 90-km horizontal resolution and 12-sigma levels.

Comparisons were made by linearly interpolating the four nearest gridpoints to GPS-receiver sites in Germany, Switzerland and Poland. The GPS data were processed using two different processing schemes, one at the International GPS Service at the University of Bern, Switzerland, and the other at the Institute of Space Research, Department of Satellite Geodesy in Graz, Austria.

When compared with the NWP, the GPS data was again consistently drier than the model output, with a 5.5 mm RMSE with the Bern processing software, and a 6.3 mm RMSE with the Graz processing software.

**2.4.6 Summary.** Overall, this sample of studies involving GPS-derived precipitable water with NWP has shown the GPS data's reliability, along with its excellent spatial and temporal resolution. For these studies, GPS-derived PW was clearly a value-added data source. Independent data comparisons showed how well GPS compares with radiosonde data, and could reduce consistent biases in many NWP models. Also, assimilation studies have proven on numerous occasions how moisture-related variables are more accurate when GPS data are included.

### III. Methodology

#### 3.1 Data Collection

**3.1.1 GPS-Meteorology Data.** The National Oceanic and Atmospheric Administration Forecast Systems Laboratory (NOAA/FSL) controls the American network of GPS Precipitable Water receivers. Their network of over 50 sites in the CONUS and four sites in Alaska produces precipitable water readings every 30 minutes and posts a comprehensive output file to an FTP site for public viewing and download. Table 2 is an example of the downloaded data from the NOAA/FSL database. Figure 4 shows NOAA's GPS Meteorology network as of May 2001. See Appendix A for terrain, network, and gridding details for each GPS site.

The NOAA/FSL GPS-MET website contains the geodesy and hardware specifications for the sites. Most of the sensors are either Trimble 4000 SSI or Ashtech LP Z-XII3 receivers, and the data is processed with the University of Hawaii/Scripps Institute for Oceanography GAMIT software suite using predicted orbit information.

Table 2. Sample GPS-MET Data from Bartlett, NH for 6 July 2001

| ID   | Year | Julian Date | IPW (cm) | Press (mb) | Temp (C) | RH (%) | Total Delay (m) | Wet Delay (m) | Hydro Delay (m) | Mean Temp (K) | $\Pi$ (cm) |
|------|------|-------------|----------|------------|----------|--------|-----------------|---------------|-----------------|---------------|------------|
| BARN | 2001 | 187.010     | 2.512    | 986.73     | 19.42    | 84.7   | 2.4035          | 0.1567        | 2.2468          | 280.85        | 6.239      |
| BARN | 2001 | 187.031     | 2.381    | 986.95     | 18.17    | 89.4   | 2.3963          | 0.149         | 2.2473          | 279.95        | 6.259      |
| BARN | 2001 | 187.052     | 2.385    | 987.25     | 17.63    | 89.7   | 2.3974          | 0.1495        | 2.2479          | 279.562       | 6.268      |
| BARN | 2001 | 187.073     | 2.617    | 987.65     | 17.4     | 89.3   | 2.413           | 0.1641        | 2.2489          | 279.396       | 6.271      |
| BARN | 2001 | 187.094     | 2.62     | 987.88     | 17.28    | 87     | 2.4138          | 0.1644        | 2.2494          | 279.31        | 6.273      |
| BARN | 2001 | 187.115     | 2.539    | 987.82     | 17.02    | 85.2   | 2.4087          | 0.1594        | 2.2492          | 279.122       | 6.277      |





Figure 4. The American GPS Precipitable Water Receiver Network as of 31 May 2001. Courtesy of NOAA/FSL.

**3.1.2 MM5 Data.** The MM5 data for the CONUS and Alaska 15 km grids were obtained from AFWA. The GRIB output was downloaded daily from 06 July 2001 through 31 October 2001. Only four parameters needed to be stripped from the GRIB files: longitude (LUN), latitude (LOT), terrain height (TERHGT), and precipitable water (PWAT). The first three parameters are necessary for properly placing the GPS data on the MM5 grid. Processing of the PWAT data will be discussed later in this chapter.

**3.1.3 RAOB Data.** RAOB sites were chosen based on their proximity to GPS-receiver sites. There was a challenge of finding collocated sites since the NOAA/FSL-controlled GPS network is not concurrent with established WMO weather observation sites. Using guidance from Köpken (2001), the estimated range of atmosphere included in a GPS-derived PW value has 40 km radius. Therefore, only upper air sites within 45

km of GPS sites were chosen for comparison. However, Springfield, MO (SGF)'s RAOB site was also considered, due to its location in the Tornado Alley region of the country, despite it being nearly 70 km from the nearest GPS site, Conway, MO (CNWM).

The radiosonde-based PW values were downloaded from the GPS-MET website (<http://www.gpsmet.noaa.gov>). This website provides radiosonde output in an easy-to-process format. Because this data was pre-formatted, reading it into FORTRAN programs was simple and requires no further discussion in this section.

### **3.2 Sources of Error**

Prior to explaining the data analysis process, it is important to address the sources of error faced in working with GPS data in concert with MM5 and RAOB data. The following is a discussion of possible sources of error. Further details are available in Feng (1998).

**3.2.1 Make and model of GPS equipment.** This is not an explicit source of error that has been measured, but the varying makes and models of GPS equipment provides a lack of consistency in how a GPS-MET sample was taken. Table 3 shows a representation of the makes and models of GPS receiver and antenna equipment, in no particular order.

Table 3. Representation of Makes and Models of GPS Receivers

| <b>Receiver Models</b> | <b>Description</b>  |
|------------------------|---|
| Trimble 4000 SSE       | Dual frequency P-code on L1 and L2                                  |
| Trimble 4000 SSI       | Dual frequency P-code on L1 and L2                                  |
| Ashtech LP Z-XII3      | 12 Channel, L1/L2, P1/P2 w/ continuous reference station capability |
| Ashtech LP Z12         | 12 Channel, L1/L2   |

**3.2.2 Antenna configuration and height.** The type of antenna is a bonafide source of error in processing GPS-MET data. There are two types of GPS antennas well known in the navigation world: the choke ring and the fixed groundplane. Many older antenna models still have a fixed groundplane configuration, and this could be a source of error in GPS calculations. The choke ring antenna is the International GPS Service (IGS) standard for computing phase center corrections (Feng 1998). Table 4 provides information about the various antennas involved in this study.

Table 4. Representation of Makes and Models of GPS Antennas

| <b>Antenna Models</b>    | <b>Shape</b>              |
|--------------------------|---------------------------|
| Trimble 33429            | Fixed Groundplane         |
| Trimble 29659            | Dorne Margolin Choke Ring |
| Trimble 22020            | Fixed Groundplane         |
| Trimble 14532            | Fixed Groundplane         |
| Trimble 23903            | Fixed Groundplane         |
| Ashtech 700829 "Whopper" | Fixed Groundplane         |

### **3.2.3 Elevation differences**

#### **3.2.3.1 Differences between GPS site elevation and MM5 TERHGT**

**value.** A significant source of error in the comparisons between GPS and MM5 PW

values is the difference in elevation at each GPS site. The model height of the GPS site was calculated by linear interpolation of the TERHGT value for four surrounding grid points. This was compared with the established height of the GPS receiver, provided by the network administrators. No adjustments were made to correct for the differences in terrain in this study. Elevation residuals are shown in the location data in Appendix A.

**3.2.3.2 Differences between GPS site elevation and RAOB site.** Like the MM5 elevations, the differences between the GPS sites and their nearest RAOB locations can be significant. This elevation difference can be corrected using assumptions of constant relative humidity and a typical lapse rate, but the RAOB sites used in this study had similar enough elevations that such differences were negligible. The elevation residuals between the GPS and RAOB locations are shown with the location data in Appendix A.

**3.2.4 Horizontal differences between GPS site and RAOB site locations.** As discussed in Section 3.1.3, only RAOB sites that were within 45 km of the GPS site were chosen for this study (plus Springfield, MO, as explained in Section 3.1.3). Due to the setup of the GPS network, this resulted in very few RAOB sites being available. The horizontal differences between the GPS sites and RAOB sites are of particular interest due to several of the sites being near coastlines. When a RAOB sites is near a coastline, there is a chance of the balloon drifting over the ocean and being exposed to increased moisture compared to an inland GPS site. These distance differences are shown in Appendix B.

**3.2.5 Orbit calculations.** The orbit calculation methods are another source of error in GPS-MET parameter calculations. Knowledge of ephemeris data is essential to calculate ZHD and ZWD. There are 5 variations on the type of orbit information, outlined in Table 5.

Table 5. Comparison of GPS Orbit Calculations Available in GPS-MET Processing (NASA 2001).

| <b>GPS Orbit Calculation</b> | <b>Accuracy</b> | <b>Latency</b> | <b>Update Frequency</b> |
|------------------------------|-----------------|----------------|-------------------------|
| Broadcast                    | ~260 cm         | real time      | --                      |
| Scripps Hourly               | ~20 cm          | real time      | hourly                  |
| Predicted (Ultra Rapid)      | ~25 cm          | real time      | twice daily             |
| Rapid                        | ~ 5 cm          | 17 hours       | daily                   |
| Final                        | < 5 cm          | ~ 13 days      | weekly                  |

The NOAA/FSL GPS network uses the Scripps Hourly orbit product, which provides the most up-to-date, real-time orbit information for operational processing of GPS-MET data. Their standard for accuracy is 25 cm, so the Scripps product is within that tolerance.

**3.2.6 Processing software.** This potential for error arises from the varying methods of processing the data. There are several software suites available for calculating tropospheric, hydrostatic and wet delays, from which PW is extracted. A list of the most widely used programs is listed in Table 6. A study was conducted comparing the GPS-MET data from these three software packages with varying orbital calculations. It was concluded that BERNESE and GAMIT had comparable accuracies, and that other factors besides software accuracy can be taken into account to decide on which software package is better (Department of Commerce 1995). The NOAA/FSL network employs the GAMIT software suite.

Table 6. Available GPS Processing Software

| <b>Software</b> | <b>Developer</b>  |
|-----------------|---|
| GAMIT           | Massachusetts Institute of Technology/Scripps Institute of Oceanography |
| BERNESE         | University of Bern  |
| PAGES           | National Geodetic Survey  |

**3.2.7 Empirical estimates of parameters in GPS-MET calculations.** Many calculations in processing GPS-MET parameters require constants of proportionality. These constants were empirically defined with studies involving thousands of radiosondes.

The mean temperature for  $\Pi$  in Equation (4) is routinely calculated for CONUS and Alaska using Bevis' (1992) empirical correlation based on 8718 radiosonde calculations over 2 years. Other studies have been conducted in Europe and Taiwan that derive other mean temperature correlations. These correlations are sufficient for meteorological use of GPS, and their relative error is less than 1%. Nonetheless, this is still a contribution to the error budget.

The refractivity constants,  $k_2$  and  $k_3$ , in Equations (3) and (4) also are empirically defined. Bevis et al. (1994) provides historical commentary on their derivations. Bevis et al. (1994) also derived his own values for the refractivity constants and assumed them to be within 2 standard deviations of the true values.

Bevis et al. (1994) concluded that the error in mean temperature is much greater than that of the refractivity constants, and that most of the error in the  $\Pi$  calculation is due to the mean temperature.

### ***3.2.8 Differences in PW calculation methods between GPS, RAOB and MM5.***

Another significant source of error is the differences in how PW is calculated among the three data sources.

The GPS PW is calculated using the equations outlined in Chapter II. Note that there is no reference to typical humidity parameters, such as mixing ratio, dew point or specific humidity.

The RAOB PW is calculated using a NOAA algorithm and it integrates mixing ratio over all pressure levels. Mixing ratio is defined as the ratio of water vapor to dry air (Glickman 2000). If the sounding from which mixing ratio is being calculated runs out of data before encountering the highest possible level, then those levels are simply left off; if the top level is less than 5 km elevation, the sounding is thrown out.

MM5 PW is calculated by integrating specific humidity over all pressure levels. For all intents and purposes, it is acceptable to interchange specific humidity and mixing ratio (Glickman 2000). A typical mid-latitude mixing ratio value varies from a specific humidity value by not more than 0.1%. It has been observed that some operational versions of the MM5 may interchange specific humidity and mixing ratio in calculations (Swanson 2001).

### **3.3 Coding of Processing Programs**

**3.3.1 Overview.** A number of variables required custom procedures for each of the theaters processed. The following steps needed to be completed: (1) extract relevant information from GPS, MM5 and RAOB input data and read the data from the various sources into FORTRAN arrays, (2) perform linear interpolation of MM5 data to GPS sites, (3) write out arrays of GPS data with RAOB sites, (4) write out the GPS, MM5 and RAOB values by domain and by location, (5) calculate comparative statistics and write them out to delimited text files. These text files were then imported into Microsoft Excel for statistical processing. Now each step will be reviewed in more detail.

**3.3.2 Extract Relevant Information.** Each of the three data sources (GPS, MM5 and RAOB) required unique programs to extract the relevant information. The GPS data came from the FSL FTP site grouped according to location. First, appending all locations' files created a large file. Then a program was developed which brought in the GPS output file and read the columns into arrays according to data type (i.e. year, id, Julian date). A second pass was then performed to conduct several tasks at once. It first threw out the lines with missing PW values. Then it searched through the Julian date arrays to strip out only those values that contained a particular DTG. Those lines were written to a new formatted file named after the Julian DTG.

The MM5 output required more work than the GPS and RAOB data, due to its two-dimensional nature and binary format. The PWAT parameter that was stripped from each GRIB file had to be converted to a binary format and then read into FORTRAN arrays.



The RAOB data was relatively easy to work with. The files were downloaded from the NOAA/FSL website in a long string of formatted soundings with no definitive breaks. To divide the data into separate soundings, an IDL routine was employed. The end result was one file for each of the soundings, named according to sounding location and DTG.

**3.3.3 Perform linear interpolation of MM5 data to GPS sites.** Each GPS site had a grid coordinate corresponding to the MM5 grid position calculated, based on a FORTRAN subroutine from AFWA. The subroutine brought in parameters describing the MM5 grid, along with an array of latitudes and longitudes of the GPS sites, and wrote out an array of IX/JX positions. The interpolation program reads in the MM5 GRIB data and linearly interpolates the values of the sixteen surrounding grid points to the GPS receiver location's IX/JX position.

Sixteen grid points, rather than four, were chosen due to the horizontal extent of a GPS-derived PW observation. Figure 5 shows the trigonometric relationship of the horizontal expanse of an averaged GPS-derived PW reading. The conditions assume a 7° elevation angle (which is the elevation cutoff for the NOAA/FSL network) and that 98% of the column water vapor resides in the lowest 5 km of the atmosphere. This results in a horizontal coverage of approximately 5200 km<sup>2</sup>.

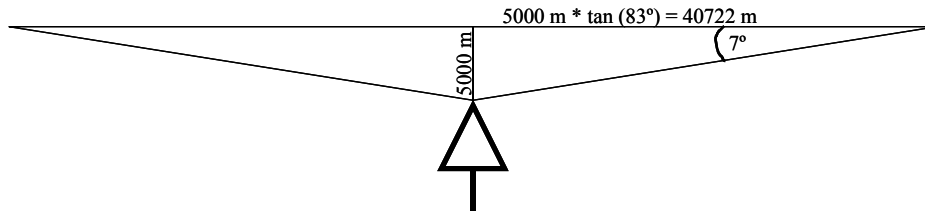


Figure 5. Area of Influence of a GPS-Derived Precipitable Water Reading. Diagram not to scale.

In a 15 km resolution model, the horizontal expanse of sixteen grid points will cover 2025 km<sup>2</sup>. Figure 6 illustrates this. Even though the coverage areas aren't exactly the same, choosing an additional ring of grid points would have resulted in an area much larger than that of the GPS observation. The 7° cutoff will result in a larger area of influence, but expanding the MM5 grid points any farther would cause negligible differences in PWAT values, due to the nature of the interpolation scheme.

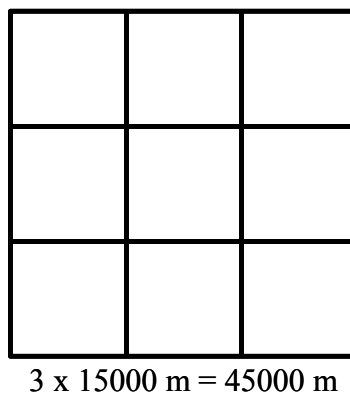


Figure 6. Area of Influence in MM5 Grid. The GPS site is positioned somewhere in the center box.

**3.3.4 Write out arrays of GPS data with RAOB sites.** To calculate precipitable water from each of the RAOB soundings another FORTRAN program was required. The foundation for this program came from Thomas Schlatter and Donald Baker in the PROFS Program Office, NOAA Environmental Research Laboratories, Boulder, Colorado. Schlatter and Baker developed a suite of FORTRAN algorithms in 1981 to

calculate moisture parameters. This suite is the standard throughout NOAA and the National Weather Service. For the precipitable water algorithm, the method of choice was to integrate dimensionless mixing ratios through the pressure levels.

Each sounding was run through the precipitable water algorithm and the output was grouped by location into files. An example of one of these files is in Table 7.

Table 7. Sample RAOB-Based Precipitable Water for Charleston, SC

| ID  | MO | DY | HR | PW     |
|-----|----|----|----|--------|
| CHS | 7  | 6  | 0  | 5.2679 |
| CHS | 7  | 6  | 12 | 4.7164 |
| CHS | 7  | 7  | 0  | 4.5271 |
| CHS | 7  | 7  | 12 | 4.8938 |
| CHS | 7  | 8  | 0  | 3.6750 |
| CHS | 7  | 8  | 12 | 4.7439 |
| CHS | 7  | 9  | 0  | 6.7243 |
| CHS | 7  | 9  | 12 | 6.3339 |

These data were run through a program to generate files of GPS-derived PW and RAOB-derived PW together, as seen in Table 8.

Table 8. Sample GPS vs. RAOB Comparison File for Slidell, LA

| DTG    | GPS Site | GPS PW | RAOB Site | RAOB PW |
|--------|----------|--------|-----------|---------|
| 187.01 | NDBC     | 5.2130 | SIL       | 5.8068  |
| 187.51 | NDBC     | 4.4710 | SIL       | 5.0915  |
| 188.01 | NDBC     | 4.5440 | SIL       | 5.2191  |
| 188.51 | NDBC     | 3.7530 | SIL       | 4.3528  |
| 189.01 | NDBC     | 3.7390 | SIL       | 4.4593  |
| 189.51 | NDBC     | 3.9020 | SIL       | 4.8850  |
| 190.01 | NDBC     | 3.8940 | SIL       | 4.3743  |
| 190.51 | NDBC     | 5.0740 | SIL       | 5.7159  |
| 191.01 | NDBC     | 4.4040 | SIL       | 5.3123  |
| 191.51 | NDBC     | 4.6320 | SIL       | 5.3905  |

**3.3.5 Output by DTG.** Next, the GPS-derived PW and MM5 interpolated PW values were written to a file titled by Julian date/Julian time/forecast integration time. Table 9 is an example of one of these output files.

Table 9. Sample Output File for a 45-Hour Forecast Valid 8 July 2001 03 UTC. PW values are in centimeters.

| <b>ID</b> | <b>Lat</b> | <b>Long</b> | <b>IX</b> | <b>JX</b> | <b>GPS PW</b> | <b>MM5 PW</b> |
|-----------|------------|-------------|-----------|-----------|---------------|---------------|
| BLRW      | 43.22      | -90.53      | 218.54    | 138.78    | 1.5330        | 1.8270        |
| DQUA      | 34.11      | -94.29      | 200.33    | 72.17     | 4.2180        | 5.0045        |
| FBYN      | 40.08      | -97.31      | 182.79    | 115.33    | 3.3970        | 3.7789        |
| HKLO      | 35.68      | -95.86      | 190.83    | 83.49     | 3.5200        | 4.5889        |
| JTNT      | 33.02      | -100.98     | 159.43    | 65.04     | 2.8280        | 2.8529        |
| RWDN      | 40.09      | -100.65     | 164.43    | 116.09    | 2.2000        | 2.6036        |
| MBWW      | 41.90      | -106.19     | 135.74    | 131.80    | 2.0060        | 1.8064        |

**3.3.6 Output by location.** The next task was to group all data together by location. This involved a new program that took the output GPS and MM5 data from a particular DTG and wrote each location's line to a new file, which is shown in Table 10.

Table 10. Location-specific PW Data for Spokane, WA.

| <b>DTG</b>  | <b>ID</b> | <b>GPS PW</b> | <b>MM5 PW</b> |
|-------------|-----------|---------------|---------------|
| 187.500.06H | SPN1      | 0.8400        | 1.2588        |
| 187.625.09H | SPN1      | 1.5220        | 1.2732        |
| 187.750.12H | SPN1      | 2.0170        | 1.2030        |
| 187.875.15H | SPN1      | 1.3900        | 1.0499        |
| 188.000.06H | SPN1      | 1.3970        | 1.1243        |
| 188.000.18H | SPN1      | 1.3970        | 1.0859        |
| 188.125.09H | SPN1      | 1.5500        | 1.1666        |
| 188.125.21H | SPN1      | 1.5500        | 1.1892        |

**3.3.7 Comparative statistics calculations.** Summary statistics were calculated from each of the previously described files. A statistics subroutine was developed that calculated the mean values, bias, correlation, root mean square (RMS) error, standard deviation, and n, the number of observations available in each calculation, based on equations from Wilks (1995). Table 11 shows an example of a summary statistics file for a single DTG. The contents of this file can easily be imported into PC-based programs for additional grouping and processing.

Table 11. Sample Statistical Summary by DTG. This file collected all 06H forecasts from the 06 UTC initialization MM5 runs in CONUS. One line of data was generated for each DTG file described above in Table 9.

| DTG/Forecast | Init | Corr   | Bias    | RMSE   | StDev  | Mean GPS | Mean MM5 | n  |
|--------------|------|--------|---------|--------|--------|----------|----------|----|
| 187.500.06H  | 06Z  | 0.9666 | -0.2678 | 0.4472 | 0.3622 | 2.9663   | 3.2341   | 46 |
| 188.500.06H  | 06Z  | 0.9485 | -0.2737 | 0.4861 | 0.4066 | 3.0918   | 3.3655   | 44 |
| 189.500.06H  | 06Z  | 0.9449 | -0.3391 | 0.5044 | 0.3782 | 3.4527   | 3.7917   | 42 |
| 190.500.06H  | 06Z  | 0.9090 | -0.3363 | 0.5912 | 0.4921 | 3.3689   | 3.7052   | 44 |
| 191.500.06H  | 06Z  | 0.9568 | -0.3813 | 0.5404 | 0.3874 | 3.4713   | 3.8526   | 45 |
| 192.500.06H  | 06Z  | 0.9635 | -0.3721 | 0.5262 | 0.3765 | 3.4880   | 3.8601   | 45 |
| 193.500.06H  | 06Z  | 0.9581 | -0.1280 | 0.3958 | 0.3789 | 3.3698   | 3.4978   | 45 |
| 194.500.06H  | 06Z  | 0.9674 | -0.2316 | 0.4229 | 0.3579 | 3.4582   | 3.6898   | 46 |

By-location files were also run through the statistical summary subroutine to generate data for each location: mean values, residuals, bias, correlation, and regression equation slopes and intercepts. Table 12 shows an example of this combined summary.

Table 12. Sample Statistical Summary File by Location. Each line was generated from stripping off location lines from each of the files listed such as that in Table 10.

| ID   | Corr   | Bias    | RMSE   | RMSE%   | StDev  | %Stdev  | Mean GPS | Mean MM5 | n  |
|------|--------|---------|--------|---------|--------|---------|----------|----------|----|
| ANP1 | 0.9938 | -0.2673 | 0.2968 | 11.6236 | 0.1345 | 5.2659  | 2.5538   | 2.8211   | 13 |
| ARP3 | 0.8072 | -0.3427 | 0.5228 | 12.5932 | 0.4029 | 9.7060  | 4.1512   | 4.4939   | 25 |
| AZCN | 0.9554 | -0.1466 | 0.2595 | 15.0628 | 0.2208 | 12.8136 | 1.7229   | 1.8695   | 17 |
| BARH | 0.9295 | -0.0166 | 0.4668 | 16.5490 | 0.5387 | 19.0971 | 2.8210   | 2.8376   | 4  |
| BARN | 0.9474 | -0.0101 | 0.2459 | 10.9260 | 0.2509 | 11.1516 | 2.2502   | 2.2603   | 24 |
| BIL1 | 0.7005 | 0.0075  | 0.2624 | 15.0918 | 0.2704 | 15.5499 | 1.7388   | 1.7313   | 17 |
| BLKV | 0.9844 | -0.2897 | 0.3549 | 11.2416 | 0.2128 | 6.7391  | 3.1574   | 3.4472   | 14 |
| BLMM | 0.9528 | -0.4392 | 0.5988 | 21.5478 | 0.4196 | 15.0979 | 2.7789   | 3.2181   | 17 |
| BLRW | 0.9500 | -0.5849 | 0.6719 | 28.9181 | 0.3535 | 15.2167 | 2.3234   | 2.9082   | 8  |

## IV. Results and Discussion

### 4.1 CONUS

**4.1.1 Case Studies.** Local storage restrictions limited the amount of MM5 data that could be downloaded from AFWA's FTP site. The MM5 data download was for only 90 days, so the cases available were restricted to a time period during the summer of 2001. Four cases were chosen and are discussed below. Each case was approximately 8 days long, resulting in four independent time periods totaling 30 days. The statistics developed were for a combination of the four cases.

**4.1.1.1 6-14 July 2001 "Ring of Fire".** In this case, strong high pressure centered near Memphis, TN dominated the eastern two-thirds of the country and restricted precipitation to the periphery of the air mass.

The southwest monsoon brought rain to Arizona and New Mexico. The stationary front dropped significant rainfall over Kansas, Missouri and the Ohio River Valley. Over the course of the week, a new system entered the through the Pacific northwest and worked its way across the country. Once it entered the plains, it prompted a strong squall line that worked its way across the country. See Figure 7 for a representative radar mosaic.

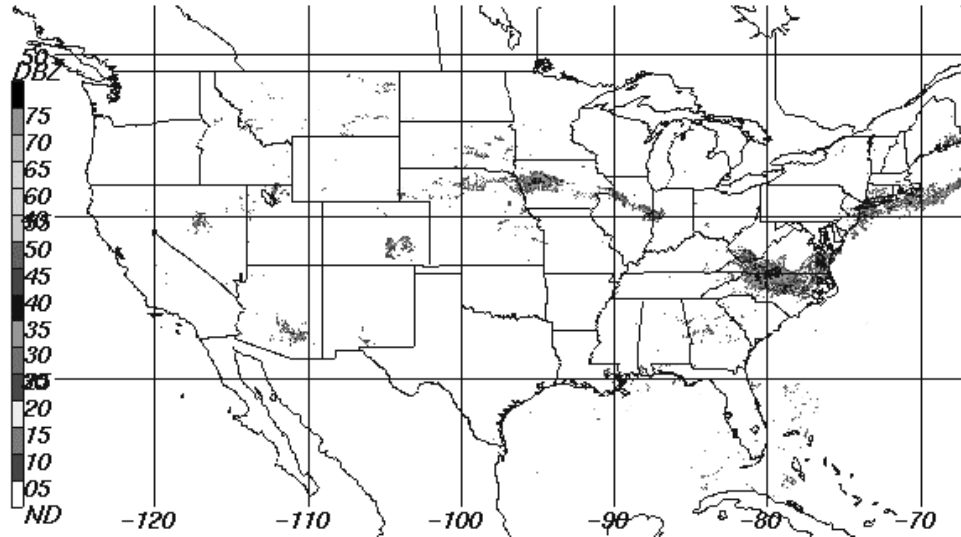


Figure 7. NEXRAD Mosaic Image from 15 UTC 8 July 2001. Note the radar reflectivities arcing across the northern plains and the Midwest. Image courtesy National Oceanic and Atmospheric Administration (NOAA 2002).

**4.1.1.2 25 July – 2 August 2001 “Central Plains Squall Line”.** At the beginning of this time period, the Bermuda high was dominating the southeast quadrant of the nation, while a stationary front draped across the central plains. The southwest monsoon was bringing rain to Arizona and New Mexico. The stationary front was sending significant rainfall over Kansas, Missouri, and the Ohio River Valley. Over the course of the week, a new system entered the country through the Pacific Northwest and worked its way across the country. Once it entered the plains, it prompted a strong squall line. Figure 8 shows a representative radar mosaic.

**4.1.1.3 11 - 18 August 2001 “Dirty Subtropical High”.** During this time period, the Bermuda high was the primary influence east of the Rockies. As seen in Figure 9, scattered showers and garden-variety thunderstorms erupted every afternoon. The monsoon was continuing to influence the desert southwest.

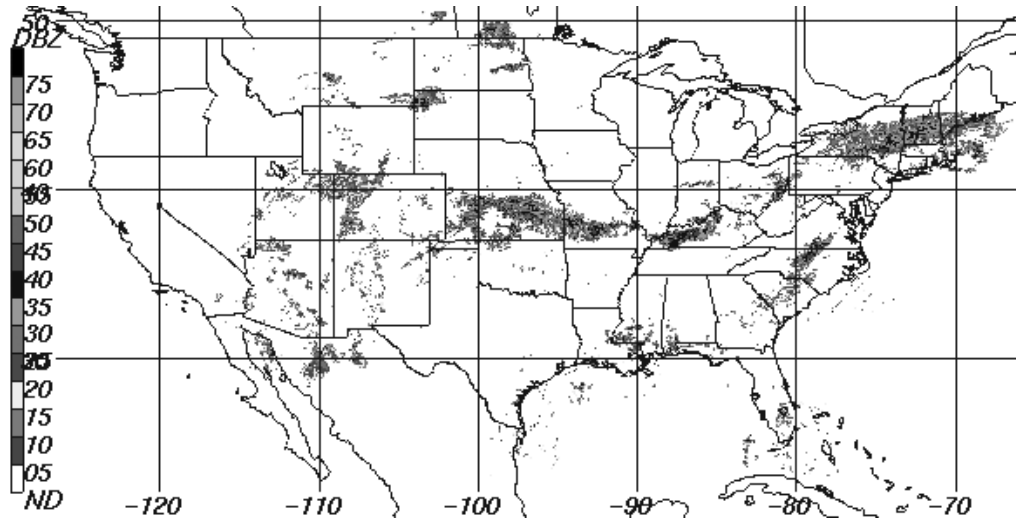


Figure 8. NEXRAD Mosaic Image from 09 UTC 25 July 2001. A stationary front bisected the nation and generated daily squall lines. Image courtesy of NOAA (2001).

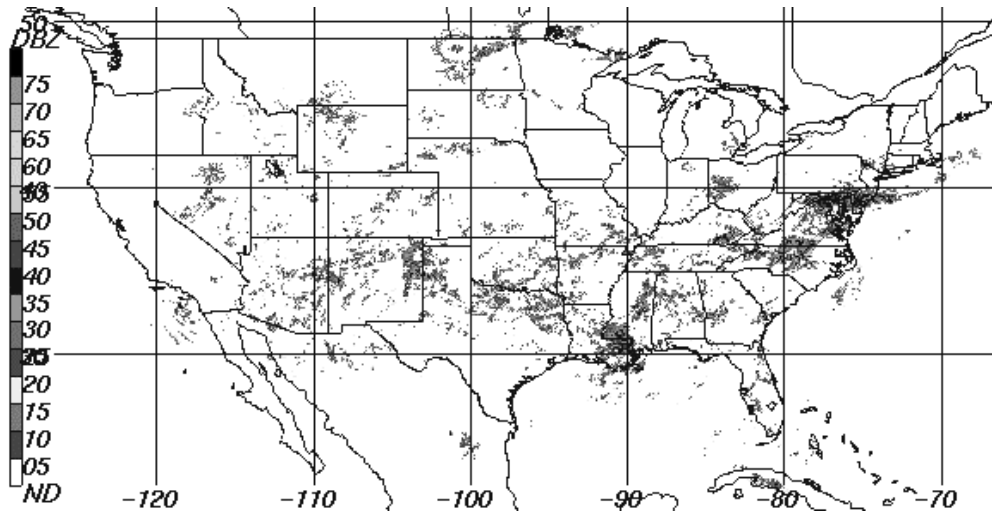


Figure 9. NEXRAD Mosaic Image from 00 UTC 12 August 2001. Image courtesy of NOAA (2001).

**4.1.1.4 10 – 15 September 2001 “Hurricane Gabrielle”.** Figure 10 shows mosaic imagery from just after Tropical Storm Gabrielle’s landfall. Gabrielle formed over the southeastern Gulf of Mexico and cut across the Florida peninsula. At the same time, the southwest monsoon was pumping moisture all the way up into the northern plains, causing showers and thunderstorms throughout.



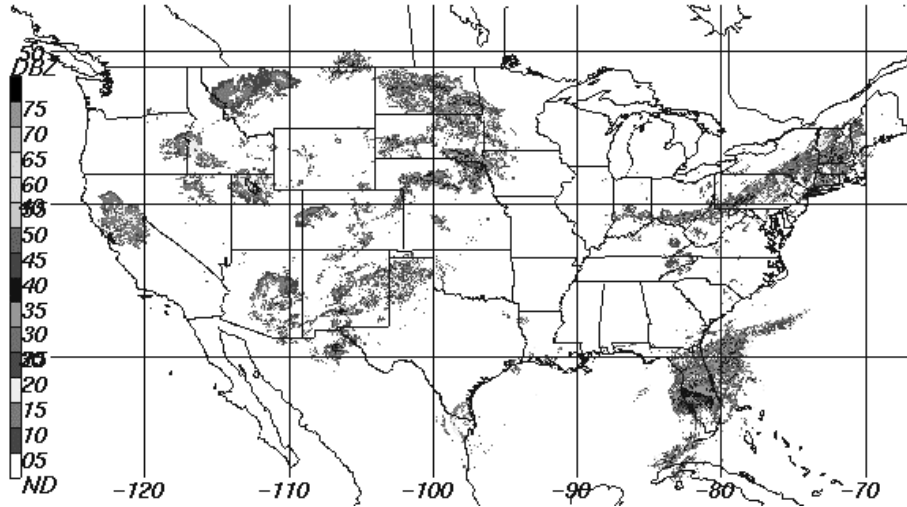


Figure 10. NEXRAD Mosaic Image from 08 UTC 14 September 2001. This image was from just after Tropical Storm Gabrielle's landfall near Venice, FL. Image courtesy of NOAA (2001).

**4.1.2 Domain Summary.** Figure 11 shows summaries of the domain-wide comparisons between GPS-derived and MM5-calculated precipitable water. In order to properly assess the data, it is important to understand the local diurnal patterns. Figure 11a shows the mean GPS and MM5 PW values for each forecast period. Note the significant diurnal variation in the GPS PW. The GPS PW was higher during the daylight hours and this results in higher correlations, lower root mean square errors and lower standard deviations when compared against the 06 UTC initialization products.

The maximum seen in the GPS-derived PW at the 06 UTC initialization occurs at 1500 local Central Standard Time, which is the estimated time of maximum heating. The minimum seen in the GPS 18 UTC Initialization occurs just before local sunrise. Note the 06 UTC and 18 UTC patterns crossing over each other just before 09H and 21H. This signature is hereafter referred to as a “crossover” in the graph. Both GPS-derived PW crossovers occur at their respective local sunrise and sunset. Note the MM5's lack of crossover compared to the GPS values.

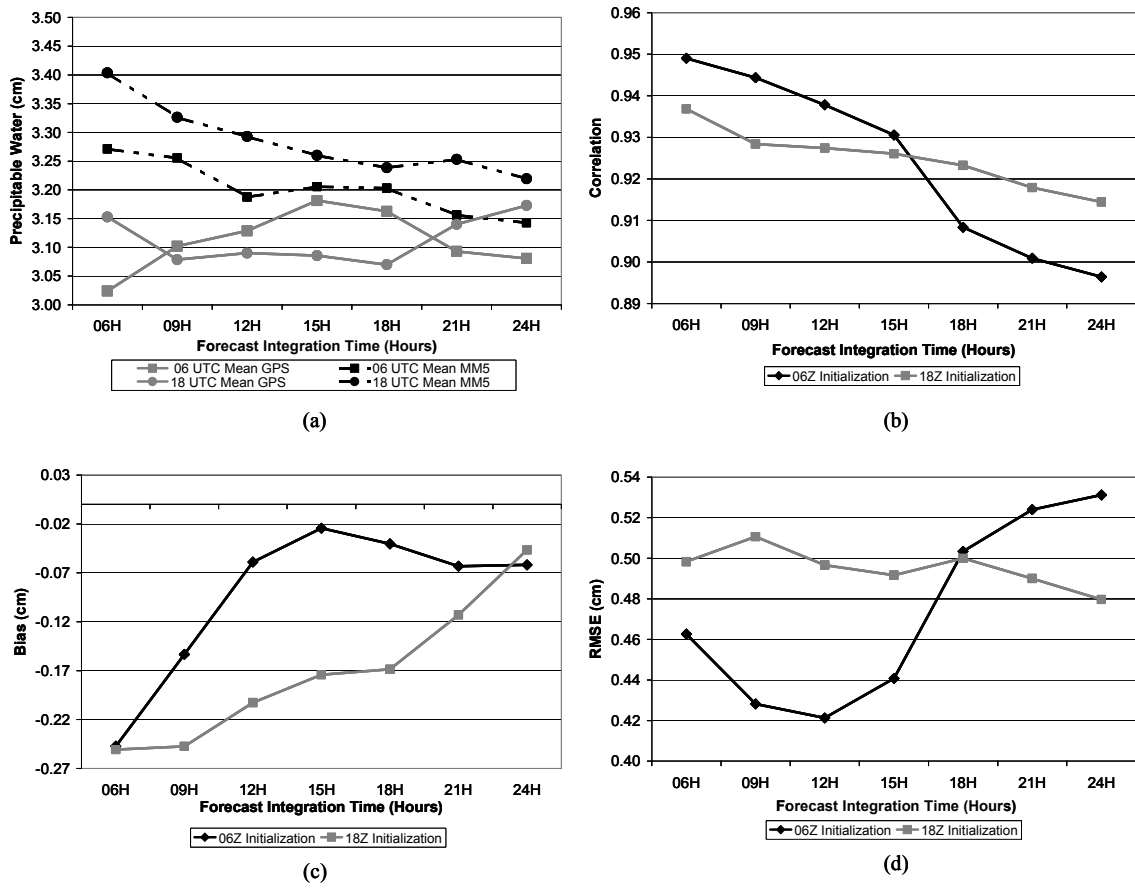


Figure 11. CONUS Domain-Wide Statistical Summaries. (a) Mean GPS-Derived PW and MM5 Calculated PW. (b) Correlation: GPS-Derived PW – MM5-Calculated PW. (c) Bias: GPS-Derived PW – MM5-Calculated PW. (d) RMSE of GPS-Derived PW – MM5-Calculated PW.

The highest correlations (Figure 11b) seemed to occur during the hours of sunlight, which could be attributed to the higher precipitable water content during the day. The crossover occurs just after local maximum heating in the 06 UTC initialization, and just before sunrise in the 18 UTC initialization. In addition, the local minima in bias (Figure 11c) seemed to occur during the day, as the hours approached that of maximum heating. However, in both cases, data noise must be taken into account as the forecast integration time progressed. Decreasing correlation and bias with forecast time is

expected, owing to the nature of numerical weather prediction: the further in the future one attempts to predict, the higher the error of the predictand.

The model's consistent moist bias (Figure 11c) arises from the nature of the moisture variables that are assimilated into the model. For the 06 UTC model run, drier moisture variables are entering the model, and that lack of moisture carries throughout. The converse is true with the 18 UTC model run. Figure 11a shows the model's lack of diurnal variation that the GPS-derived PW can provide.

RMSE in Figure 11d shows the same trends as correlation and bias. The highest values of GPS PW, which occurred during daylight hours, produced the least RMSE. The crossover occurred just after maximum heating in the 06 UTC run and just after minimum heating in the 18 UTC run.

**4.1.3 By-Location Summary Data.** Each forecast period for both initialization times was analyzed for each location in the CONUS GPS network. A thorough discussion of the 6-hour forecasts for both initialization times will be provided here; results for all forecast times are in Appendix C. Sections 4.1.2.1 and 4.1.2.2 discuss all locations' statistics, while Sections 4.1.2.3 and 4.1.2.4 review relationships that surfaced from analysis of these statistics.

**4.1.3.1 Summary statistics for the 06 UTC model initialization.** In this section, trends in comparisons between the GPS site and the MM5 output for each location will be reviewed. Figure 12 shows the mean correlation of each location's 06 hour forecast in the CONUS GPS network. Medicine Bow, Wyoming's (MBWW) low correlation stands out, but its low corresponding number of samples will explain the

anomaly. The mean correlation for all GPS receiver locations was 90.0%, while the mean correlation for locations with more than 10 samples was 91.5%.

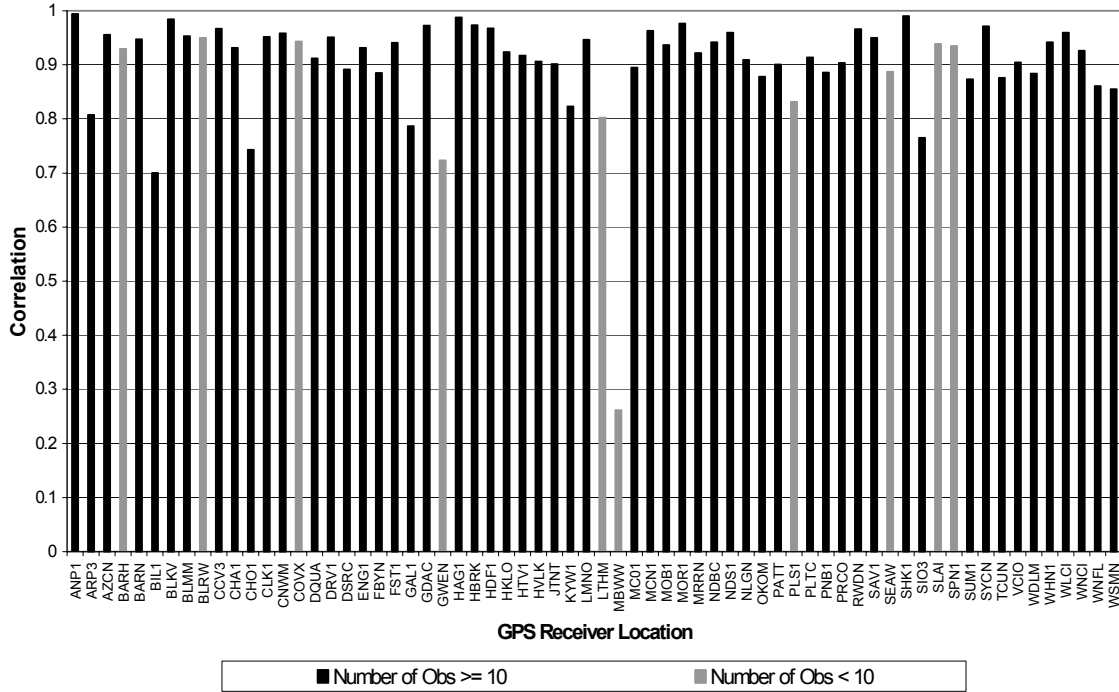


Figure 12. Mean Correlation of Each GPS Receiver Location: CONUS 06 UTC Initialization, 06-Hour Forecast. The locations with gray columns were calculated with less than 10 samples.

Figure 13 shows the mean bias at each location. As is seen in the domain-wide bias summary (Figure 11c), there was an overwhelming moist bias in the majority of the locations. It is interesting to point out that of the eleven sites with positive bias, nine of the sites are west of the Mississippi River. The dependence of the bias on the number of samples in each location calculation seems to be of minimal value in this case: the mean bias of all locations was  $-0.240$  cm, while the mean bias of only locations with more than 10 samples was  $-0.241$  cm. The western sites' drier model outputs most likely were the cause of a positive bias. Sites with a mean GPS PW reading of more than 4 cm had a

bias of  $-0.38$  cm, while those with mean PW readings of less than 2 cm had a bias of  $-0.19$  cm.

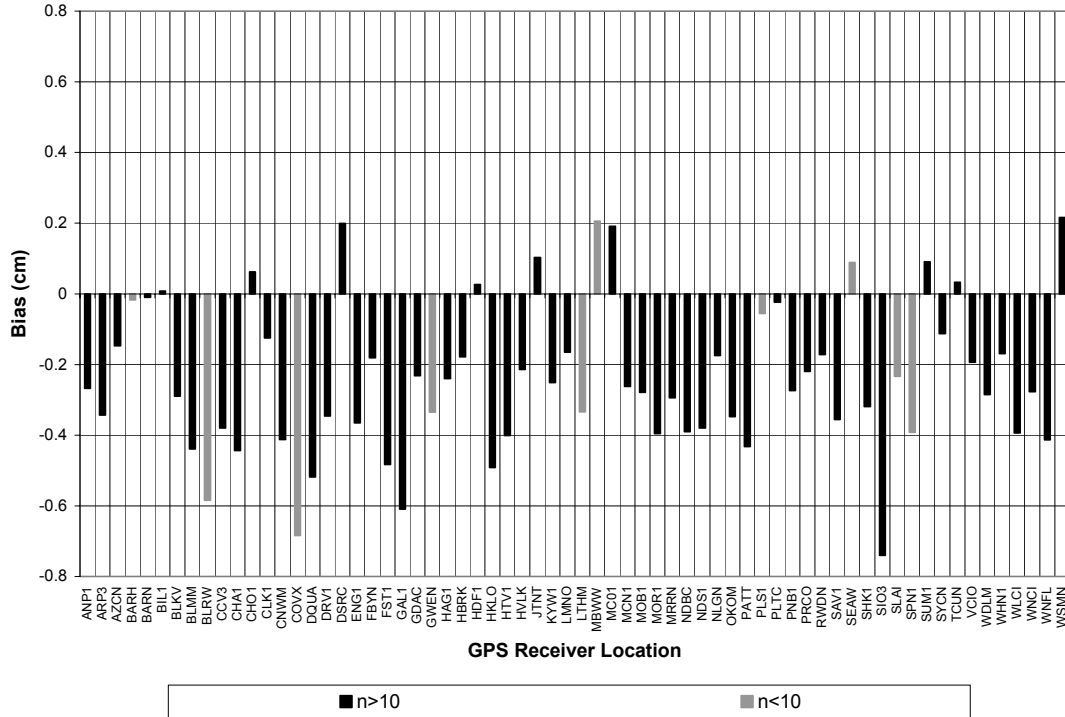


Figure 13. Mean Bias of Each GPS Receiver Location: CONUS 06 UTC Initialization, 06-Hour Forecast. The gray columns are locations that had less than 10 samples in the statistic's calculation. A negative bias signifies the model having more moisture than the GPS receiver site.

Figure 14 shows the RMSE expressed as a percentage of the location's mean GPS precipitable water value. This normalizes the environmental differences between arid (i.e., Arizona) and humid (i.e., Florida) regions throughout the domain. Like correlation and bias, most of the high RMSE locations also happen to have a low sample set. However, if we were to remove all low sample set sites, two sites still stand out as having high RMSEs, Flagstaff, AZ (FST1) and La Jolla, CA (SIO3). The mean normalized RMSE for all sites is 16.49% of the mean GPS PW value, while the mean for sites with more than 10 samples is 15.5%.

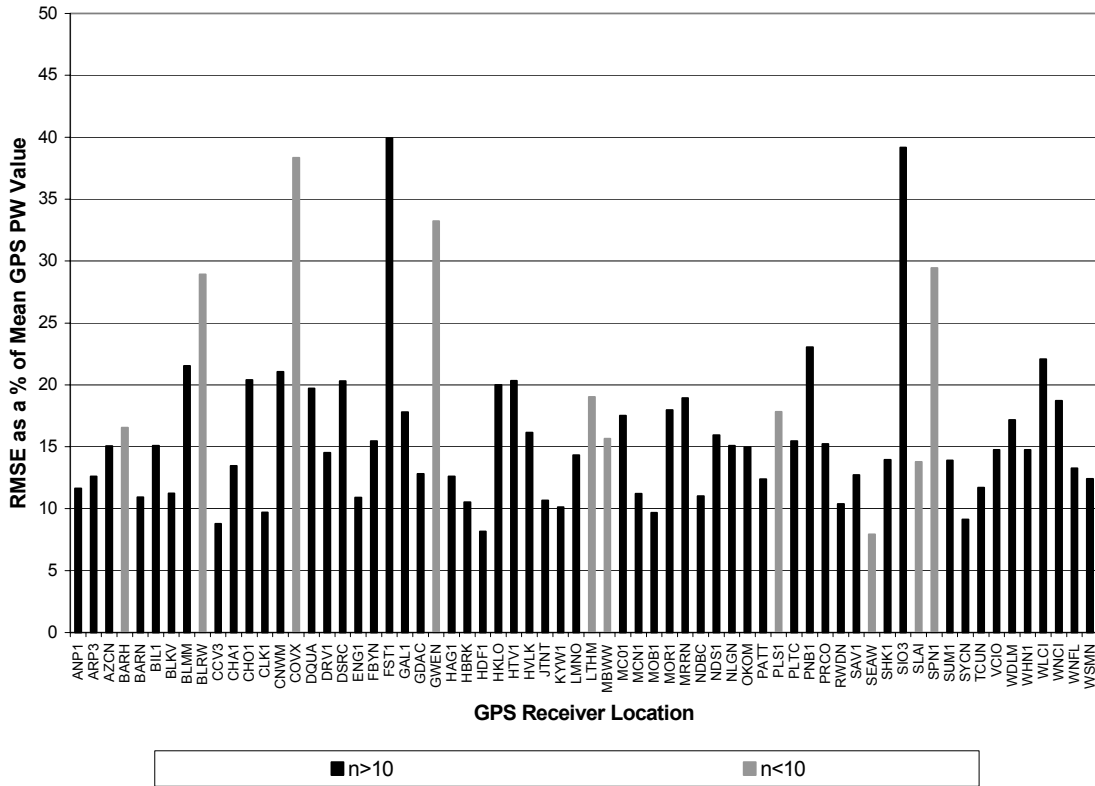


Figure 14. Mean Normalized RMSE of Each GPS Receiver Location: CONUS 06 UTC Initialization, 06 Hour Forecast. The value calculated as  $(RMSE/\text{mean GPS PW}) \times 100$ . The gray columns are locations that had less than 10 samples in the statistic's calculation.

Standard deviation as a percentage of mean GPS precipitable water is shown in Figure 15. Again, by considering those sites with less than 10 samples as questionable, many of the highest standard deviation-sites can be eliminated from the summary. Even if the low-sample sites are eliminated, La Jolla, CA (SIO3) remains as an anomalously high standard deviation. All GPS sites produced a mean normalized standard deviation of 12.37%, while the mean of sites with more than 10 samples was 11.8%.

**4.1.3.2 Summary statistics for the 18 UTC model initialization.** The 18 UTC model output was treated as a separate entity in this study to offset any diurnal differences between the twice-daily runs.

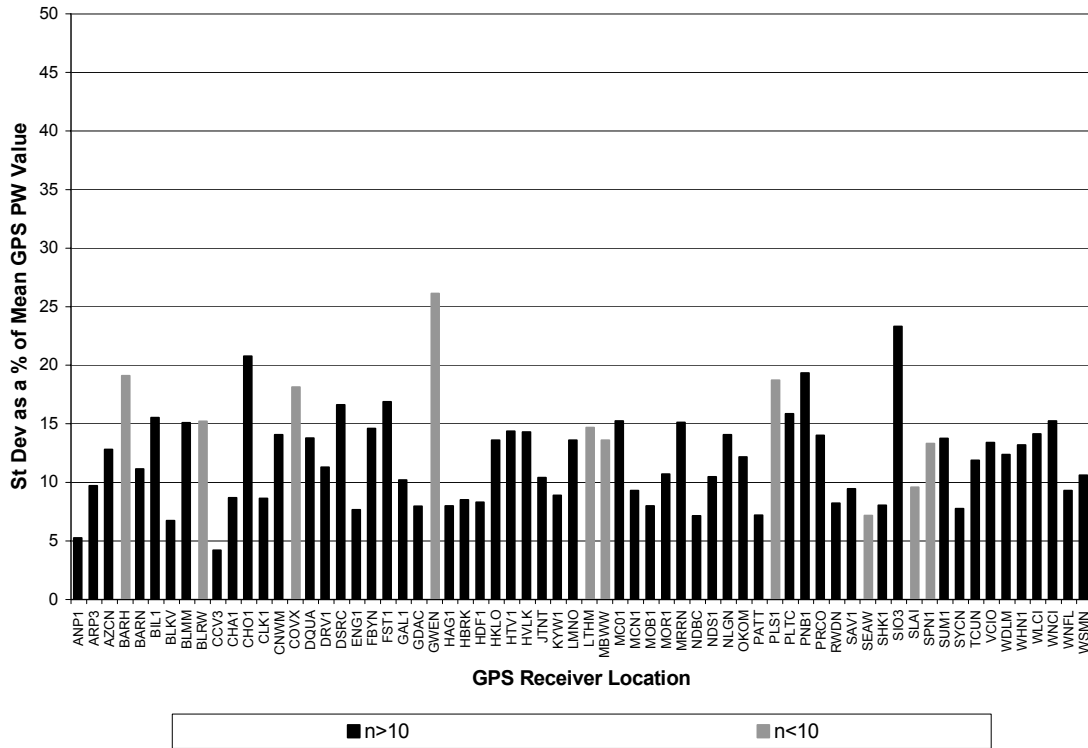


Figure 15. Mean Normalized Standard Deviation of Each GPS Receiver Location: CONUS 06 UTC Initialization, 06 Hour Forecast. The value is calculated as (standard deviation/mean GPS PW)\*100. The gray columns are locations that had less than 10 samples in the statistic's calculation.

Correlation at each of the GPS sites is shown in Figure 16. Again, the lowest correlations have less than 10 samples available for calculation, but Flagstaff, AZ (FST1) still has a low value. The mean correlation of all sites was 84.2%, while the mean correlation of all sites with more than 10 samples was 87.1%.

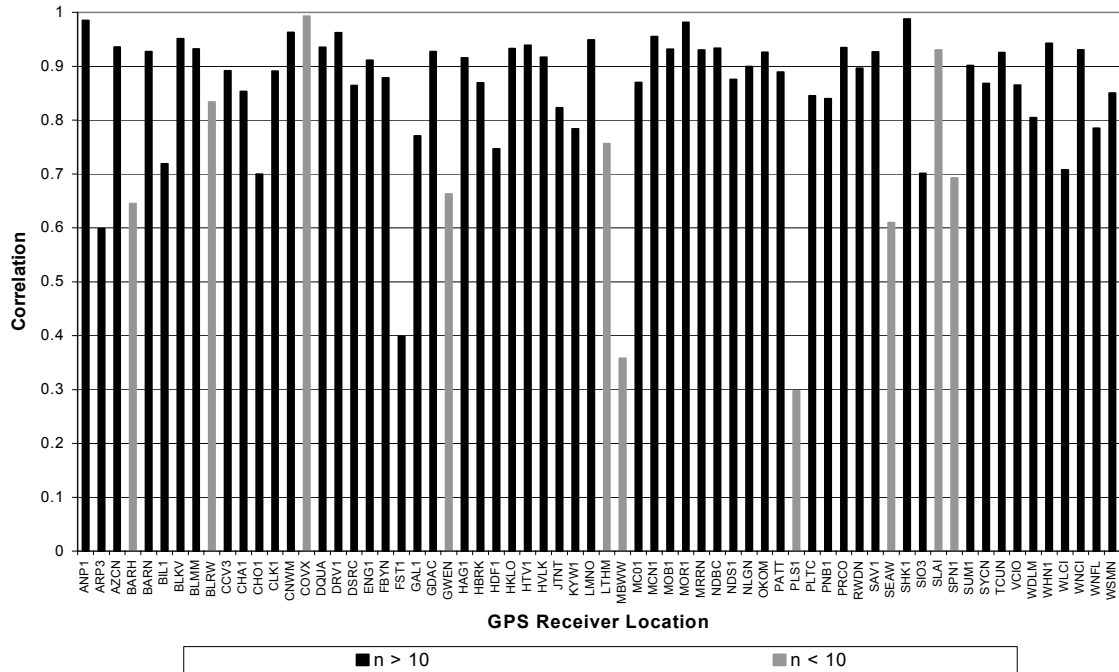


Figure 16. Mean Correlation of Each GPS Receiver Location: CONUS 18 UTC Initialization, 06-Hour Forecast. The locations with gray columns were calculated with less than 10 samples.

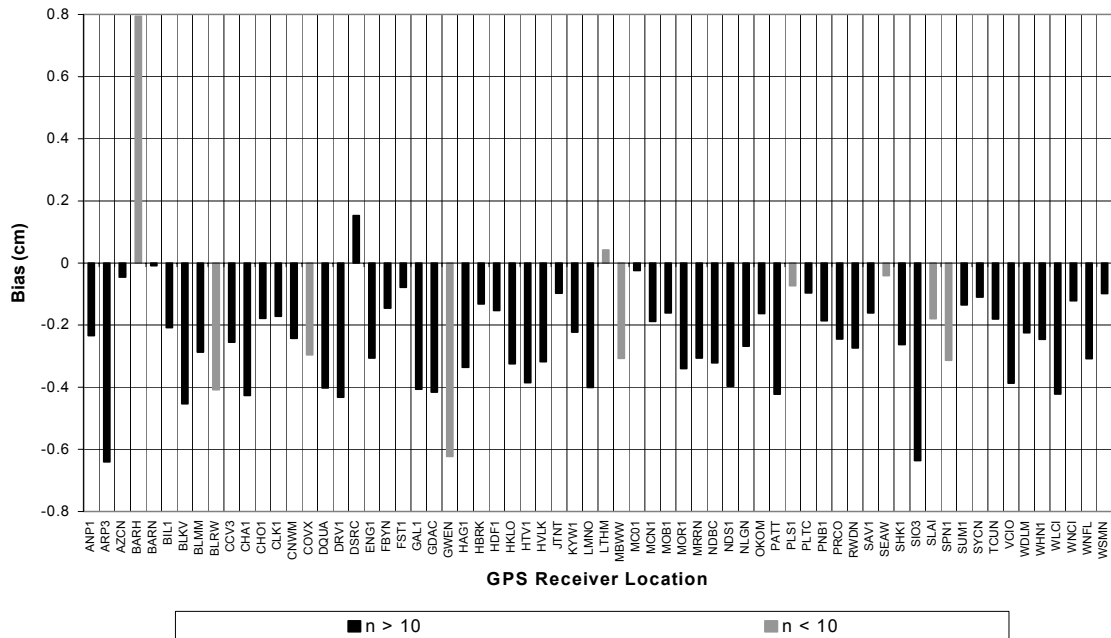


Figure 17. Mean Bias of Each GPS Receiver Location: CONUS 18 UTC Initialization, 06-Hour Forecast. The locations with gray columns were calculated with less than 10 samples. A negative bias signifies the model having more moisture than the GPS receiver site.



Figure 17 shows the mean bias for each GPS site. Like the 06 UTC model run, there are very few locations with positive bias. Two of the three positive bias locations had low samples, and the remaining site is Boulder, CO (DSRC), which is in a relatively arid location. The mean bias of all sites was  $-0.237$ , while the mean bias of sites with more than 10 samples was  $-0.255$ , more negative due to removing Bartlett, NH's (BARH) anomalous statistic.

Figure 18 shows the normalized mean RMSE for the 18 UTC model run. The anomalous sites with more than 10 samples were Chico, CA (CHO1), Flagstaff, AZ (FST1), La Jolla, CA (SIO3), and Wolcott, IN (WLCI). The mean normalized RMSE for all sites was 17.9%, while that for sites with more than 10 samples was 16.7%.

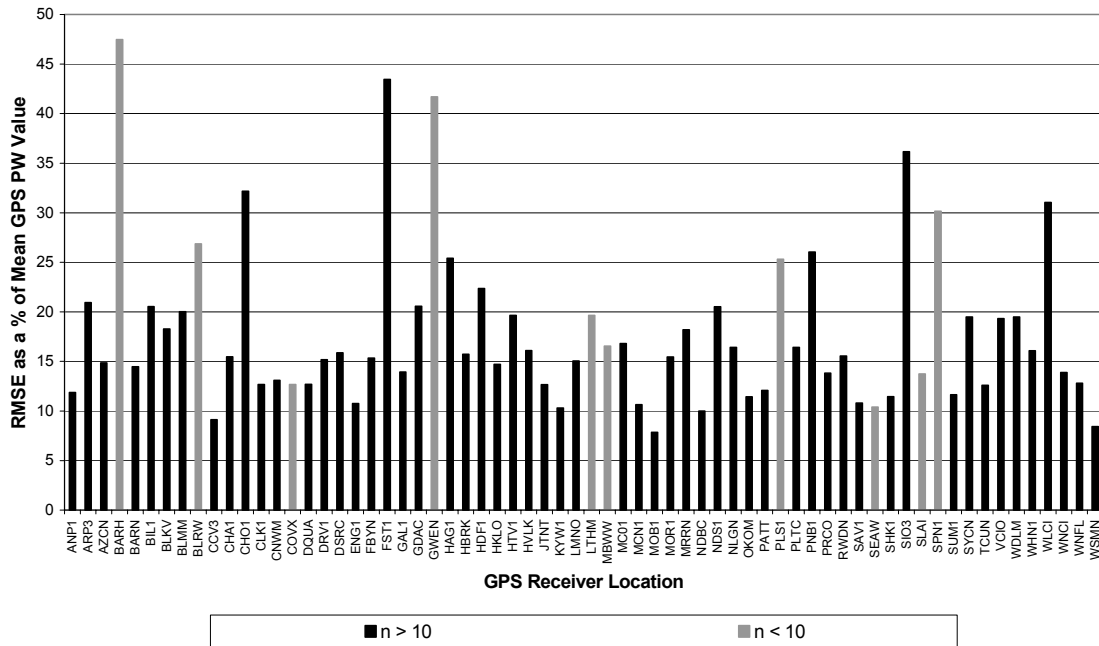


Figure 18. Mean Normalized RMSE of Each GPS Receiver Location: CONUS 18 UTC Initialization, 06-Hour Forecast. The value is calculated as  $(RMSE/mean\ GPS\ PW) * 100$ . The locations with gray columns were calculated with less than 10 samples.

The mean normalized standard deviation is shown in Figure 19. The mean normalized standard deviation for all sites was 15.16%, while those sites with more than 10 samples had a mean of 14.15%.

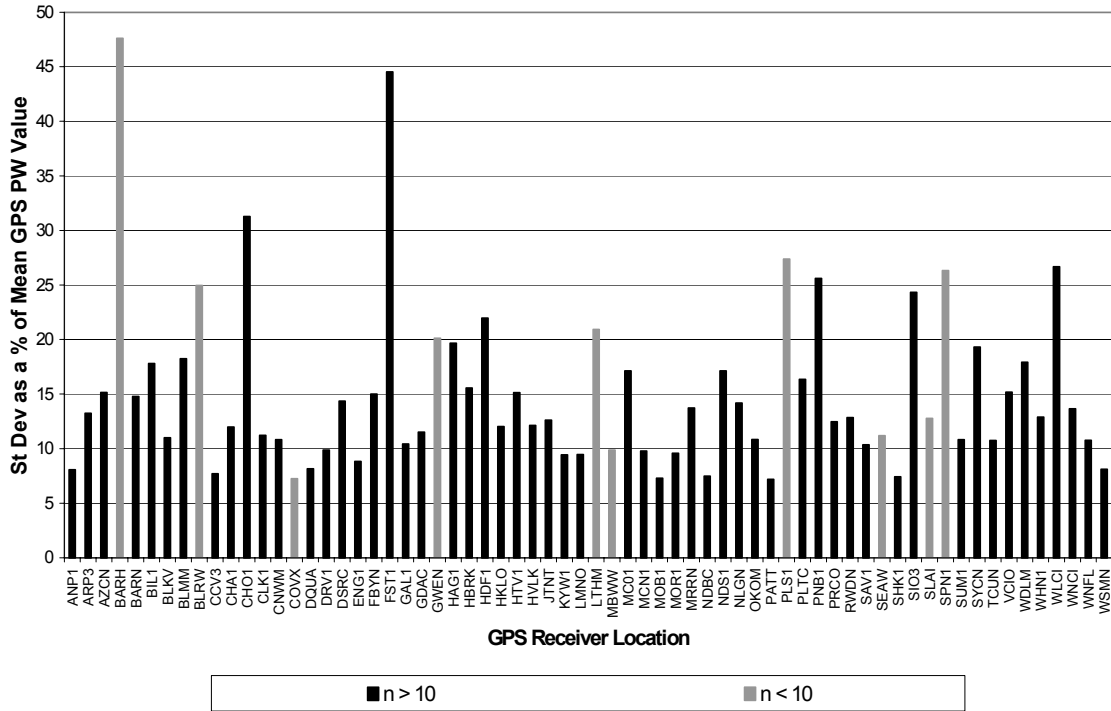


Figure 19. Mean Normalized Standard Deviation of Each GPS Receiver Location: CONUS 18 UTC Initialization, 06-Hour Forecast. The value is calculated as  $(\text{standard deviation}/\text{mean GPS PW}) \times 100$ . The locations with gray columns were calculated with less than 10 samples.

**4.1.3.3 Dependence on number of observations.** As evidenced by the previous two sections, many of the statistics were altered due to some locations having few GPS observations available. Figures 20 and 21 show the number of data points available for generating the statistics in Sections 4.1.2.1 and 4.1.2.2. The mean n for the calculations from the 06 UTC 06 hour forecasts was 18.4, while stripping the sites with less than 10 samples provided a mean n of 20.4. For the 18 UTC model run, the total mean n was 17.3, while the mean n of those sites with 10 or more samples was 19.3.

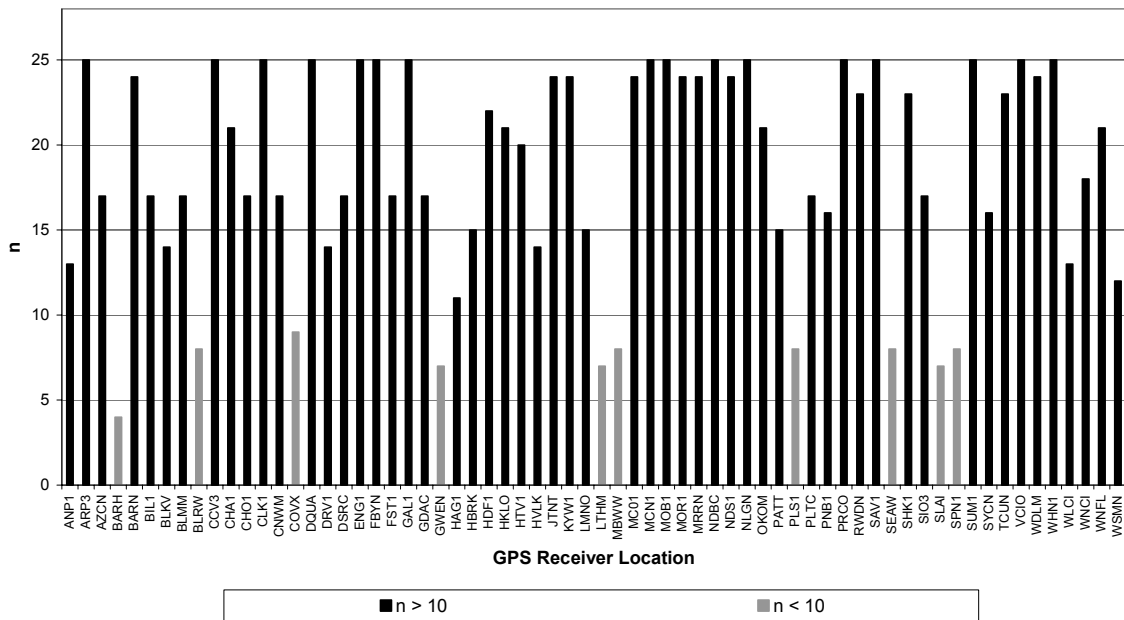


Figure 20. Number of Observations Available for Calculating the 06 UTC Initialization, 06 Hour Forecast Statistics.

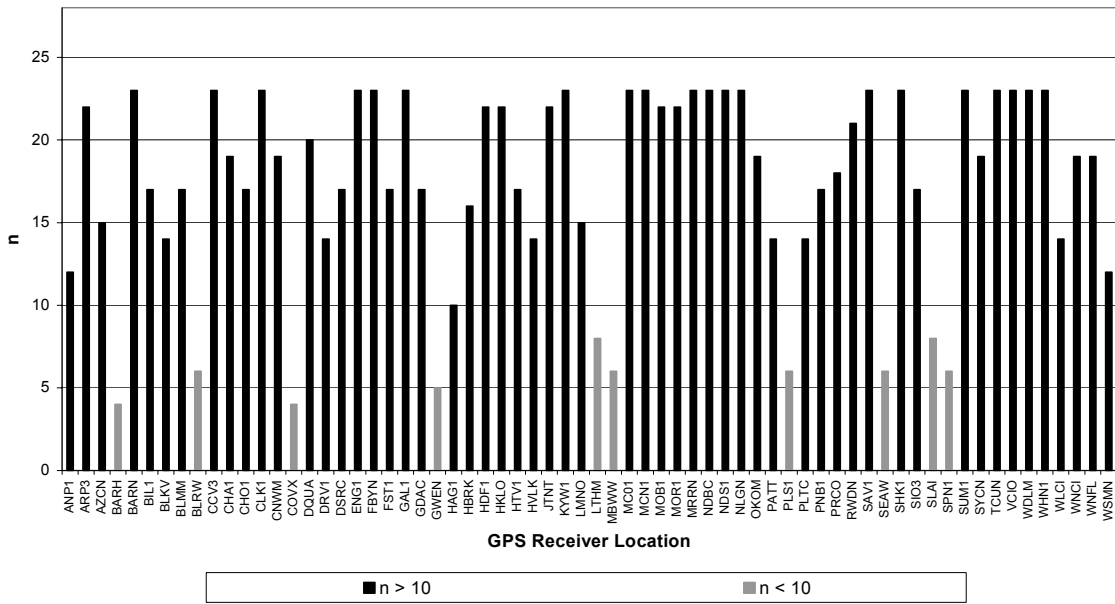


Figure 21. Number of Observations Available for Calculating the 18 UTC Initialization, 06 Hour Forecast Statistics.

#### 4.1.4 Special Studies.

**4.1.4.1 Moist vs. Dry Regimes.** The differences between moist regime and dry regime sites are shown here. The statistics were separated into those sites with mean GPS PW values greater than 4 cm, and those with mean GPS PW values of less than 2 cm. The 18 UTC initialization, 6 hour forecast is the only one reviewed here. Other date/time groups performed comparably. Figure 22 shows the increased error and noise attributed to the less humid GPS receiver sites, and how the MM5 depicts those moisture patterns.

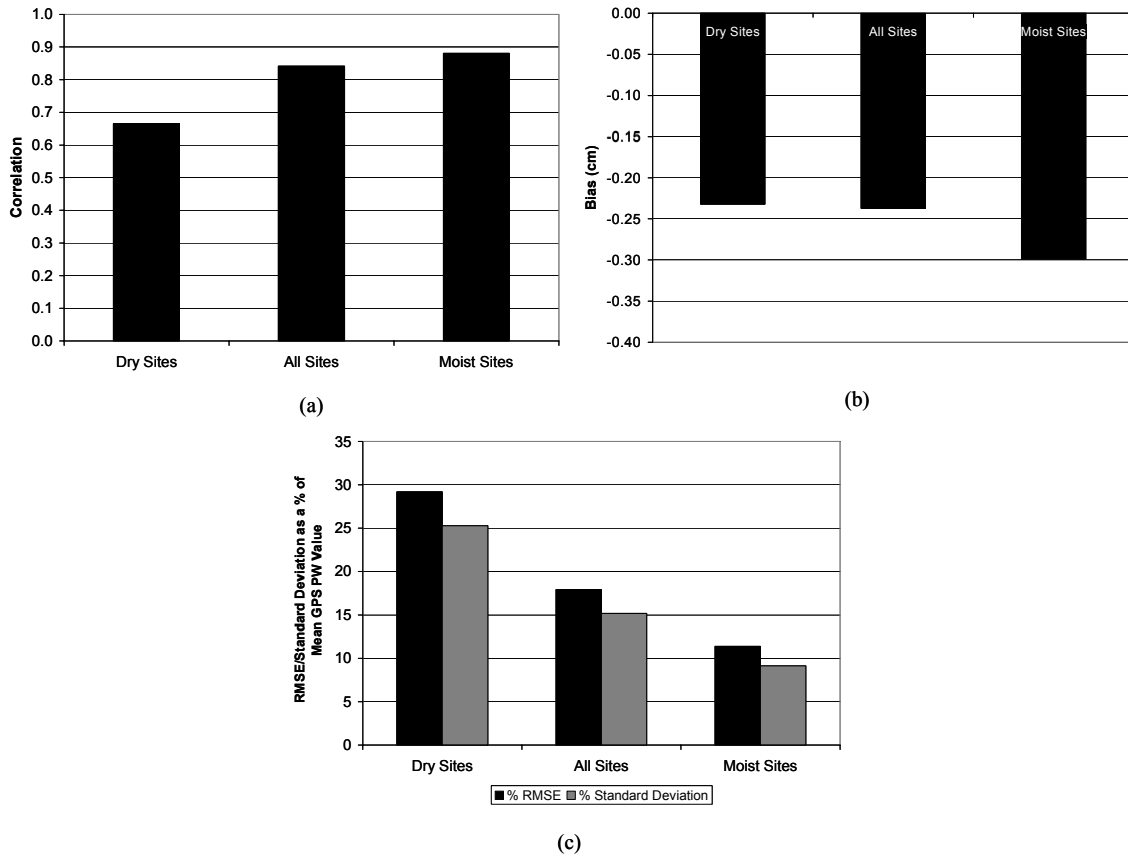


Figure 22. Moist Sites vs. Dry Sites Statistical Summaries: CONUS 18 UTC Initialization, 06 Hour Forecast. (a) Correlation (b) Mean Bias. Bias is defined as (GPS PW – MM5 PW) (c) Mean Normalized RMSE and Standard Deviation. RMSE calculated as  $(RMSE/mean\ GPS\ PW)*100$  and standard deviation calculated as  $(st\ dev/mean\ GPS\ PW)*100$ . Dry sites had a mean GPS PW values of less than 2 cm, while the moist sites had a mean GPS PW values of more than 4 cm.

**4.1.4.2 Error Dependence on Elevation and Elevation Residual.** One of

the sources of error in this study was the terrain height difference between each GPS site and its MM5-interpolated site elevation, based on the GRIB file’s terrain height parameter. In addition, the inverse proportion between site elevation and mean precipitable water had an impact on the statistics. The elevation values for each GPS receiver site are in Appendix A.

The mean normalized standard deviation for each site was plotted against the GPS site elevations and the difference between the GPS site elevation and the MM5 interpolated elevation. The expected relationship for this comparison was that the lower elevation sites, having more vertical atmosphere through which a GPS signal could refract, would have the highest standard deviation, and that the higher elevation sites would have smaller standard deviations, such that an inverse proportionality would exist.

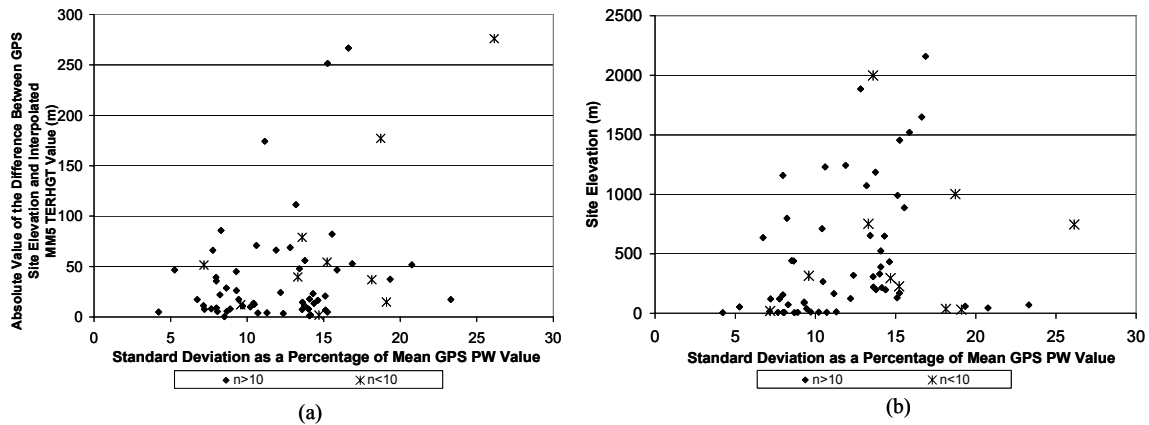


Figure 23. Elevation Comparisons: CONUS 06 UTC Initialization, 06 Hour Forecast. The diamonds are sites with  $n \geq 10$ , while the stars are sites with  $n < 10$ . (a) Mean Normalized Standard Deviation Plotted Against Absolute Value of Elevation Residual. (b) Mean Normalized Standard Deviation Plotted Against GPS Site Elevation.

Figure 23 shows the results of the two comparisons. Sites with less than 10 samples in the calculation were displayed in a different shape to highlight their positions on the chart. The expected relationship did not appear in these cases, but there are numerous other factors that could be clouding the expected relationship, such as model performance at high elevations.

The results seen in Figure 23 seemed to agree better with the comparison made in Section 4.1.3, that drier GPS sites had higher standard deviations than more humid sites. Most of the high-elevation GPS sites were in arid locations, to include Aztec, NM, Grand Junction, CO and Flagstaff, AZ.

**4.1.5 RAOB Comparison.** GPS sites within a prescribed distance of a RAOB site (as explained in Section 3.1.3) underwent additional analysis. The results are shown and discussed below.

Table 13. Summary of GPS-RAOB Comparisons in CONUS. Geodetic information about the RAOB sites is provided in Appendix C.

| RAOB Site | GPS ID | Mean GPS |        | Mean RAOB |        | Correlation |        | Bias    |        | %RMSE   |        | %StDev  |        | n  |
|-----------|--------|----------|--------|-----------|--------|-------------|--------|---------|--------|---------|--------|---------|--------|----|
|           |        | Coastal  | Inland | Coastal   | Inland | Coastal     | Inland | Coastal | Inland | Coastal | Inland | Coastal | Inland |    |
| CHS       | CHA1   | 4.30     |        | 4.66      |        | 0.97        |        | -0.37   |        | 10.11   |        | 5.46    |        | 49 |
| CRP       | ARP3   | 4.32     |        | 4.42      |        | 0.91        |        | -0.09   |        | 9.81    |        | 9.63    |        | 85 |
| DEN       | DSRC   |          | 1.80   |           | 1.88   |             | 0.95   |         | -0.08  |         | 12.16  |         | 11.30  | 85 |
| FLG       | FST1   |          | 1.30   |           | 1.54   |             | 0.98   |         | -0.23  |         | 19.93  |         | 8.97   | 64 |
| SGF       | CNWM   |          | 3.10   |           | 3.29   |             | 0.96   |         | -0.19  |         | 12.53  |         | 10.77  | 61 |
| SIL       | NDBC   | 4.27     |        | 4.49      |        | 0.98        |        | -0.21   |        | 7.49    |        | 5.63    |        | 88 |
| XMR       | CCV3   | 5.14     |        | 5.12      |        | 0.85        |        | 0.02    |        | 6.87    |        | 6.94    |        | 43 |
| Means     |        | 4.30     | 2.07   | 4.52      | 2.24   | 0.95        | 0.96   | -0.22   | -0.17  | 9.13    | 14.87  | 6.91    | 10.35  | 72 |

Table 13 shows the summaries of the GPS-RAOB comparisons. Note the differences between inland and coastal sites. All sites showed the radiosondes producing higher average PW measurements than the GPS receivers. A likely explanation for this

negative bias is the possibility of moisture loading when a radiosonde travels through a cloud or precipitation layer.

This study was conducted during the warmest and most humid of the year (July-September 2001). This impacts how high the PW readings can become, particularly along the coast. Another reason for such high radiosonde readouts is the coastal sites are all on the eastern coasts (either Atlantic or Gulf of Mexico), thus being susceptible to the prevailing westerly winds that would tend to send the radiosonde balloons over the water, perhaps to air with higher PW. In addition, it is appropriate to point out the differences in how GPS-derived PW is calculated compared to radiosonde PW, as detailed in Section 3.2.8. Recall that the GPS measurements infer PW from the refraction of the signal through the total atmosphere, while the RAOB is integrating layers of mean mixing ratio through the troposphere and perhaps part of the stratosphere. Figure 24 shows some statistics comparing inland and coastal sites. The statistics in this figure are calculated only from the sites listed in Table 13.

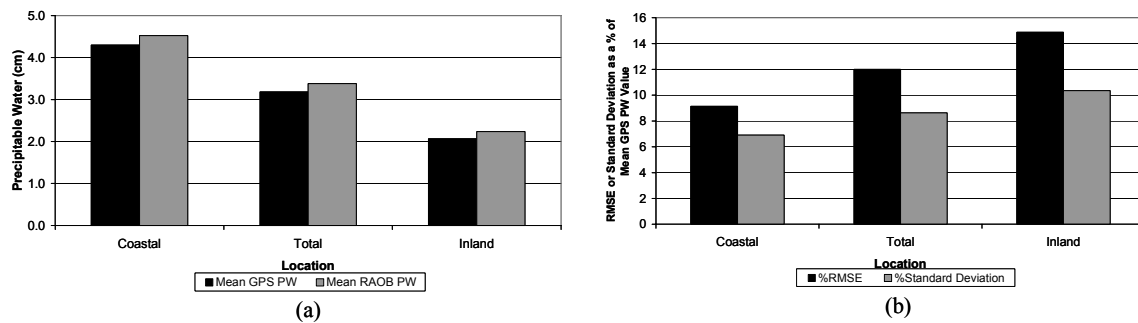


Figure 24. GPS/RAOB Coastal vs. Inland Statistical Summaries. (a) Mean GPS and RAOB PW Grouped by Region. (b) Mean Normalized RMSE and Standard Deviation. The RMSE is calculated as  $(\text{RMSE}/\text{mean GPS PW value}) \times 100$  and standard deviation is calculated as  $(\text{standard deviation}/\text{mean GPS PW value}) \times 100$ .

## 4.2 Alaska

**4.2.1 Case Study.** There was little choice in finding a time period for study in Alaska. The choices for which days to perform comparisons was restricted to the 90-day archive of MM5 GRIB data. During the period of time covered in AFIT's MM5 archive, there was only one 24-day window with GPS-MET observations encompassing all four Alaska GPS sites. At the other times, at least one of the receiver sites did not produce data. Therefore, the Alaska study took place from 6 – 29 July 2001. A number of extratropical cyclones still traversed the study area, bringing the variations in moisture that were desired for a good sample. Figure 25 shows a representative satellite image, with an extratropical cyclone moving across the state. During this period of study, a cyclone such as this one traversed the state approximately once a week. The satellite images available for this time period could only resolve the southern two-thirds of the state, but this didn't impact the quality of the study, for all four of the Alaska GPS receiver sites were in the southern two-thirds of the state.

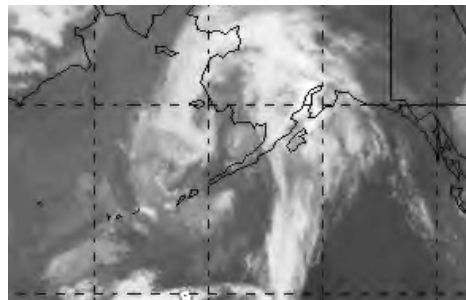


Figure 25. Representative Alaska IR Satellite Image from 12 UTC 19 July 2001. Image courtesy of NOAA (2001).

**4.2.2 Domain Summary.** Figure 26 shows the summaries of the domain-wide comparisons between the Alaska GPS-MET network and the 15 km Alaska MM5



window. The GPS observations were only those that were compared with MM5 data. If no MM5 data was available on a particular model run, then no GPS data was collected for that DTG.

Figure 26a shows the mean GPS PW and mean MM5 PW. The maximum seen in the GPS 12 UTC initialization occurs at 1800 Alaska Time, which is the estimated time of maximum heating. The minimum seen in the GPS 00 UTC initialization occurs just before local sunrise. Both crossovers occur just before their local sunset. Note the lack of diurnal variation in the MM5 lines. The diurnal variations are similar to what is seen in Figure 11 for CONUS.

It is important to point out that diurnal cycles are different in Alaska than in CONUS. In Fairbanks, sunrise in July was between 0213 (1 July) and 0349 (31 July) local time, while its sunsets ranged from 2335 (1 July) through 2203 (31 July). This resulted in a larger maximum in the mean GPS PW plot to accommodate for the longer period of heating. On these charts, sunrise occurred between the 12- and 15-hour forecasts on the 00 UTC initialization only. Sunsets were at the 09-hour forecast time on the 00 UTC line and the 21-hour forecast on the 12 UTC line. Like the CONUS scenario, the MM5 output doesn't seem to reflect the impacts of daily heating on its precipitable water values.

Figure 26b is the mean correlation of the Alaska domain, while Figure 26c shows the mean bias throughout the domain. The crossover between the 06- and 09-hour forecast occurs as the 00 UTC model run is about to experience sunset, while, at the same time, the 12 UTC model has experienced sunrise. The best correlation seemed to occur in the 00 UTC initialization, when maximum heating was *not* taken into account during

this time period. As is expected, the model run with the minimum of bias has the better correlation. The model had a dry bias in this theater, and the model's lack of diurnal variation resulted in a better-looking performance at the 00 UTC model run.

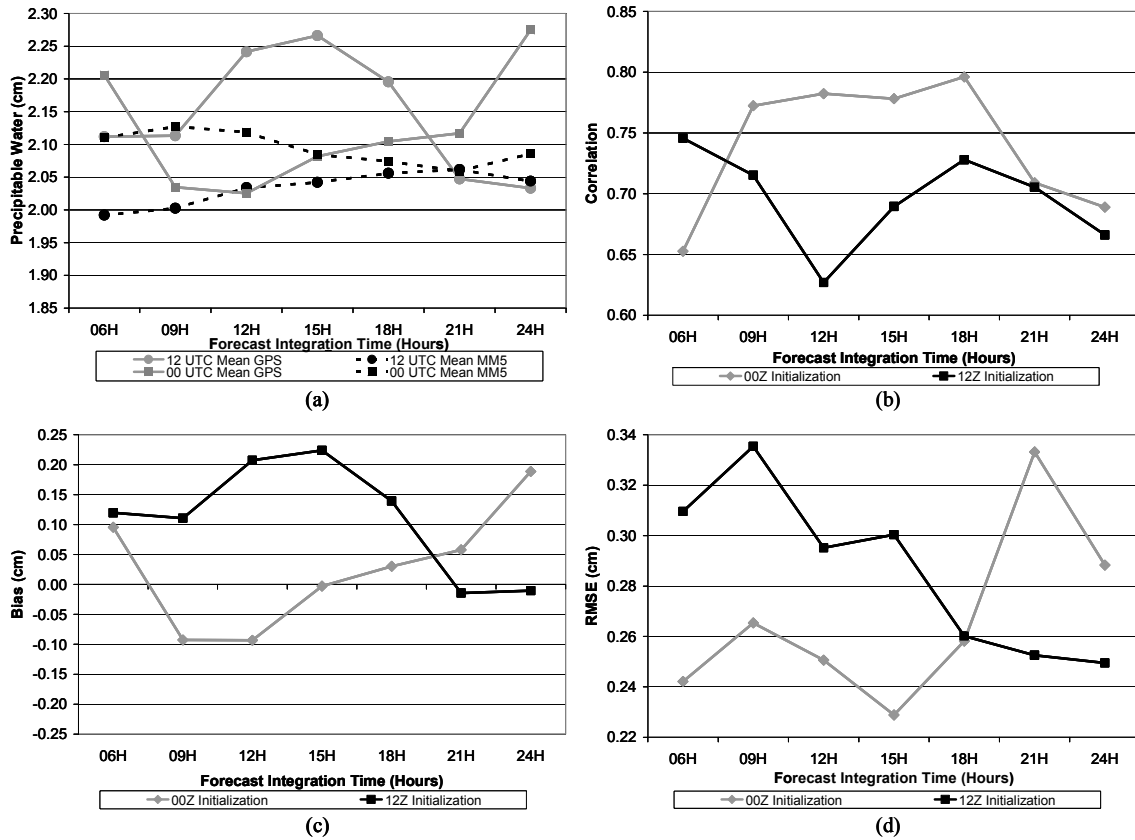


Figure 26. Alaska Domain-Wide Statistical Summaries. (a) Mean GPS-Derived and MM5-Calculated PW. (b) Correlation: GPS-Derived PW – MM5-Calculated PW (c) Bias: GPS-Derived PW – MM5-Calculated PW. (d) RMSE of GPS-Derived PW – MM5-Calculated PW.

Finally, Figure 26d shows the RMSE for the comparisons. Again, the errors seemed to be highest during the parts of the day with solar heating. The lowest errors occur at nighttime, between midnight and 0600L. It is unusual that the 12 UTC initialization's RMSE starts out lower at the 06-hour forecast, and then increases with

forecast integration time. This is again attributed to the onset of maximum heating as the forecast period progresses.

**4.2.3 By-Location Summary Data.** A clearer picture of the comparison can be seen looking at individual location data. The 06-hour forecasts for the 00 and 12 UTC model runs will be discussed here, while the complete data summaries are provided in Appendix C.

**4.2.3.1 Summary statistics for the 00 UTC model initialization.** In this section, trends in comparisons between the GPS site and the MM5 output for each location will be reviewed. In this theater, all locations averaged more than 10 observations, so no separate “low-n” statistics needed to be computed.

Figure 27a shows the mean correlation of the 00 UTC 06 hour forecast. All correlations were at least 80%, which is a desirable value. The mean correlation was 89%.

Figure 27b is the mean bias of each location. As was seen in the domain-wide data, most of this case study showed the model having a dry bias compared to the GPS network. This is corroborated here, showing only a minimal moist bias at the two northernmost sites, Central (CENA) and College (CLGO). The mean bias was 0.8 mm, with the GPS sites more moist than the MM5.

Figures 27c and 27d are the mean normalized RMSE and standard deviation for the Alaska locations. All of the sites performed well, with a mean normalized RMSE of 10.9%, and the mean normalized standard deviation of only 8.81%. College, AK, performed significantly better than the other three sites, bringing to light a concern about

the differences between the GPS sensors. The College GPS site is part of a sub-network independent of NOAA’s wind profiler network, which controls the other three GPS-MET sites in Alaska. The College sensor has a different antenna than the other three locations, a TRM33429.00 L1/L2 Micro Centered with Ground Plane, compared to the TRM22020 L1/L2 Compact with Ground Plane at the other three sites.

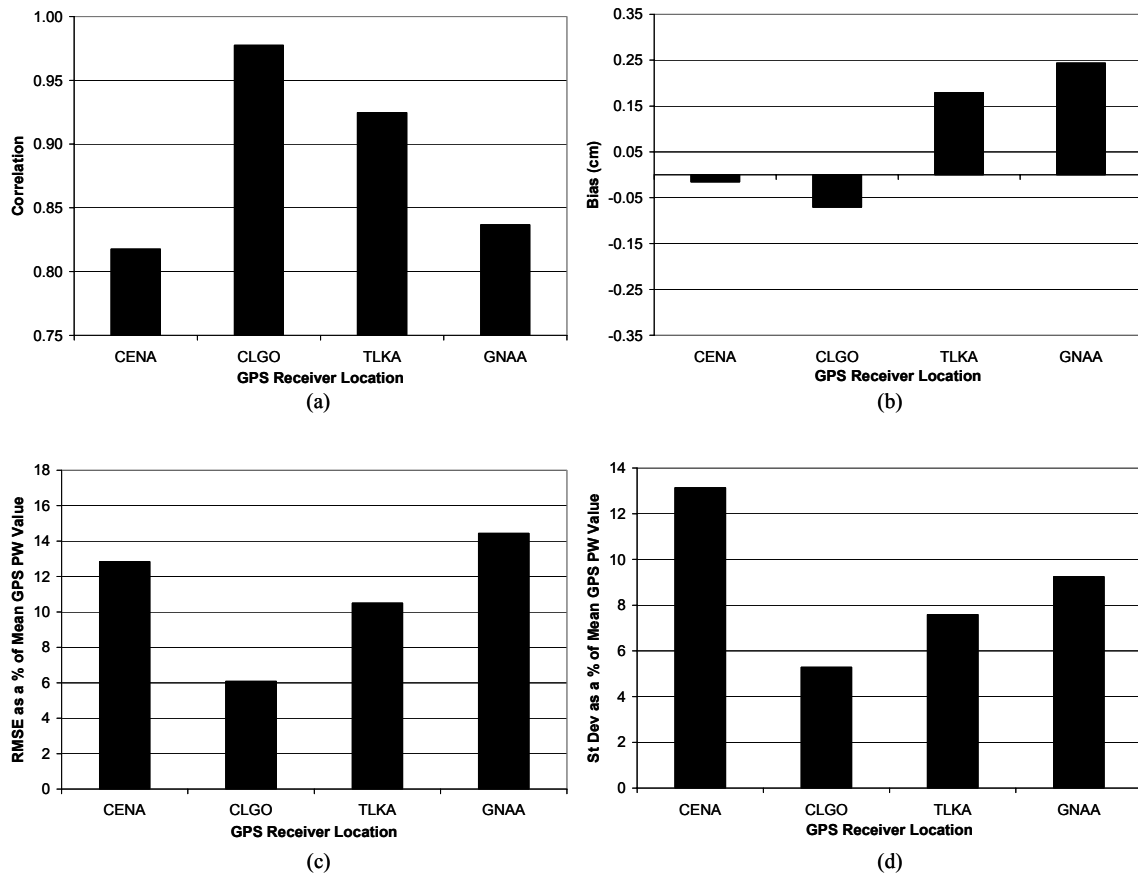


Figure 27. Alaska By-Location Statistical Summaries: 00 UTC Initialization, 06 Hour Forecast. (a) Mean Correlation. (b) Mean Bias. A negative bias signifies the model having more moisture than the GPS receiver site. (c) Mean Normalized RMSE. The value is calculated as  $(RMSE/mean\ GPS\ PW)*100$ . (d) Mean Normalized Standard Deviation. The value is calculated as  $(standard\ deviation/mean\ GPS\ PW)*100$ .

**4.2.3.2 Summary statistics for the 12 UTC model initialization.** In this

section, trends in comparisons from the 12 UTC model run will be reviewed.

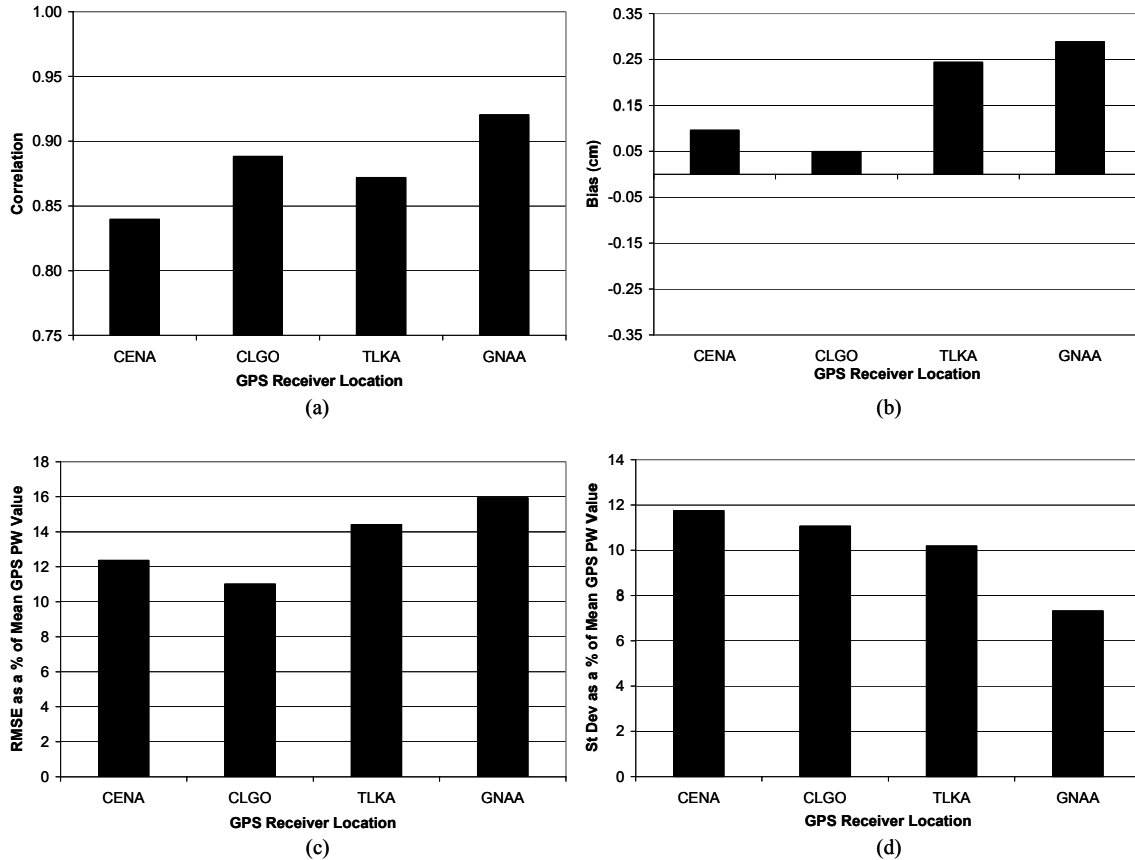


Figure 28. Alaska By-Location Statistical Summaries: 12 UTC Initialization, 06 Hour Forecast. (a) Mean Correlation. (b) Mean Bias. A negative bias signifies the model having more moisture than the GPS receiver site. (c) Mean Normalized RMSE. The value is calculated as  $(\text{RMSE}/\text{mean GPS PW value}) \times 100$ . (d) Mean Normalized Standard Deviation. The value is calculated as  $(\text{standard deviation}/\text{mean GPS PW}) \times 100$ .

Figure 28a shows the correlation between the GPS network observations and the model observations' 6 hour forecasts that were valid at the same time. All four sites showed reasonable correlations, with the mean of all sites being 88.01%. Figure 28b is the bias for the four locations. Note the distinct positive bias at all four locations, which coincided with the stronger positive bias on the 12 UTC forecast line in Figure 26c, the domain-wide mean bias. Talkeetna and Glenallen have the strongest biases, and it is of note that those two stations are the furthest south. The mean bias for all four sites is 1.69 mm.

Figure 28c shows the mean normalized RMSE for all four locations. As is the case with the bias, the southernmost two sites have the highest percentages of RMSE, with the mean through all four sites being 13.43%. The mean normalized standard deviation is shown in Figure 28d. In this case, the stations with the highest standard deviations, College and Central, have the smallest biases and RMSEs.

**4.2.4 RAOB Comparison.** In the Alaska theater, only one of the four GPS sites was near a RAOB site: College (CLGO) is 5.59 km away from the Fairbanks (FAI) radiosonde launch site. The raw radiosonde data was downloaded from the NOAA FSL RAOB site (<http://raob.fsl.noaa.gov>) and PW was computed using a NOAA algorithm. However, the algorithm, when computed on only the mandatory and significant levels that the web site provides, tends to overestimate the radiosonde PW values. This method of computation is different than how NOAA ordinarily computes PW. NOAA has the ability to use the balloon output that's transmitted every second, providing a much more robust database.

Thirty-seven soundings were evaluated with their respective GPS PW measurements and the summary statistics are shown in Table 14 below. Like in CONUS, the RAOB produced a higher average PW value, but in this case the differences are attributed to the errors inherent in computing the radiosonde PWs without using enough levels.

Table 14. Summary Statistics of Fairbanks GPS-PW and RAOB-PW Comparison.

| <b>Statistic</b>   | <b>Value</b> |
|--------------------|--------------|
| Mean GPS PW        | 2.07         |
| Mean RAOB PW       | 2.70         |
| Correlation        | 0.86         |
| Bias               | -0.63        |
| RMSE               | 0.50         |
| Standard Deviation | 0.33         |
| n                  | 37           |

## **V. Conclusions**

This study compared GPS-derived precipitable water with the AFWA MM5, in hopes of recommending future Air Force actions regarding the precipitable water data set. The potential impacts of the GPS PW on moisture forecasts provide much promise for assimilation into Air Force operational models, particularly when the 3DVAR assimilation system comes on line at AFWA. In addition, AFWA could also investigate placement of their own GPS-MET sensors in data sparse locations; the passive remote sensing capability would serve military operations well.

It is important to point out here that the results generated in this study were restricted to the summer season only, so they may not accurately represent other times of year. Also, the errors that did develop cannot be singly attributed to either shortcomings in the GPS observing network nor that of the MM5. These conclusions emphasize the quantitative differences between the two data sets and qualitative observations about the model and the GPS observing system.

The variations that were expected between the two theaters do exist, but it is not known which data set contributed more to the differences. It is likely that the MM5 physics packages, which are the same in both CONUS and Alaska, act differently in the two climate regimes.



The biases that originated from these comparisons were expected to have been the same order of magnitude as other independent comparisons between GPS networks and NWP models. This was found to be true in both CONUS and Alaska.

## **5.1 CONUS Conclusions**

**5.1.1 Domain-Wide Conclusions.** The GPS PW patterns demonstrate the significant diurnal variations that cannot be captured with the existing radiosonde network. The MM5 values performed comparably to the GPS PW at initialization times, but the MM5 does not account for the diurnal changes that occur; the lack of diurnal changes in the MM5 resulted in increased error as the forecast progressed.

The MM5 values were consistently more moist than what was measured with the GPS receivers. This could be attributed to the consistent moist bias the radiosondes seemed to have compared to the GPS network. In addition, the MM5's 18 UTC model run initialized with higher moisture than the 06 UTC run. However, the lack of diurnal variation in the MM5 moisture patterns resulted in consistently higher moisture values throughout the period.

Additionally, the 06 UTC model runs matched the GPS network better than did the 18 UTC runs. A possible reason for this is the higher GPS values in the first 15 hours of the 06 UTC forecast matching the consistently higher MM5 forecast outputs. Finally, in both model runs, the RMSE approached minimum values during the day's local peak heating, when the GPS PW values were the highest.

**5.1.2 By-Location Conclusions.** When assessing individual location trends, it is apparent how important it is to have a sufficient sample size to compute the statistics. Any statistics calculated with less than 10 observation-model pairs were taken out of the calculation and a separate statistic was made available for comparison.

Significant errors persisted in some locations despite removing those sites with less than 10 observations available. The trend in these sites is that most were in the western United States, and one site in particular was on the west coast. Western sites may have inherent model errors due to the lack of upstream initialization information.

A comparison was made with coastal versus non-coastal sites and the differences demonstrated the impact the high number of coastal sites has on the quality of the network when compared to the MM5. It is also of note that most of the coastal sites are Coast Guard/Army Corps of Engineers sites, which often have different models of GPS receivers and antennas than many of the inland sites. The coastal sites had higher errors and biases than the inland sites.

## **5.2 Alaska Conclusions**

**5.2.1 Domain-Wide Conclusions.** Alaska's GPS network consistently observed higher PW values than the MM5 output. In this case, the best correlations occurred during minima in heating. Alaska's summertime sunrise and sunset schedules created an interesting diurnal PW pattern. These caused longer heating periods and probably drove the GPS network's readings to be much higher than the MM5.

**5.2.2 By-Location Conclusions.** Two interesting points came out of the by-location analyses. First, the northern sites, College (CLGO) and Central (CENA) had a negative model bias in the 00 UTC model run, likely due to the model initializing right before local sunset, thus driving the GPS values lower than the MM5.

Secondly, the College (CLGO) GPS site performed markedly better than the other three sites. Two possibilities arise from this observation. One is that the CLGO antenna is a different model than the other three in Alaska. The other option is the terrain surrounding the stations having an impact on the prevailing localized weather patterns.

### **5.3 Recommendations for Future Work**

Three major areas require attention for future work: comparisons of GPS-derived PW from other networks with other AFWA MM5 global domains, assimilation of GPS-derived values into the MM5, and vertical profiling of GPS-derived moisture parameters.

Many other GPS-Meteorology networks exist worldwide for various research endeavors. Matching other AFWA MM5 domain windows with these GPS-MET networks allows many opportunities for additional data and comparisons. Examples of additional research areas include Japan, Taiwan, Southern Europe, and Scandinavia.

Secondly, the next logical step would be to assimilate the GPS-MET data into the operational MM5. Using the 3DVAR assimilation would aptly take advantage of the temporal availability of the GPS data. To do this would require intimate knowledge of the MM5 code and would work best in an advanced degree program with a numerical weather prediction emphasis.

Finally, it would serve well to investigate how to take the one-dimensional precipitable water values and derive a vertical profile, based on other thermodynamic variables. The other variables could be either observed through other sources or else inferred from the 3DVAR initialization. Vertical profiling of GPS-MET data with GOES sounder data is currently being researched and the results have been promising.

## Bibliography

- Applequist, Scott, AFWA/DNXM, Scientist, Mesoscale Modeling Branch, Offutt AFB, NE, Personal Correspondence, August 2001.
- Bevis, Michael, Steven Businger, Steven Chiswell, Thomas A. Herring, Richard A. Anthes, Christian Rocken, and Randolph H. Ware, 1994: GPS Meteorology: Mapping zenith wet delays onto precipitable water. *Journal of Applied Meteorology*, **33**, 379-386.
- Bevis, Michael, Steven Businger, Thomas A. Herring, Christian Rocken, Richard A. Anthes, and Randolph H. Ware, 1992: GPS Meteorology: Remote sensing of atmospheric water vapor using the Global Positioning System. *Journal of Geophysical Research*, **97**, No D14, 15,787-15,801.
- Borbas, E., 1998: Derivation of precipitable water from GPS data: an application to meteorology. *Physics and Chemistry of the Earth*, **23**, 87-90.
- Businger, Steven, Steven R. Chiswell, Michael Bevis, Jingping Duan, Richard A. Anthes, Christian Rocken, Randolph H. Ware, Michael Exner, T. VanHove, Fredrick S. Solheim, 1996: The promise of GPS in atmospheric monitoring. *Bulletin of the American Meteorological Society*, **77**, 5-18.
- Craig, Robert, AFWA/DNXM, *MM5 Model Physics*, 20 June 2000 [online article: <ftp://ws1-ftp.afwa.af.mil/pubs/aboutmm5/toc/physics/index.htm>].
- Cucurull, Lidia, Jordi Vila, Pepa Sedo and Antonia Rius, October 2001: MASS/MM5 meteorological model validation and data assimilation. *Meteorological Applications of GPS Integration Column Water Vapor Measurements in the Western Mediterranean Final Report*, Report to the European Commission, Document No. D01233, 72-84.
- Cucurull, L., B. Navascues, G. Ruffini, P. Elosegui, A. Rius and J. Vila, 2000: The use of GPS to validate NWP systems: The HIRLAM model. *Journal of Atmospheric and Oceanic Technology*, **17**, 773-787.
- Dana, Peter H., 1999: *The Geographer's Craft Project*, Department of Geography, The University of Colorado at Boulder [online web tutorial <http://www.colorado.edu/geography/gcraft/contents.html>.]
- De Ponte, Manuel S.F.V., Xiaolei Zou, 2001: A case study of the variational assimilation of GPS zenith delay observations into a mesoscale model. *Journal of Applied Meteorology*, **40**, 1559-1576.

- Department of Commerce, National Oceanic and Atmospheric Administration.  
*Precipitable Water Vapor Comparisons Using Various GPS Processing Technique*. Document No. 1203-GP-36, 28 August 1995.
- Emardson, T. Ragne and Henrico J.P. Derks, 2000: On the relation between the wet delay and the integrated precipitable water vapour in the European atmosphere. *Meteorological Applications*, **7**, 61-68.
- Glickman, Todd S., et al., 2000: *Glossary of Meteorology*. American Meteorological Society, 855 pp.
- Grell, G.A., J. Dudhia, and D. Stauffer, 1995: *A Description of the Fifth Generation Penn State/NCAR Mesoscale Model (MM5)*. NCAR Tech. Note TN-398+STR, 122 pp.
- Gutman, Seth I., Benjamin, Stanley G., 2001: The role of ground-based GPS meteorological observation in numerical weather prediction. *GPS Solutions*, **4**, 16-24.
- Hoffman-Wellenhof, B. and Herbert Lichtenegger, 1993: *GPS: Theory and Practice*. Springer-Verlag, 326 pp.
- Kopken, Christina, 2001: Validation of integrated water vapor from numerical models using ground-based GPS, SSM/I, and water vapor radiometer measurements. *Journal of Applied Meteorology*, **40**, 1105-1117.
- Kuo, Ying-Hwa, Yong-Run Guo, and Ed R. Westwater, 1993: Assimilation of precipitable water measurements into a mesoscale numerical model. *Monthly Weather Review*, **121**, 1215-1238.
- Leick, Alfred, 1990: *GPS Satellite Surveying*. John Wiley, 352 pp.
- Liou, Yuei-An, Yu-Tun Teng, T. Van Hove, J. Liljegren, 2001: Comparison of precipitable water observations in the near tropics by GPS, microwave radiometer, and radiosondes. *Journal of Applied Meteorology*, **40**, 5-15.
- National Aeronautics and Space Administration, Jet Propulsion Laboratory, *International GPS Service Data and Products*, May 2001, [online article: <http://igsceb.jpl.nasa.gov/components/prods.html>].
- National Oceanic and Atmospheric Administration, National Climatic Data Center, *NEXRAD National Mosaic Reflectivity Image Database*, 2002, [online: <http://lwf.ncdc.noaa.gov/oa/ncdc.html>].

- Niell, A.E., A.J. Coster, F.S. Solheim, V.B. Mendes, P.C. Toor, R.B. Langley, and C.A. Upham, 2001: Comparison of measurements of atmospheric wet delay by radiosonde, water vapor radiometer, GPS and VLBI. *Journal of Atmospheric and Oceanic Technology*, **18**, 830-850.
- Ritz, Richard L., Michael D. McAtee, Robert T. Swanson, Jr., July 2001: Data assimilation at the Air Force Weather Agency. Preprint Volume, *14<sup>th</sup> Conference on Numerical Weather Prediction*.
- Saastamoinen, J., 1972: Atmospheric correction for the troposphere and stratosphere in radio ranging of satellites. *The Use of Artificial Satellites for Geodesy, Geophysical Monograph Series*, **15**, 247-251.
- Smith, Bruce A., 30 July 2001: Boeing Satellite Systems to Build GPS Block 2F. *Aviation Week and Space Technology*, **155**, 30.
- Smith, Tracy, Stanley G. Benjamin, Barry E. Schwartz, and Seth I. Gutman, 2000: Using GPS-IPW in a 4-D data assimilation system. *Earth Planets Space*, **52**, 921-926.
- Swanson, Robert T., AFWA/DNXT, Chief, Technology Transition Branch, Offutt AFB, NE, Personal Correspondence, October 2001.
- Trimble Navigation Inc., *How GPS Works*, [online tutorial, <http://www.trimble.com/gps>], 1996.
- Ware, Randolph H., David W. Fulker, Seth A. Stein, David N. Anderson, Susan K. Avery, Richard D. Clark, Kelvin K. Droegemeier, Joachim P. Kuettnner, J. Bernard Minster, and Soroosh Sorooshian, 2000: SuomiNet: A real-time national GPS network for atmospheric research and education. *Bulletin of the American Meteorological Society*, **81**, 677-693.
- Wilks, Daniel S., 1995: *Statistical Methods in the Atmospheric Sciences*. Academic Press, 467 pp.
- Wolfe, Daniel E., Seth I. Gutman, 2000: Developing an operational, surface-based, GPS, water vapor observing system for NOAA: Network design and results. *Journal of Atmospheric and Oceanic Technology*, **17**, 426-440.
- Yang, Xiaohua, Bent H. Sass, Gunnar Elgered, Jan M. Johansson, T. Ragne Emardson, 1999: A comparison of precipitable water vapor estimates by an NWP simulation and GPS observations. *Journal of Applied Meteorology*, **38**, 941-956.

## Appendix A: Geodetic Information

This data is provided to give the reader detailed information about the locations, elevations and model positioning for each of the GPS-MET sites and their nearby RAOB sites (if a RAOB site is within range). The MM5 IX and MM5 JX columns are the grid positions on the AFWA 15 km MM5 grid and are used to assist in grid-to-station interpolation. Table A-1 is the CONUS geodetic information, while Table A-2 is Alaska's information.

Table A-1. CONUS Geodetic Information

| ID   | Location             | Latitude | Longitude | MM5 IX | MM5 JX | GPS Receiver Elevation (m) | MM5 Interpolated Elevation (m) | MM5-GPS dz (m) | RAOB | RAOB dx (m) | RAOB-GPS dz (m) |
|------|----------------------|----------|-----------|--------|--------|----------------------------|--------------------------------|----------------|------|-------------|-----------------|
| ANP1 | Annapolis, MD        | 39.01    | -76.61    | 297    | 120.2  | 53                         | 6.24                           | 46.7569        |      |             |                 |
| ARP3 | Aransas Pass, TX     | 27.84    | -97.06    | 182.5  | 25.32  | 11                         | 0                              | 11             | CRP  | 44.01       | 3               |
| AZCN | Aztec, NM            | 36.84    | -107.91   | 120.8  | 96.54  | 1885                       | 1816.17                        | 68.8204        |      |             |                 |
| BARH | Bar Harbor, ME       | 44.40    | -68.22    | 328.8  | 170.2  | 31                         | 16.12                          | 14.8733        |      |             |                 |
| BARN | Bartlett, NH         | 44.10    | -71.16    | 315.2  | 163.3  | 165                        | 339.19                         | -174.198       |      |             |                 |
| BIL1 | Billings, MT         | 45.97    | -108.00   | 130.1  | 161.5  | 887                        | 969.19                         | -82.1951       |      |             |                 |
| BLKV | Blacksburg, VA       | 37.20    | -80.41    | 278.8  | 102.7  | 636                        | 653.26                         | -17.267        |      |             |                 |
| BLMM | Bloomfield, MO       | 36.88    | -89.97    | 224.4  | 93.02  | 130                        | 109.08                         | 20.9145        |      |             |                 |
| BLRW | Blue River, WI       | 43.22    | -90.53    | 218.1  | 138.3  | 226                        | 280.42                         | -54.4268       |      |             |                 |
| CCV3 | Cape Canaveral, FL   | 28.46    | -80.55    | 290.3  | 39.66  | 5                          | 0                              | 5              | XMR  | 2.23        | 0               |
| CHA1 | Charleston, SC       | 32.76    | -79.84    | 288.5  | 71.72  | 6                          | 0.26                           | 5.7305         | CHS  | 23.63       | 9               |
| CHO1 | Chico, CA            | 39.43    | -121.66   | 49.28  | 132.8  | 45                         | 96.61                          | -51.6135       |      |             |                 |
| CLK1 | Clark, SD            | 44.93    | -97.96    | 179.6  | 149.7  | 440                        | 468.63                         | -28.6326       |      |             |                 |
| CNWM | Conway, MO           | 37.52    | -92.70    | 208.4  | 96.72  | 390                        | 388.60                         | 1.3908         | SGF  | 69.82       | 4               |
| COVX | Chesapeake Light, VA | 36.90    | -75.71    | 305.7  | 106.7  | 37                         | 0                              | 37             |      |             |                 |
| DQUA | Dequeen, AR          | 34.11    | -94.29    | 199.9  | 71.69  | 199                        | 143.04                         | 55.9553        |      |             |                 |
| DRV1 | Driver, VA           | 36.96    | -76.56    | 300.9  | 105.9  | 13                         | 8.88                           | 4.1195         |      |             |                 |
| DSRC | Boulder, CO          | 39.99    | -105.26   | 138.6  | 117.1  | 1649                       | 1915.70                        | -266.702       | DEN  | 40.66       | -38             |
| ENGI | English Turn, LA     | 29.88    | -89.94    | 228.5  | 41.95  | 9                          | 0.78                           | 8.2178         |      |             |                 |
| FBYN | Fairbury, NE         | 40.08    | -97.31    | 182.3  | 114.8  | 433                        | 449.53                         | -16.5334       |      |             |                 |
| FST1 | Flagstaff, AZ        | 35.22    | -111.82   | 96.16  | 88.92  | 2159                       | 2211.78                        | -52.7822       | FLG  | 1.11        | 20              |
| GAL1 | Galveston, TX        | 29.33    | -94.74    | 197.7  | 36.45  | 10                         | 0                              | 10             |      |             |                 |
| GDAC | Granada, CO          | 37.78    | -102.18   | 154.3  | 99.57  | 1159                       | 1119.58                        | 39.4105        |      |             |                 |
| GWEN | Appleton, WA         | 45.78    | -121.33   | 65.19  | 175.5  | 746                        | 470.05                         | 275.9499       |      |             |                 |
| HAG1 | Hagerstown, MD       | 39.55    | -77.71    | 290.2  | 122.5  | 155                        | 190.75                         | -35.7526       |      |             |                 |
| HBRK | Hillsboro, KS        | 38.30    | -97.29    | 182.2  | 102    | 443                        | 442.67                         | 0.3285         |      |             |                 |
| HDF1 | Hudson Falls, NY     | 43.27    | -73.54    | 305.2  | 154    | 72                         | 157.94                         | -85.9444       |      |             |                 |
| HKLO | Haskell, OK          | 35.68    | -95.86    | 190.4  | 83.01  | 221                        | 206.32                         | 14.681         |      |             |                 |
| HTV1 | Hartsville, TN       | 36.36    | -86.09    | 247.2  | 91.51  | 198                        | 211.47                         | -13.4706       |      |             |                 |
| HVLK | Haviland, KS         | 38.30    | -99.11    | 171.9  | 102.3  | 648                        | 624.85                         | 23.1503        |      |             |                 |
| JTNT | Jayton, TX           | 33.02    | -100.98   | 159    | 64.56  | 711                        | 724.64                         | -13.6392       |      |             |                 |
| KYW1 | Key West, FL         | 24.58    | -81.65    | 288.4  | 9.54   | 8                          | 0                              | 8              |      |             |                 |
| LMNO | Lamont, OK           | 36.69    | -97.48    | 180.9  | 90.41  | 308                        | 315.52                         | -7.5227        |      |             |                 |
| LTHM | Lathrop, MO          | 39.58    | -94.17    | 199.7  | 111.3  | 295                        | 293.18                         | 1.8147         |      |             |                 |
| MBWW | Medicine Bow, WY     | 41.90    | -106.19   | 135.3  | 131.3  | 1999                       | 2078.07                        | -79.0701       |      |             |                 |
| MC01 | Grand Junction, CO   | 39.09    | -108.53   | 119.8  | 113.1  | 1454                       | 1705.46                        | -251.458       |      |             |                 |
| MCN1 | Macon, GA            | 32.70    | -83.56    | 266    | 67.21  | 88                         | 114.17                         | -26.1736       |      |             |                 |
| MOB1 | Mobile Point, AL     | 30.23    | -88.02    | 240.5  | 45.61  | 9                          | 0                              | 9              |      |             |                 |
| MOR1 | Moriches, NY         | 40.79    | -72.75    | 314.2  | 138.1  | 8                          | 3.99                           | 4.0127         |      |             |                 |



## Appendix A: Geodetic Information

Table A-1 (continued): CONUS Geodetic Information

| ID   | Location             | Latitude | Longitude | MM5 IX | MM5 JX | GPS Receiver Elevation (m) | MM5 Interpolated Elevation (m) | MM5-GPS dz (m) | RAOB | RAOB dx (m) | RAOB-GPS dz (m) |
|------|----------------------|----------|-----------|--------|--------|----------------------------|--------------------------------|----------------|------|-------------|-----------------|
| MRRN | Merriman, NE         | 42.90    | -101.70   | 159.6  | 136.1  | 991                        | 997.79                         | -6.7922        |      |             |                 |
| NDBC | Stennis, MS          | 30.36    | -89.61    | 230.3  | 45.66  | 16                         | 4.71                           | 11.2897        | SIL  | 20.45       | -8              |
| NDS1 | Neodesha, KS         | 37.30    | -95.60    | 191.8  | 94.75  | 266                        | 253.50                         | 12.4971        |      |             |                 |
| NLGN | Neligh, NE           | 42.21    | -97.80    | 180    | 130.2  | 525                        | 542.78                         | -17.7815       |      |             |                 |
| OKOM | Okolona, MS          | 34.08    | -88.86    | 232.6  | 73.28  | 125                        | 100.58                         | 24.4151        |      |             |                 |
| PATT | Palestine, TX        | 31.78    | -95.72    | 191.3  | 54.51  | 121                        | 113.27                         | 7.7337         |      |             |                 |
| PLS1 | Polson, MT           | 47.66    | -114.11   | 102.9  | 178.9  | 1002                       | 1179.05                        | -177.053       |      |             |                 |
| PLTC | Platteville, CO      | 40.18    | -104.73   | 141.7  | 118.1  | 1521                       | 1474.26                        | 46.7418        |      |             |                 |
| PNB1 | Penobscot, ME        | 44.45    | -68.77    | 326    | 169.6  | 59                         | 21.40                          | 37.5984        |      |             |                 |
| PRCO | Purcell, OK          | 34.98    | -97.52    | 180.5  | 78     | 331                        | 339.06                         | -8.0615        |      |             |                 |
| RWDN | Mccook, NE           | 40.09    | -100.65   | 164    | 115.6  | 799                        | 820.98                         | -21.9778       |      |             |                 |
| SAV1 | Savannah, GA         | 32.14    | -81.70    | 278    | 65.08  | 40                         | 22.42                          | 17.5801        |      |             |                 |
| SEAW | Seattle WFO, WA      | 47.69    | -122.26   | 65.19  | 189.9  | 20                         | 71.47                          | -51.4691       |      |             |                 |
| SHK1 | Sandy Hook, NJ       | 40.47    | -74.01    | 308.2  | 134    | 9                          | 3.44                           | 5.559          |      |             |                 |
| SIO3 | Scripps/La Jolla, CA | 32.86    | -117.25   | 60.25  | 79.69  | 71                         | 53.60                          | 17.4031        |      |             |                 |
| SLAI | Slater, IA           | 41.90    | -93.69    | 201.9  | 128    | 315                        | 302.78                         | 12.2155        |      |             |                 |
| SPN1 | Spokane, WA          | 47.52    | -117.52   | 86.71  | 182    | 752                        | 712.35                         | 39.646         |      |             |                 |
| SUM1 | Summerfield, TX      | 34.83    | -102.51   | 150.7  | 78.4   | 1186                       | 1197.10                        | -11.1024       |      |             |                 |
| SYCN | Syracuse, NY         | 43.12    | -76.09    | 292.6  | 149.5  | 122                        | 188.15                         | -66.1533       |      |             |                 |
| TCUN | Tucumcari, NM        | 35.09    | -103.61   | 144.3  | 80.87  | 1243                       | 1309.37                        | -66.3683       |      |             |                 |
| VCIO | Vici, OK             | 36.07    | -99.22    | 170.7  | 86.21  | 653                        | 605.20                         | 47.7974        |      |             |                 |
| WDLM | Wood Lake, MN        | 44.67    | -95.44    | 192.4  | 147.7  | 319                        | 315.47                         | 3.5298         |      |             |                 |
| WHN1 | Whitney, NE          | 42.74    | -103.33   | 151    | 135.6  | 1072                       | 1183.34                        | -111.336       |      |             |                 |
| WLCI | Wolcott, IN          | 40.81    | -87.05    | 238.1  | 122.8  | 215                        | 212.79                         | 2.2077         |      |             |                 |
| WNCI | Winchester, IL       | 39.65    | -90.48    | 220.1  | 112.8  | 170                        | 174.93                         | -4.9254        |      |             |                 |
| WNFL | Winfield, LA         | 31.90    | -92.78    | 209.6  | 55.79  | 95                         | 49.94                          | 45.0612        |      |             |                 |
| WSMN | White Sands, NM      | 32.41    | -106.35   | 125.6  | 63.28  | 1229                       | 1299.96                        | -70.955        |      |             |                 |

Table A-2. Alaska Geodetic Information

| ID   | Location      | Latitude | Longitude | MM5 IX | MM5 JX | Elevation (m) | MM5 Interpolated Elevation (m) | MM5-GPS dz (m) | RAOB | RAOB dx (m) | RAOB-GPS dz (m) |
|------|---------------|----------|-----------|--------|--------|---------------|--------------------------------|----------------|------|-------------|-----------------|
| CENA | Central, AK   | 65.5     | -144.68   | 75.52  | 81.41  | 273           | 528.34                         | -255.34        |      |             |                 |
| GNAA | Glenallen, AK | 62.11    | -145.97   | 79.29  | 56.64  | 586           | 619.99                         | -33.99         |      |             |                 |
| TLKA | Talkeetna, AK | 62.31    | -150.42   | 64.22  | 54.04  | 154           | 155.8                          | -1.8           |      |             |                 |
| CLGO | College, AK   | 64.87    | -147.86   | 67.63  | 74.19  | 196           | 227.2                          | -31.2          | FAI  | 5.59        | -61             |

## Appendix B: RAOB Geodetic Information

This information is provided to give the location and elevation information for each of the RAOB sites used in this study.

Table B-1. RAOB Geodetic Information for CONUS and Alaska

| Site ID       | Site Name          | Latitude (degrees) | Longitude (degrees) | Elevation (m) | Nearest GPS Site                | Distance from Nearest GPS Site (km) |
|---------------|--------------------|--------------------|---------------------|---------------|---------------------------------|-------------------------------------|
| <b>CONUS</b>  |                    |                    |                     |               |                                 |                                     |
| CHS           | Charleston, SC     | 32.90              | -80.03              | 15            | Charleston, SC (CHA1)           | 23.63                               |
| CRP           | Corpus Christi, TX | 27.77              | -97.50              | 14            | Aransas Pass, TX (ARP3)         | 44.01                               |
| DEN           | Denver, CO         | 39.77              | -104.88             | 1611          | Boulder, CO (DSRC)              | 40.66                               |
| FLG           | Flagstaff, AZ      | 35.23              | -111.82             | 2179          | Flagstaff, AZ (FST1)            | 1.11                                |
| OTX           | Spokane, WA        | 47.68              | -117.63             | 728           | Spokane, WA (SPN1)              | 19.63                               |
| SGF           | Springfield, MO    | 37.23              | -93.40              | 394           | Conway, MO (CNWM)               | 69.82                               |
| SIL           | Slidell, LA        | 30.33              | -89.82              | 8             | Stennis Space Center, MS (NDBC) | 20.45                               |
| XMR           | Cape Canaveral, FL | 28.48              | -80.55              | 5             | Cape Canaveral, FL (CCV3)       | 2.23                                |
| <b>Alaska</b> |                    |                    |                     |               |                                 |                                     |
| FAI           | Fairbanks, AK      | 64.82              | -147.87             | 135           | College, AK (CLGO)              | 5.59                                |

### **Appendix C: Location-Specific Statistics**

The following tables provide the full statistics that complement the summary values discussed in Chapter 4 of the thesis text. Bias is defined as the observed GPS-MET PW value minus the MM5 PW value. %RMSE is defined as the RMSE value divided by the Mean GPS PW value times 100, while the %StDev is defined as the Standard Deviation value divided by the Mean GPS PW times 100. The tables in the C-1 series are for CONUS, while the tables in the C-2 series are for Alaska.

## Appendix C: Location-Specific Statistics

Table C-1-1. CONUS Statistics: 06 UTC Initialization, 06H Forecast

| ID              | Correlation | Bias    | RMSE   | RMSE%   | StDev  | %Stdev  | Mean GPS | Mean MM5 | n    |
|-----------------|-------------|---------|--------|---------|--------|---------|----------|----------|------|
| ANP1            | 0.9938      | -0.2673 | 0.2968 | 11.6236 | 0.1345 | 5.2659  | 2.5538   | 2.8211   | 13   |
| ARP3            | 0.8072      | -0.3427 | 0.5228 | 12.5932 | 0.4029 | 9.706   | 4.1512   | 4.4939   | 25   |
| AZCN            | 0.9554      | -0.1466 | 0.2595 | 15.0628 | 0.2208 | 12.8136 | 1.7229   | 1.8695   | 17   |
| BARH            | 0.9295      | -0.0166 | 0.4668 | 16.549  | 0.5387 | 19.0971 | 2.821    | 2.8376   | 4    |
| BARN            | 0.9474      | -0.0101 | 0.2459 | 10.926  | 0.2509 | 11.1516 | 2.2502   | 2.2603   | 24   |
| BIL1            | 0.7005      | 0.0075  | 0.2624 | 15.0918 | 0.2704 | 15.5499 | 1.7388   | 1.7313   | 17   |
| BLKV            | 0.9844      | -0.2897 | 0.3549 | 11.2416 | 0.2128 | 6.7391  | 3.1574   | 3.4472   | 14   |
| BLMM            | 0.9528      | -0.4392 | 0.5988 | 21.5478 | 0.4196 | 15.0979 | 2.7789   | 3.2181   | 17   |
| BLRW            | 0.95        | -0.5849 | 0.6719 | 28.9181 | 0.3535 | 15.2167 | 2.3234   | 2.9082   | 8    |
| CCV3            | 0.9664      | -0.3803 | 0.431  | 8.7934  | 0.2069 | 4.222   | 4.9012   | 5.2815   | 25   |
| CHA1            | 0.9313      | -0.4432 | 0.5701 | 13.4673 | 0.3675 | 8.6806  | 4.2333   | 4.6765   | 21   |
| CHO1            | 0.7429      | 0.0623  | 0.397  | 20.3961 | 0.4041 | 20.763  | 1.9465   | 1.8841   | 17   |
| CLK1            | 0.952       | -0.1244 | 0.2539 | 9.7102  | 0.2259 | 8.6393  | 2.6145   | 2.7389   | 25   |
| CNWM            | 0.9584      | -0.4121 | 0.5415 | 21.0561 | 0.3621 | 14.0798 | 2.5715   | 2.9836   | 17   |
| COVX            | 0.9435      | -0.6836 | 0.7638 | 38.3409 | 0.3614 | 18.1411 | 1.9922   | 2.6758   | 9    |
| DQUA            | 0.9121      | -0.5181 | 0.7112 | 19.7001 | 0.4973 | 13.7747 | 3.61     | 4.1281   | 25   |
| DRV1            | 0.9508      | -0.3458 | 0.5224 | 14.5276 | 0.4064 | 11.3011 | 3.5958   | 3.9415   | 14   |
| DSRC            | 0.8919      | 0.1996  | 0.3286 | 20.2971 | 0.2691 | 16.6207 | 1.6188   | 1.4193   | 17   |
| ENGI            | 0.9313      | -0.3655 | 0.5038 | 10.8976 | 0.3539 | 7.655   | 4.6229   | 4.9884   | 25   |
| FBYN            | 0.885       | -0.1806 | 0.4809 | 15.448  | 0.4549 | 14.6129 | 3.1133   | 3.2939   | 25   |
| FST1            | 0.9406      | -0.4827 | 0.5292 | 39.9312 | 0.2235 | 16.869  | 1.3252   | 1.8079   | 17   |
| GAL1            | 0.7866      | -0.6096 | 0.7371 | 17.7861 | 0.4229 | 10.2044 | 4.1441   | 4.7537   | 25   |
| GDAC            | 0.9725      | -0.2316 | 0.2906 | 12.8006 | 0.1809 | 7.9692  | 2.27     | 2.5016   | 17   |
| GWEN            | 0.7232      | -0.3349 | 0.489  | 33.2146 | 0.3848 | 26.138  | 1.4721   | 1.8071   | 7    |
| HAG1            | 0.9878      | -0.2398 | 0.3006 | 12.6031 | 0.1902 | 7.9753  | 2.3855   | 2.6252   | 11   |
| HBRK            | 0.9732      | -0.1779 | 0.2855 | 10.5157 | 0.2312 | 8.5146  | 2.7153   | 2.8932   | 15   |
| HDF1            | 0.9675      | 0.0262  | 0.2166 | 8.1659  | 0.2201 | 8.2966  | 2.6528   | 2.6265   | 22   |
| HKLO            | 0.9236      | -0.4914 | 0.6575 | 20.001  | 0.4476 | 13.6149 | 3.2872   | 3.7787   | 21   |
| HTV1            | 0.9169      | -0.4016 | 0.5539 | 20.3297 | 0.3915 | 14.3668 | 2.7248   | 3.1264   | 20   |
| HVLK            | 0.9063      | -0.2141 | 0.4123 | 16.1384 | 0.3657 | 14.3123 | 2.555    | 2.7691   | 14   |
| JTNT            | 0.9017      | 0.1029  | 0.3452 | 10.6816 | 0.3366 | 10.4153 | 3.2315   | 3.1286   | 24   |
| KYWI            | 0.8231      | -0.2513 | 0.4924 | 10.1183 | 0.4325 | 8.8882  | 4.866    | 5.1173   | 24   |
| LMNO            | 0.9466      | -0.1658 | 0.4158 | 14.3238 | 0.3947 | 13.5965 | 2.9027   | 3.0685   | 15   |
| LTHM            | 0.8025      | -0.3338 | 0.4775 | 19.015  | 0.3689 | 14.6873 | 2.5114   | 2.8452   | 7    |
| MBWW            | 0.2617      | 0.2061  | 0.3533 | 15.6566 | 0.3067 | 13.5945 | 2.2564   | 2.0503   | 8    |
| MC01            | 0.8949      | -0.1913 | 0.3661 | 17.5081 | 0.3189 | 15.2499 | 2.0912   | 1.8999   | 24   |
| MEN1            | 0.9625      | -0.2617 | 0.4495 | 11.2018 | 0.3731 | 9.2961  | 4.013    | 4.2747   | 25   |
| MOB1            | 0.9367      | -0.2791 | 0.4756 | 9.6658  | 0.3931 | 7.9881  | 4.9206   | 5.1997   | 25   |
| MOR1            | 0.9766      | -0.3957 | 0.4869 | 17.9803 | 0.2899 | 10.7035 | 2.7082   | 3.1039   | 24   |
| MRRN            | 0.9218      | -0.2942 | 0.4718 | 18.938  | 0.3767 | 15.1227 | 2.4912   | 2.7854   | 24   |
| MDBC            | 0.942       | -0.3904 | 0.5059 | 11.0003 | 0.3284 | 7.1408  | 4.5987   | 4.989    | 25   |
| NDS1            | 0.9593      | -0.3796 | 0.4955 | 15.945  | 0.3253 | 10.4675 | 3.1075   | 3.4871   | 24   |
| NLGN            | 0.9091      | -0.1741 | 0.4316 | 15.0765 | 0.4031 | 14.0796 | 2.863    | 3.0372   | 25   |
| OKOM            | 0.8777      | -0.3475 | 0.5726 | 14.9628 | 0.4663 | 12.1853 | 3.8269   | 4.1744   | 21   |
| PATT            | 0.9006      | -0.4324 | 0.5227 | 12.3924 | 0.3039 | 7.2059  | 4.2177   | 4.6501   | 15   |
| PLS1            | 0.8317      | -0.0558 | 0.2976 | 17.832  | 0.3125 | 18.7248 | 1.6691   | 1.725    | 8    |
| PLTC            | 0.9137      | -0.0239 | 0.2635 | 15.4535 | 0.2705 | 15.8633 | 1.7053   | 1.7292   | 17   |
| PNB1            | 0.8856      | -0.2739 | 0.4698 | 23.045  | 0.3942 | 19.3376 | 2.0385   | 2.3124   | 16   |
| PRCO            | 0.9036      | -0.2195 | 0.5058 | 15.2317 | 0.4651 | 14.0059 | 3.3209   | 3.5404   | 25   |
| RWDN            | 0.9663      | -0.1716 | 0.2718 | 10.3739 | 0.2155 | 8.2251  | 2.6203   | 2.792    | 23   |
| SAVI            | 0.9496      | -0.3556 | 0.5192 | 12.7087 | 0.386  | 9.4493  | 4.0851   | 4.4407   | 25   |
| SEAW            | 0.8869      | 0.089   | 0.1669 | 7.9361  | 0.151  | 7.1779  | 2.103    | 2.014    | 8    |
| SHK1            | 0.9899      | -0.3189 | 0.3865 | 13.9472 | 0.2233 | 8.0571  | 2.771    | 3.0899   | 23   |
| SIO3            | 0.765       | -0.7397 | 0.9062 | 39.151  | 0.5396 | 23.3127 | 2.3147   | 3.0544   | 17   |
| SLAI            | 0.9387      | -0.2334 | 0.3052 | 13.7735 | 0.2124 | 9.5858  | 2.2157   | 2.4491   | 7    |
| SPN1            | 0.9348      | -0.3917 | 0.4321 | 29.4426 | 0.1953 | 13.3028 | 1.4677   | 1.8594   | 8    |
| SUM1            | 0.8731      | 0.091   | 0.3769 | 13.8794 | 0.3733 | 13.7464 | 2.7158   | 2.6248   | 25   |
| SYCN            | 0.9714      | -0.1132 | 0.1993 | 9.1287  | 0.1694 | 7.7595  | 2.1828   | 2.296    | 16   |
| TCUN            | 0.8757      | 0.0326  | 0.3017 | 11.6945 | 0.3067 | 11.8875 | 2.58     | 2.5474   | 23   |
| VCIO            | 0.9045      | -0.1938 | 0.4281 | 14.7395 | 0.3895 | 13.4132 | 2.9042   | 3.098    | 25   |
| WDLM            | 0.8835      | -0.2854 | 0.4025 | 17.1685 | 0.2899 | 12.3653 | 2.3444   | 2.6298   | 24   |
| WHN1            | 0.9421      | -0.1687 | 0.3492 | 14.7591 | 0.3121 | 13.1903 | 2.3661   | 2.5347   | 25   |
| WLCI            | 0.9595      | -0.3937 | 0.4997 | 22.0671 | 0.3203 | 14.1443 | 2.2645   | 2.6582   | 13   |
| WNCI            | 0.9261      | -0.2766 | 0.4527 | 18.7061 | 0.3687 | 15.2377 | 2.4198   | 2.6964   | 18   |
| WNFL            | 0.8607      | -0.4127 | 0.5653 | 13.2649 | 0.3959 | 9.2897  | 4.2616   | 4.6743   | 21   |
| WSMN            | 0.8554      | 0.216   | 0.3762 | 12.4052 | 0.3216 | 10.6066 | 3.0323   | 2.8162   | 12   |
|                 |             |         |        |         |        |         |          |          |      |
| Means           | 0.9003      | -0.2401 | 0.4393 | 16.4977 | 0.3303 | 12.3741 | 2.8460   | 3.0861   | 18.4 |
| Means of n > 10 | 0.9146      | -0.2411 |        | 15.5030 |        | 11.8041 |          |          | 20.4 |

## Appendix C: Location-Specific Statistics

Table C-1-2. CONUS Statistics: 06 UTC Initialization, 09H Forecast

| ID                        | Correlation   | Bias           | RMSE          | RMSE%          | StDev         | %Stdev         | Mean GPS      | Mean MM5      | n              |
|---------------------------|---------------|----------------|---------------|----------------|---------------|----------------|---------------|---------------|----------------|
| ANP1                      | 0.9662        | -0.2061        | 0.2996        | 13.392         | 0.2281        | 10.1955        | 2.2373        | 2.4434        | 11             |
| ARP3                      | 0.7696        | -0.1978        | 0.4653        | 11.0849        | 0.4306        | 10.2587        | 4.1975        | 4.3953        | 23             |
| AZCN                      | 0.9677        | -0.152         | 0.2215        | 11.7897        | 0.1672        | 8.9005         | 1.8786        | 2.0305        | 14             |
| BARH                      | 0.8814        | -0.0719        | 0.4163        | 15.8226        | 0.4735        | 17.9963        | 2.6312        | 2.7031        | 4              |
| BARN                      | 0.9637        | 0.0542         | 0.2347        | 10.0751        | 0.2334        | 10.0232        | 2.3291        | 2.2749        | 23             |
| BIL1                      | 0.8433        | 0.0031         | 0.2062        | 11.1914        | 0.214         | 11.6126        | 1.8429        | 1.8398        | 14             |
| BLKV                      | 0.9687        | -0.1482        | 0.3125        | 10.1154        | 0.2854        | 9.2406         | 3.0889        | 3.2371        | 14             |
| BLMM                      | 0.9644        | -0.3172        | 0.4568        | 15.9668        | 0.3411        | 11.9231        | 2.8611        | 3.1783        | 14             |
| BLRW                      | 0.9416        | -0.3009        | 0.4729        | 18.9949        | 0.3899        | 15.6644        | 2.4894        | 2.7903        | 8              |
| CCV3                      | 0.9228        | -0.189         | 0.4065        | 8.2278         | 0.368         | 7.4479         | 4.9407        | 5.1297        | 23             |
| CHAI                      | 0.9109        | -0.2158        | 0.4895        | 11.3671        | 0.4514        | 10.4821        | 4.3061        | 4.5219        | 19             |
| CHO1                      | 0.672         | -0.006         | 0.4935        | 25.1216        | 0.512         | 26.068         | 1.9643        | 1.9703        | 14             |
| CLK1                      | 0.8914        | -0.1466        | 0.3287        | 12.0181        | 0.3009        | 10.9988        | 2.7353        | 2.8819        | 23             |
| CNWM                      | 0.9506        | -0.2544        | 0.4603        | 16.1201        | 0.3954        | 13.8469        | 2.8552        | 3.1096        | 17             |
| COVX                      | 0.7363        | -0.7674        | 0.8402        | 49.3239        | 0.3746        | 21.9909        | 1.7033        | 2.4707        | 6              |
| DQUA                      | 0.9121        | -0.4096        | 0.6093        | 16.4071        | 0.4612        | 12.4195        | 3.7134        | 4.123         | 23             |
| DRV1                      | 0.9536        | -0.317         | 0.4991        | 14.047         | 0.4           | 11.2582        | 3.5529        | 3.8699        | 14             |
| DSRC                      | 0.84          | 0.2528         | 0.3778        | 21.5792        | 0.2905        | 16.5964        | 1.7507        | 1.4978        | 15             |
| ENGI                      | 0.9272        | -0.0984        | 0.4183        | 8.9069         | 0.4156        | 8.8514         | 4.6958        | 4.7942        | 23             |
| FBYN                      | 0.8755        | -0.1145        | 0.433         | 13.5235        | 0.427         | 13.3356        | 3.2021        | 3.3166        | 23             |
| FST1                      | 0.9231        | -0.4587        | 0.518         | 37.7366        | 0.2491        | 18.1439        | 1.3727        | 1.8315        | 15             |
| GAL1                      | 0.6988        | -0.3315        | 0.6166        | 14.4575        | 0.5315        | 12.4638        | 4.2647        | 4.5963        | 23             |
| GDAC                      | 0.9267        | -0.1068        | 0.2926        | 11.6518        | 0.282         | 11.228         | 2.5113        | 2.6182        | 15             |
| GWEN                      | 0.9235        | -0.2644        | 0.3321        | 23.0152        | 0.2172        | 15.0472        | 1.4431        | 1.7075        | 7              |
| HAG1                      | 0.8543        | -0.2549        | 0.3905        | 20.9685        | 0.3137        | 16.848         | 1.8622        | 2.1171        | 9              |
| HBRK                      | 0.9415        | -0.0743        | 0.3172        | 11.2044        | 0.3209        | 11.3371        | 2.8308        | 2.9051        | 13             |
| HDF1                      | 0.9449        | 0.0528         | 0.2935        | 11.0329        | 0.2958        | 11.1208        | 2.6601        | 2.6073        | 21             |
| HKLO                      | 0.8826        | -0.3213        | 0.5718        | 16.6982        | 0.4846        | 14.1535        | 3.4242        | 3.7455        | 21             |
| HTV1                      | 0.9639        | -0.2224        | 0.3563        | 11.946         | 0.2865        | 9.6047         | 2.9826        | 3.205         | 18             |
| HVLK                      | 0.8037        | -0.1894        | 0.4184        | 14.9268        | 0.3883        | 13.8539        | 2.8031        | 2.9925        | 13             |
| JTNT                      | 0.9276        | 0.082          | 0.2736        | 8.2202         | 0.2669        | 8.0186         | 3.3279        | 3.2459        | 23             |
| KYW1                      | 0.6845        | -0.3385        | 0.6684        | 14.0113        | 0.5893        | 12.3528        | 4.7703        | 5.1088        | 23             |
| LMNO                      | 0.9429        | -0.082         | 0.4029        | 13.3636        | 0.4094        | 13.578         | 3.015         | 3.097         | 14             |
| LTHM                      | 0.6285        | -0.2002        | 0.6339        | 23.8474        | 0.6589        | 24.7862        | 2.6583        | 2.8586        | 6              |
| MBWW                      | 0.4179        | 0.1652         | 0.2776        | 12.8449        | 0.2385        | 11.0367        | 2.1612        | 1.9961        | 8              |
| MC01                      | 0.8878        | 0.3091         | 0.4289        | 19.2372        | 0.3044        | 13.65          | 2.2298        | 1.9206        | 22             |
| MCN1                      | 0.9711        | -0.1493        | 0.3662        | 9.1416         | 0.3419        | 8.5343         | 4.0057        | 4.155         | 23             |
| MOB1                      | 0.9353        | -0.2096        | 0.4635        | 9.5291         | 0.4227        | 8.6902         | 4.8643        | 5.0739        | 23             |
| MOR1                      | 0.9761        | -0.2264        | 0.3755        | 13.4532        | 0.3063        | 10.9745        | 2.7912        | 3.0176        | 23             |
| MRRN                      | 0.9406        | -0.2083        | 0.3596        | 13.5277        | 0.2998        | 11.2755        | 2.6585        | 2.8668        | 23             |
| NDBC                      | 0.9497        | -0.158         | 0.3558        | 7.6583         | 0.3259        | 7.0152         | 4.6453        | 4.8034        | 23             |
| NDS1                      | 0.9109        | -0.2488        | 0.4816        | 14.8608        | 0.4216        | 13.0096        | 3.2407        | 3.4896        | 23             |
| NLGN                      | 0.933         | -0.1142        | 0.3428        | 11.4778        | 0.3305        | 11.066         | 2.9868        | 3.1009        | 23             |
| OKOM                      | 0.8586        | -0.1505        | 0.4871        | 12.3612        | 0.476         | 12.0787        | 3.9408        | 4.0913        | 19             |
| PATT                      | 0.864         | -0.2352        | 0.4379        | 10.2401        | 0.3833        | 8.9633         | 4.2763        | 4.5115        | 14             |
| PLS1                      | 0.876         | 0.025          | 0.286         | 17.3021        | 0.3077        | 18.6167        | 1.6527        | 1.6277        | 7              |
| PLTC                      | 0.791         | -0.0423        | 0.3426        | 18.4802        | 0.3519        | 18.9828        | 1.854         | 1.8963        | 15             |
| PNB1                      | 0.9128        | -0.0825        | 0.3858        | 17.7833        | 0.3901        | 17.9814        | 2.1694        | 2.2519        | 15             |
| PRCO                      | 0.8836        | -0.0305        | 0.4313        | 12.5302        | 0.4399        | 12.7797        | 3.4419        | 3.4724        | 23             |
| RWDN                      | 0.9151        | -0.0924        | 0.2942        | 10.3849        | 0.2855        | 10.0803        | 2.8325        | 2.925         | 23             |
| SAV1                      | 0.9428        | -0.3098        | 0.4967        | 12.4594        | 0.397         | 9.9577         | 3.9867        | 4.2965        | 23             |
| SEAW                      | 0.7223        | 0.0988         | 0.2012        | 8.8402         | 0.1874        | 8.2332         | 2.2764        | 2.1776        | 8              |
| SHR1                      | 0.9803        | -0.2394        | 0.3714        | 13.3742        | 0.2904        | 10.457         | 2.7773        | 3.0166        | 23             |
| SIO3                      | 0.7239        | -0.8963        | 1.0694        | 46.43          | 0.6038        | 26.2152        | 2.3033        | 3.1997        | 15             |
| SLAI                      | 0.9164        | -0.3162        | 0.374         | 18.9378        | 0.2189        | 11.0821        | 1.975         | 2.2912        | 6              |
| SPN1                      | 0.785         | -0.1697        | 0.3578        | 22.1991        | 0.3402        | 21.1075        | 1.6117        | 1.7815        | 7              |
| SUM1                      | 0.8329        | 0.1295         | 0.3797        | 13.7901        | 0.3654        | 13.268         | 2.7538        | 2.6242        | 22             |
| SYCN                      | 0.9217        | -0.0811        | 0.2347        | 10.6373        | 0.2271        | 10.2897        | 2.2066        | 2.2877        | 17             |
| TCUN                      | 0.9156        | 0.0723         | 0.2506        | 9.6456         | 0.2456        | 9.4528         | 2.5983        | 2.526         | 22             |
| VCIO                      | 0.8714        | -0.1481        | 0.4078        | 13.5016        | 0.3889        | 12.8762        | 3.0201        | 3.1682        | 22             |
| WDLM                      | 0.8755        | -0.2322        | 0.4133        | 16.2017        | 0.3495        | 13.703         | 2.5507        | 2.7829        | 23             |
| WHN1                      | 0.93          | -0.0592        | 0.3142        | 12.3518        | 0.3155        | 12.4029        | 2.5438        | 2.603         | 23             |
| WLCI                      | 0.9464        | -0.3195        | 0.4193        | 19.2158        | 0.2817        | 12.9126        | 2.1819        | 2.5013        | 14             |
| WNCI                      | 0.8982        | -0.133         | 0.4325        | 17.3851        | 0.4242        | 17.0519        | 2.4879        | 2.6209        | 17             |
| WNFL                      | 0.9276        | -0.2993        | 0.4228        | 10.0077        | 0.3067        | 7.2616         | 4.2243        | 4.5236        | 19             |
| WSMN                      | 0.6947        | 0.3864         | 0.4821        | 14.8125        | 0.3039        | 9.337          | 3.255         | 2.8686        | 10             |
| <b>Means</b>              | <b>0.8760</b> | <b>-0.1557</b> | <b>0.4132</b> | <b>15.4357</b> | <b>0.3534</b> | <b>12.9089</b> | <b>2.9001</b> | <b>3.0558</b> | <b>17.0303</b> |
| <b>Means of n &gt; 10</b> | <b>0.8933</b> | <b>-0.1495</b> |               | <b>14.3029</b> |               | <b>12.1742</b> |               |               | <b>19.0545</b> |

## Appendix C: Location-Specific Statistics

Table C-1-3. CONUS Statistics: 06 UTC Initialization, 12H Forecast

| <b>ID</b>                 | <b>Correlation</b> | <b>Bias</b>    | <b>RMSE</b>   | <b>RMSE%</b>   | <b>StDev</b>  | <b>%Stdev</b>  | <b>Mean GPS</b> | <b>Mean MM5</b> | <b>n</b>       |
|---------------------------|--------------------|----------------|---------------|----------------|---------------|----------------|-----------------|-----------------|----------------|
| ANP1                      | 0.9318             | 0.008          | 0.479         | 18.7213        | 0.5002        | 19.551         | 2.5583          | 2.5503          | 12             |
| ARP3                      | 0.7457             | -0.0885        | 0.5055        | 12.1451        | 0.5089        | 12.2264        | 4.1625          | 4.251           | 23             |
| AZCN                      | 0.9264             | -0.1235        | 0.289         | 16.34          | 0.2705        | 15.2927        | 1.7687          | 1.8921          | 15             |
| BARH                      | 0.9338             | 0.0999         | 0.3356        | 12.0706        | 0.37          | 13.3059        | 2.7805          | 2.6806          | 4              |
| BARN                      | 0.9511             | 0.1163         | 0.3052        | 12.4717        | 0.2882        | 11.7777        | 2.4467          | 2.3304          | 24             |
| BIL1                      | 0.8432             | -0.0729        | 0.2337        | 12.57          | 0.2305        | 12.3946        | 1.8593          | 1.9321          | 14             |
| BLKV                      | 0.9561             | -0.0405        | 0.3068        | 10.5692        | 0.3156        | 10.872         | 2.9025          | 2.943           | 14             |
| BLMM                      | 0.9603             | -0.0226        | 0.4183        | 14.5586        | 0.4313        | 15.014         | 2.8729          | 2.8955          | 16             |
| BLRW                      | 0.9654             | -0.1333        | 0.3544        | 13.0842        | 0.3511        | 12.9613        | 2.709           | 2.8423          | 8              |
| CCV3                      | 0.8982             | -0.1008        | 0.4102        | 8.3117         | 0.4065        | 8.2381         | 4.935           | 5.0358          | 23             |
| CHA1                      | 0.8075             | -0.023         | 0.5443        | 12.0874        | 0.5587        | 12.4075        | 4.5027          | 4.5257          | 19             |
| CHO1                      | 0.8312             | 0.0268         | 0.3356        | 16.2542        | 0.3472        | 16.8138        | 2.065           | 2.0382          | 14             |
| CLK1                      | 0.8505             | -0.1611        | 0.4176        | 15.1638        | 0.3939        | 14.3048        | 2.7538          | 2.9149          | 23             |
| CNWM                      | 0.9481             | -0.1227        | 0.4066        | 13.8767        | 0.3983        | 13.5922        | 2.9304          | 3.0531          | 19             |
| COVX                      | 0.9223             | -0.7379        | 0.819         | 42.6817        | 0.3797        | 19.7906        | 1.9188          | 2.6567          | 8              |
| DQUA                      | 0.9092             | -0.1745        | 0.4698        | 11.8163        | 0.4475        | 11.2564        | 3.9757          | 4.1501          | 20             |
| DRV1                      | 0.9784             | -0.1697        | 0.3467        | 9.4823         | 0.3147        | 8.6066         | 3.6562          | 3.8258          | 13             |
| DSRC                      | 0.9036             | 0.2187         | 0.3275        | 18.7493        | 0.2518        | 14.4138        | 1.7469          | 1.5282          | 16             |
| ENG1                      | 0.8989             | -0.0387        | 0.4616        | 9.661          | 0.4703        | 9.8434         | 4.7783          | 4.8169          | 23             |
| FBYN                      | 0.942              | -0.1046        | 0.3117        | 10.108         | 0.2999        | 9.7268         | 3.0835          | 3.1881          | 24             |
| FST1                      | 0.9233             | -0.3609        | 0.4368        | 29.5735        | 0.2547        | 17.2473        | 1.4769          | 1.8378          | 15             |
| GAL1                      | 0.806              | -0.1512        | 0.3757        | 8.7511         | 0.3517        | 8.1909         | 4.2932          | 4.4444          | 23             |
| GDAC                      | 0.9365             | -0.0558        | 0.2618        | 10.7814        | 0.2641        | 10.8787        | 2.4281          | 2.484           | 16             |
| GWEN                      | 0.8213             | -0.1681        | 0.3292        | 22.4562        | 0.3058        | 20.8564        | 1.4661          | 1.6342          | 7              |
| HAG1                      | 0.9782             | -0.1619        | 0.2683        | 12.0739        | 0.2255        | 10.1501        | 2.222           | 2.3839          | 10             |
| HBRK                      | 0.9532             | -0.0736        | 0.3327        | 11.8752        | 0.3358        | 11.987         | 2.8013          | 2.875           | 15             |
| HDF1                      | 0.9336             | 0.1594         | 0.4085        | 15.1836        | 0.385         | 14.3084        | 2.6906          | 2.5312          | 22             |
| HKLO                      | 0.8965             | -0.089         | 0.459         | 13.322         | 0.4604        | 13.3632        | 3.4454          | 3.5344          | 23             |
| HTV1                      | 0.9574             | 0.0999         | 0.4159        | 12.9132        | 0.4169        | 12.9462        | 3.2206          | 3.1207          | 16             |
| HVLK                      | 0.908              | -0.1488        | 0.3295        | 11.8808        | 0.3051        | 11.0007        | 2.7736          | 2.9224          | 14             |
| JTNT                      | 0.95               | 0.0777         | 0.2356        | 7.1782         | 0.2272        | 6.922          | 3.2828          | 3.2051          | 24             |
| KYWI                      | 0.6529             | -0.2981        | 0.7199        | 14.9295        | 0.67          | 13.8951        | 4.8219          | 5.12            | 23             |
| LMNO                      | 0.9615             | -0.1512        | 0.3315        | 11.1526        | 0.3054        | 10.2736        | 2.9727          | 3.1239          | 15             |
| LTHM                      | 0.9316             | -0.0882        | 0.4434        | 16.2816        | 0.476         | 17.4794        | 2.7233          | 2.8115          | 6              |
| MBWW                      | 0.8873             | 0.048          | 0.1389        | 6.4572         | 0.1394        | 6.4786         | 2.1514          | 2.1034          | 8              |
| MC01                      | 0.865              | 0.2535         | 0.4069        | 19.2064        | 0.3255        | 15.3608        | 2.1188          | 1.8652          | 23             |
| MCN1                      | 0.9342             | 0.1823         | 0.5432        | 13.4403        | 0.5232        | 12.9454        | 4.0418          | 3.8595          | 23             |
| MOB1                      | 0.9435             | -0.1455        | 0.3961        | 8.231          | 0.3767        | 7.8281         | 4.8127          | 4.9582          | 23             |
| MOR1                      | 0.9494             | -0.0881        | 0.3964        | 14.05          | 0.3952        | 14.0061        | 2.8213          | 2.9095          | 23             |
| MRRN                      | 0.9449             | -0.1479        | 0.3215        | 12.2894        | 0.2916        | 11.1456        | 2.6158          | 2.7638          | 24             |
| NDBC                      | 0.9276             | -0.0816        | 0.3983        | 8.3372         | 0.3982        | 8.3358         | 4.7775          | 4.8591          | 24             |
| NDS1                      | 0.9164             | -0.1178        | 0.4505        | 13.9677        | 0.4441        | 13.772         | 3.225           | 3.3427          | 24             |
| NLGN                      | 0.9365             | -0.0416        | 0.3349        | 10.9213        | 0.3394        | 11.0698        | 3.0664          | 3.108           | 24             |
| OKOM                      | 0.8431             | 0.1161         | 0.5349        | 13.8298        | 0.535         | 13.8333        | 3.8677          | 3.7516          | 21             |
| PATT                      | 0.9412             | -0.2158        | 0.3404        | 7.958          | 0.2732        | 6.3869         | 4.2769          | 4.4927          | 14             |
| PLS1                      | 0.7711             | 0.0191         | 0.2849        | 16.9416        | 0.307         | 18.258         | 1.6816          | 1.6625          | 7              |
| PLTC                      | 0.865              | -0.1259        | 0.286         | 17.2709        | 0.2664        | 16.0914        | 1.6557          | 1.7816          | 14             |
| PNB1                      | 0.8987             | -0.2538        | 0.3875        | 19.6668        | 0.303         | 15.38          | 1.9701          | 2.224           | 15             |
| PRCO                      | 0.9158             | 0.0577         | 0.4079        | 11.9608        | 0.4124        | 12.0952        | 3.41            | 3.3523          | 24             |
| RWDN                      | 0.8631             | -0.1169        | 0.3923        | 13.8222        | 0.3825        | 13.4779        | 2.8383          | 2.9553          | 24             |
| SAV1                      | 0.898              | 0.0975         | 0.5037        | 11.7771        | 0.5052        | 11.8139        | 4.2766          | 4.1791          | 23             |
| SEAW                      | 0.5637             | 0.099          | 0.2487        | 10.6748        | 0.2439        | 10.4687        | 2.3295          | 2.2305          | 8              |
| SHK1                      | 0.9438             | -0.1034        | 0.4649        | 16.6171        | 0.464         | 16.5824        | 2.798           | 2.9013          | 22             |
| SIO3                      | 0.6996             | -0.8538        | 1.0533        | 46.5808        | 0.637         | 28.1718        | 2.2613          | 3.1151          | 16             |
| SLAI                      | 0.5886             | -0.0811        | 0.3383        | 15.6845        | 0.3548        | 16.4469        | 2.1571          | 2.2383          | 7              |
| SPN1                      | 0.6819             | 0.0059         | 0.4183        | 22.7785        | 0.4518        | 24.6011        | 1.8366          | 1.8307          | 7              |
| SUM1                      | 0.8874             | 0.2224         | 0.392         | 14.1018        | 0.3304        | 11.8851        | 2.7798          | 2.5573          | 22             |
| SYCN                      | 0.7176             | -0.0106        | 0.5686        | 24.5454        | 0.5872        | 25.346         | 2.3167          | 2.3273          | 16             |
| TCUN                      | 0.9175             | 0.0982         | 0.2832        | 11.091         | 0.2717        | 10.6373        | 2.5538          | 2.4556          | 23             |
| VCIO                      | 0.881              | -0.0929        | 0.4171        | 13.7654        | 0.4153        | 13.7082        | 3.0298          | 3.1227          | 24             |
| WDLM                      | 0.805              | -0.1152        | 0.4324        | 16.2754        | 0.4261        | 16.0401        | 2.6566          | 2.7718          | 23             |
| WHN1                      | 0.9269             | -0.0495        | 0.3198        | 12.7396        | 0.323         | 12.8687        | 2.51            | 2.5595          | 23             |
| WLCI                      | 0.9593             | -0.1877        | 0.2769        | 11.5909        | 0.2119        | 8.8684         | 2.389           | 2.5767          | 13             |
| WNCI                      | 0.9067             | -0.0476        | 0.3928        | 15.4473        | 0.4012        | 15.7782        | 2.5428          | 2.5903          | 18             |
| WNFL                      | 0.7993             | -0.0167        | 0.4309        | 10.1716        | 0.4412        | 10.4149        | 4.2366          | 4.2533          | 21             |
| WSMN                      | 0.829              | 0.3241         | 0.449         | 14.6322        | 0.3259        | 10.6207        | 3.0686          | 2.7445          | 11             |
| <b>Means</b>              | <b>0.8806</b>      | <b>-0.0670</b> | <b>0.4006</b> | <b>14.6348</b> | <b>0.3731</b> | <b>13.3728</b> | <b>2.9409</b>   | <b>3.0079</b>   | <b>17.4697</b> |
| <b>Means of n &gt; 10</b> | <b>0.8938</b>      | <b>-0.0623</b> | <b>0.4006</b> | <b>14.0498</b> | <b>0.3731</b> | <b>12.8921</b> | <b>2.9409</b>   | <b>3.0079</b>   | <b>19.3393</b> |

### Appendix C: Location-Specific Statistics

Table C-1-4. CONUS Statistics: 06 UTC Initialization, 15H Forecast

| ID              | Correlation | Bias    | RMSE   | RMSE%   | StDev  | %Stdev  | Mean GPS | Mean MM5 | n       |
|-----------------|-------------|---------|--------|---------|--------|---------|----------|----------|---------|
| ANP1            | 0.9511      | 0.1277  | 0.3608 | 12.9209 | 0.3502 | 12.5412 | 2.7921   | 2.6645   | 14      |
| ARP3            | 0.6655      | -0.2521 | 0.5719 | 14.5042 | 0.5244 | 13.2987 | 3.943    | 4.1952   | 24      |
| AZCN            | 0.8985      | -0.1468 | 0.3372 | 20.2073 | 0.3135 | 18.7875 | 1.6687   | 1.8156   | 16      |
| BARN            | 0.8575      | 0.1845  | 0.4894 | 19.9449 | 0.463  | 18.8705 | 2.4537   | 2.2692   | 24      |
| BIL1            | 0.6893      | -0.068  | 0.3369 | 17.8686 | 0.3415 | 18.1151 | 1.8853   | 1.9533   | 15      |
| BLKV            | 0.9289      | 0.2089  | 0.4313 | 14.5058 | 0.3915 | 13.1689 | 2.9731   | 2.7641   | 14      |
| BLMM            | 0.9546      | 0.1058  | 0.4595 | 15.5916 | 0.4618 | 15.6703 | 2.947    | 2.8412   | 16      |
| BLRW            | 0.9526      | -0.0753 | 0.3127 | 10.8612 | 0.3245 | 11.2694 | 2.8794   | 2.9547   | 8       |
| CCV3            | 0.9155      | -0.2202 | 0.4429 | 9.0844  | 0.3925 | 8.0517  | 4.8749   | 5.0951   | 24      |
| CHA1            | 0.7386      | -0.198  | 0.7569 | 17.6896 | 0.7495 | 17.5171 | 4.2789   | 4.4769   | 20      |
| CHO1            | 0.7635      | -0.1208 | 0.4224 | 21.6155 | 0.4189 | 21.44   | 1.954    | 2.0748   | 15      |
| CLK1            | 0.8922      | -0.0593 | 0.3456 | 12.2807 | 0.3478 | 12.3588 | 2.8145   | 2.8738   | 24      |
| CNWM            | 0.9347      | 0.0113  | 0.4042 | 13.6517 | 0.4151 | 14.0203 | 2.961    | 2.9497   | 19      |
| COVX            | 0.9896      | -0.3419 | 0.4535 | 20.0309 | 0.3331 | 14.7142 | 2.264    | 2.6059   | 5       |
| DQUA            | 0.9224      | 0.0591  | 0.5125 | 13.3646 | 0.5248 | 13.6841 | 3.8351   | 3.776    | 17      |
| DRV1            | 0.9424      | -0.1355 | 0.4528 | 12.2588 | 0.4484 | 12.1389 | 3.6939   | 3.8293   | 14      |
| DSRC            | 0.8995      | 0.2357  | 0.3552 | 18.8126 | 0.2745 | 14.5372 | 1.8881   | 1.6525   | 16      |
| ENG1            | 0.9169      | 0.0579  | 0.3894 | 7.9536  | 0.3933 | 8.0342  | 4.8955   | 4.8375   | 24      |
| FBYN            | 0.8981      | -0.1021 | 0.417  | 13.252  | 0.413  | 13.1248 | 3.1465   | 3.2486   | 24      |
| FST1            | 0.8866      | -0.2924 | 0.4108 | 24.9947 | 0.298  | 18.1326 | 1.6436   | 1.936    | 16      |
| GAL1            | 0.7753      | -0.1282 | 0.4298 | 9.8343  | 0.4191 | 9.5885  | 4.3703   | 4.4985   | 24      |
| GDAC            | 0.9086      | -0.1667 | 0.3474 | 14.9279 | 0.3148 | 13.5263 | 2.3275   | 2.4942   | 16      |
| GWEN            | 0.8628      | -0.209  | 0.3073 | 20.9492 | 0.2433 | 16.5869 | 1.4667   | 1.6757   | 7       |
| HAG1            | 0.9445      | -0.1647 | 0.366  | 16.1136 | 0.3415 | 15.0312 | 2.2717   | 2.4363   | 12      |
| HBRK            | 0.9399      | -0.0515 | 0.333  | 11.6824 | 0.3398 | 11.9202 | 2.8506   | 2.9022   | 16      |
| HDF1            | 0.9069      | 0.266   | 0.4632 | 16.7759 | 0.3877 | 14.0435 | 2.761    | 2.4951   | 23      |
| HKLO            | 0.8766      | 0.0098  | 0.5165 | 14.6641 | 0.528  | 14.991  | 3.5219   | 3.5121   | 23      |
| HTV1            | 0.9049      | 0.0785  | 0.5517 | 17.463  | 0.5602 | 17.7344 | 3.1591   | 3.0806   | 20      |
| HVLK            | 0.8765      | -0.1522 | 0.3698 | 13.0412 | 0.3497 | 12.3335 | 2.8357   | 2.988    | 14      |
| JTNT            | 0.9285      | 0.072   | 0.2697 | 8.2419  | 0.2655 | 8.1133  | 3.2725   | 3.2005   | 24      |
| KYWI            | 0.7329      | -0.2526 | 0.6049 | 12.4697 | 0.5614 | 11.5737 | 4.851    | 5.1036   | 24      |
| LMNO            | 0.9335      | -0.0987 | 0.3855 | 12.0205 | 0.3858 | 12.028  | 3.2073   | 3.306    | 15      |
| LTHM            | 0.8606      | -0.0469 | 0.3299 | 12.2245 | 0.3527 | 13.0696 | 2.6986   | 2.7455   | 7       |
| MBWW            | 0.7983      | -0.0184 | 0.1713 | 8.046   | 0.182  | 8.5516  | 2.1285   | 2.1469   | 8       |
| MC01            | 0.8943      | 0.217   | 0.3843 | 18.4645 | 0.3242 | 15.5796 | 2.0812   | 1.8641   | 23      |
| MCN1            | 0.915       | 0.2014  | 0.567  | 13.779  | 0.5414 | 13.1576 | 4.1147   | 3.9134   | 24      |
| MOB1            | 0.8782      | -0.046  | 0.4826 | 9.9458  | 0.4912 | 10.1231 | 4.8525   | 4.8985   | 23      |
| MOR1            | 0.8708      | -0.0083 | 0.5975 | 20.2979 | 0.6102 | 20.7324 | 2.9435   | 2.9518   | 24      |
| MRRN            | 0.9253      | -0.1502 | 0.3854 | 14.7182 | 0.3626 | 13.8458 | 2.6185   | 2.7688   | 24      |
| NDBC            | 0.9402      | -0.0249 | 0.3573 | 7.3973  | 0.3641 | 7.538   | 4.8298   | 4.8548   | 24      |
| NDS1            | 0.8967      | -0.0302 | 0.492  | 15.2463 | 0.5021 | 15.5595 | 3.2267   | 3.2569   | 23      |
| NLGN            | 0.9502      | -0.0317 | 0.2932 | 9.4295  | 0.2977 | 9.5758  | 3.1093   | 3.1411   | 24      |
| OKOM            | 0.8857      | 0.2574  | 0.5575 | 14.1499 | 0.5067 | 12.8612 | 3.9399   | 3.6825   | 21      |
| PATF            | 0.8237      | -0.1895 | 0.4674 | 10.8259 | 0.4434 | 10.27   | 4.3176   | 4.5071   | 14      |
| PLS1            | 0.6086      | -0.0046 | 0.3841 | 22.1239 | 0.4149 | 23.8949 | 1.7363   | 1.7408   | 7       |
| PLTC            | 0.8401      | -0.0867 | 0.2748 | 13.2559 | 0.2714 | 13.0932 | 2.0731   | 2.1597   | 13      |
| PNB1            | 0.8668      | -0.0906 | 0.4079 | 18.7553 | 0.4116 | 18.9283 | 2.1746   | 2.2652   | 15      |
| PRCO            | 0.8994      | 0.2487  | 0.5551 | 15.3396 | 0.5092 | 14.0699 | 3.6191   | 3.3703   | 20      |
| RWDN            | 0.9307      | -0.0382 | 0.3026 | 9.9971  | 0.3069 | 10.1401 | 3.0264   | 3.0646   | 23      |
| SAV1            | 0.8942      | 0.116   | 0.5148 | 11.8656 | 0.5124 | 11.809  | 4.3387   | 4.2226   | 24      |
| SEAW            | 0.5878      | 0.0088  | 0.2503 | 11.0643 | 0.2675 | 11.8209 | 2.2626   | 2.2538   | 8       |
| SHK1            | 0.9257      | -0.1218 | 0.4853 | 17.3736 | 0.4799 | 17.1793 | 2.7932   | 2.915    | 24      |
| SIO3            | 0.6352      | -0.842  | 1.0761 | 47.9618 | 0.6921 | 30.8453 | 2.2437   | 3.0858   | 16      |
| SLAI            | 0.7337      | -0.0195 | 0.3162 | 13.6225 | 0.3409 | 14.686  | 2.3214   | 2.3409   | 7       |
| SPN1            | 0.9121      | -0.1433 | 0.2844 | 16.6488 | 0.2654 | 15.5337 | 1.7084   | 1.8517   | 7       |
| SUM1            | 0.8734      | 0.2532  | 0.4054 | 14.4755 | 0.3237 | 11.5586 | 2.8008   | 2.5476   | 23      |
| SYCN            | 0.9207      | 0.0965  | 0.2924 | 12.4326 | 0.284  | 12.076  | 2.3517   | 2.2552   | 18      |
| TCUN            | 0.9289      | 0.1199  | 0.2878 | 11.174  | 0.2675 | 10.3858 | 2.5756   | 2.4556   | 23      |
| VCIO            | 0.8771      | -0.0859 | 0.4132 | 13.496  | 0.4129 | 13.4852 | 3.0619   | 3.1478   | 24      |
| WDLM            | 0.8222      | -0.1429 | 0.4631 | 17.0593 | 0.45   | 16.5758 | 2.7149   | 2.8578   | 24      |
| WHN1            | 0.9253      | -0.1462 | 0.3596 | 14.7539 | 0.3356 | 13.7701 | 2.4373   | 2.5834   | 24      |
| WLCI            | 0.9288      | -0.0994 | 0.2604 | 10.4746 | 0.2505 | 10.0767 | 2.4861   | 2.5855   | 13      |
| WNCI            | 0.894       | 0.0512  | 0.4363 | 15.9647 | 0.4458 | 16.314  | 2.7327   | 2.6815   | 18      |
| WNFL            | 0.8076      | 0.112   | 0.505  | 11.7632 | 0.5046 | 11.7537 | 4.2933   | 4.1814   | 21      |
| WSMN            | 0.8344      | 0.2378  | 0.361  | 12.3251 | 0.2864 | 9.776   | 2.9293   | 2.6915   | 10      |
|                 |             |         |        |         |        |         |          |          |         |
|                 |             |         |        |         |        |         |          |          |         |
| Means           | 0.8688      | -0.0349 | 0.4204 | 14.8620 | 0.3983 | 13.9320 | 2.9881   | 3.0230   | 17.9692 |
| Means of n > 10 | 0.8780      | -0.0253 |        | 14.8296 |        | 13.8474 |          |          | 19.7143 |

## Appendix C: Location-Specific Statistics

Table C-1-5. CONUS Statistics: 06 UTC Initialization, 18H Forecast

| ID                        | Correlation   | Bias           | RMSE          | RMSE%          | StDev         | %Stdev         | Mean GPS      | Mean MM5      | n              |
|---------------------------|---------------|----------------|---------------|----------------|---------------|----------------|---------------|---------------|----------------|
| ANP1                      | 0.9667        | -0.0317        | 0.3011        | 11.6734        | 0.314         | 12.1752        | 2.5791        | 2.6108        | 11             |
| ARP3                      | 0.4795        | -0.3258        | 0.6396        | 16.6419        | 0.5633        | 14.6573        | 3.8432        | 4.169         | 22             |
| AZCN                      | 0.8142        | -0.0144        | 0.4571        | 24.2496        | 0.4741        | 25.1526        | 1.885         | 1.8994        | 14             |
| BARH                      | 0.6498        | 1.0947         | 1.6049        | 47.4956        | 1.3551        | 40.1042        | 3.379         | 2.2843        | 4              |
| BARN                      | 0.9358        | 0.2447         | 0.4406        | 17.8605        | 0.3746        | 15.1851        | 2.4667        | 2.222         | 23             |
| BIL1                      | 0.7147        | -0.1466        | 0.3504        | 18.782         | 0.3287        | 17.6185        | 1.8656        | 2.0122        | 16             |
| BLKV                      | 0.9553        | 0.0639         | 0.3207        | 10.5313        | 0.3261        | 10.7097        | 3.0449        | 2.981         | 14             |
| BLMM                      | 0.8436        | 0.03           | 0.8229        | 27.0951        | 0.8494        | 27.965         | 3.0372        | 3.0071        | 16             |
| BLRW                      | 0.9055        | -0.3092        | 0.5166        | 17.415         | 0.447         | 15.0698        | 2.9664        | 3.2756        | 7              |
| CCV3                      | 0.8381        | -0.0913        | 0.4546        | 9.2289         | 0.4553        | 9.244          | 4.9259        | 5.0172        | 23             |
| CHA1                      | 0.6602        | -0.1498        | 0.7401        | 17.1312        | 0.7446        | 17.2364        | 4.3202        | 4.47          | 19             |
| CHO1                      | 0.7909        | -0.3431        | 0.5484        | 31.5158        | 0.4418        | 25.3936        | 1.74          | 2.0831        | 16             |
| CLK1                      | 0.8485        | -0.115         | 0.3933        | 14.511         | 0.3846        | 14.1886        | 2.7105        | 2.8255        | 23             |
| CNWM                      | 0.9348        | -0.0121        | 0.4303        | 14.0937        | 0.4426        | 14.4966        | 3.0531        | 3.0652        | 18             |
| COVX                      | 0.9965        | -0.1009        | 0.3763        | 14.0024        | 0.4186        | 15.5759        | 2.6875        | 2.7885        | 4              |
| DQUA                      | 0.7768        | -0.0281        | 0.6029        | 14.809         | 0.6188        | 15.1982        | 4.0713        | 4.0994        | 19             |
| DRV1                      | 0.9454        | -0.2861        | 0.5306        | 14.0992        | 0.4637        | 12.3225        | 3.7631        | 4.0492        | 14             |
| DSRC                      | 0.8334        | 0.2825         | 0.4266        | 21.2324        | 0.3302        | 16.4341        | 2.0094        | 1.7269        | 16             |
| ENG1                      | 0.9232        | -0.0754        | 0.4065        | 8.6713         | 0.4084        | 8.7123         | 4.6875        | 4.7629        | 23             |
| FBYN                      | 0.8991        | 0.0018         | 0.4236        | 12.7894        | 0.4331        | 13.0767        | 3.3123        | 3.3106        | 23             |
| FST1                      | 0.3323        | -0.1582        | 0.8042        | 46.5481        | 0.8143        | 47.1352        | 1.7276        | 1.8858        | 16             |
| GALI                      | 0.7579        | -0.2872        | 0.5226        | 12.2892        | 0.4464        | 10.4984        | 4.2524        | 4.5395        | 23             |
| GDAC                      | 0.9294        | -0.2104        | 0.3525        | 14.6877        | 0.2921        | 12.1712        | 2.4           | 2.6104        | 16             |
| GWEN                      | 0.9358        | -0.2604        | 0.3022        | 19.9054        | 0.1679        | 11.0612        | 1.518         | 1.7784        | 6              |
| HAG1                      | 0.9725        | -0.1276        | 0.2043        | 10.472         | 0.1682        | 8.6217         | 1.951         | 2.0786        | 10             |
| HBRK                      | 0.8806        | -0.0192        | 0.4627        | 15.4348        | 0.4786        | 15.9627        | 2.998         | 3.0172        | 15             |
| HDF1                      | 0.7086        | 0.0661         | 0.5536        | 21.8738        | 0.5625        | 22.2282        | 2.5308        | 2.4646        | 22             |
| HKLO                      | 0.8961        | -0.0234        | 0.5102        | 14.2331        | 0.5217        | 14.5527        | 3.5849        | 3.6083        | 22             |
| HTV1                      | 0.9606        | -0.0419        | 0.3822        | 12.5773        | 0.3916        | 12.8864        | 3.0391        | 3.0809        | 17             |
| HVLK                      | 0.8381        | -0.1679        | 0.4267        | 14.9414        | 0.4084        | 14.2979        | 2.8562        | 3.024         | 13             |
| JTNT                      | 0.8284        | 0.1307         | 0.4282        | 12.6854        | 0.4174        | 12.3648        | 3.3756        | 3.245         | 22             |
| KYW1                      | 0.6794        | -0.0985        | 0.5336        | 10.7649        | 0.5362        | 10.8176        | 4.9564        | 5.055         | 23             |
| LMNO                      | 0.9664        | -0.1307        | 0.2913        | 8.7451         | 0.2702        | 8.1113         | 3.3314        | 3.4621        | 14             |
| LTHM                      | 0.5256        | 0.1473         | 0.6398        | 22.3936        | 0.6725        | 23.5384        | 2.8571        | 2.7099        | 7              |
| MBWW                      | 0.5584        | 0.0613         | 0.39          | 16.9715        | 0.416         | 18.1034        | 2.2979        | 2.2366        | 7              |
| MC01                      | 0.8525        | 0.1718         | 0.4246        | 20.5357        | 0.3974        | 19.2224        | 2.0675        | 1.8958        | 22             |
| MCN1                      | 0.9086        | 0.2283         | 0.5961        | 14.5571        | 0.563         | 13.7492        | 4.0948        | 3.8665        | 23             |
| MOB1                      | 0.899         | -0.022         | 0.4444        | 9.0788         | 0.4543        | 9.281          | 4.895         | 4.9171        | 22             |
| MOR1                      | 0.9014        | -0.0781        | 0.565         | 19.7949        | 0.5727        | 20.0662        | 2.8541        | 2.9323        | 22             |
| MRRN                      | 0.9282        | -0.2188        | 0.4131        | 16.164         | 0.3582        | 14.0173        | 2.5556        | 2.7745        | 23             |
| NDBC                      | 0.9074        | -0.088         | 0.4132        | 8.8585         | 0.4128        | 8.85           | 4.6647        | 4.7527        | 23             |
| NDS1                      | 0.8522        | -0.0689        | 0.5721        | 17.3439        | 0.5807        | 17.6048        | 3.2987        | 3.3676        | 23             |
| NLGN                      | 0.9026        | -0.0734        | 0.3942        | 12.5946        | 0.396         | 12.6525        | 3.1297        | 3.2031        | 23             |
| OKOM                      | 0.9317        | 0.147          | 0.412         | 10.7424        | 0.3954        | 10.3101        | 3.8349        | 3.6879        | 19             |
| PATT                      | 0.7365        | -0.1906        | 0.5436        | 12.707         | 0.5283        | 12.3498        | 4.278         | 4.4686        | 14             |
| PLS1                      | 0.1974        | 0.0067         | 0.5624        | 30.8408        | 0.6074        | 33.3095        | 1.8236        | 1.8168        | 7              |
| PLTC                      | 0.862         | -0.002         | 0.3386        | 15.9971        | 0.3525        | 16.65          | 2.1169        | 2.119         | 13             |
| PNB1                      | 0.7701        | -0.0082        | 0.663         | 27.3686        | 0.6846        | 28.264         | 2.4223        | 2.4305        | 16             |
| PRCO                      | 0.8794        | 0.1563         | 0.5392        | 15.1837        | 0.5311        | 14.9529        | 3.5515        | 3.3952        | 18             |
| RWDN                      | 0.8814        | -0.0646        | 0.39          | 12.7381        | 0.3941        | 12.8725        | 3.0615        | 3.126         | 21             |
| SAV1                      | 0.8499        | 0.2856         | 0.6637        | 15.2689        | 0.6126        | 14.0933        | 4.3468        | 4.0613        | 23             |
| SEAW                      | 0.7213        | -0.0505        | 0.2185        | 9.7347         | 0.2296        | 10.23          | 2.2449        | 2.2954        | 7              |
| SHK1                      | 0.8896        | 0.129          | 0.6904        | 22.7216        | 0.6935        | 22.823         | 3.0387        | 2.9096        | 23             |
| SIO3                      | 0.6573        | -0.8678        | 1.0828        | 47.2726        | 0.6688        | 29.1985        | 2.2906        | 3.1585        | 16             |
| SLAI                      | 0.6081        | -0.0942        | 0.5755        | 23.1239        | 0.6132        | 24.64          | 2.4886        | 2.5827        | 7              |
| SPN1                      | 0.8226        | -0.1303        | 0.319         | 18.9037        | 0.3145        | 18.638         | 1.6874        | 1.8177        | 7              |
| SUM1                      | 0.8769        | 0.1634         | 0.358         | 12.9362        | 0.3257        | 11.7695        | 2.7673        | 2.604         | 23             |
| SYCN                      | 0.9008        | -0.0961        | 0.3717        | 16.8777        | 0.3695        | 16.7772        | 2.2022        | 2.2983        | 18             |
| TCUN                      | 0.8947        | 0.0247         | 0.314         | 12.2037        | 0.3201        | 12.4393        | 2.5733        | 2.5486        | 23             |
| VCIO                      | 0.8339        | 0.002          | 0.469         | 15.1261        | 0.4795        | 15.466         | 3.1004        | 3.0984        | 23             |
| WDLM                      | 0.7246        | -0.224         | 0.6087        | 23.0275        | 0.5787        | 21.8934        | 2.6434        | 2.8674        | 23             |
| WHN1                      | 0.9569        | -0.1323        | 0.283         | 11.2968        | 0.2558        | 10.2108        | 2.5053        | 2.6377        | 23             |
| WLCI                      | 0.7176        | -0.1936        | 0.592         | 25.1243        | 0.5823        | 24.7129        | 2.3564        | 2.55          | 13             |
| WNCI                      | 0.8533        | 0.2546         | 0.625         | 21.0634        | 0.5873        | 19.7939        | 2.9671        | 2.7125        | 18             |
| WNFL                      | 0.846         | 0.1445         | 0.4784        | 11.3258        | 0.4686        | 11.0928        | 4.2242        | 4.0797        | 19             |
| WSMN                      | 0.7381        | 0.236          | 0.4096        | 13.6523        | 0.3512        | 11.7033        | 3.0005        | 2.7644        | 11             |
|                           |               |                |               |                |               |                |               |               |                |
| <b>Means</b>              | <b>0.8149</b> | <b>-0.0316</b> | <b>0.4988</b> | <b>17.6139</b> | <b>0.4760</b> | <b>16.7046</b> | <b>3.0168</b> | <b>3.0484</b> | <b>17.0303</b> |
| <b>Means of n &gt; 10</b> | <b>0.8368</b> | <b>-0.0437</b> |               | <b>16.8166</b> |               | <b>15.9327</b> |               |               | <b>18.9464</b> |



## Appendix C: Location-Specific Statistics

Table C-1-6. CONUS Statistics: 06 UTC Initialization, 21H Forecast

| ID                        | Correlation   | Bias           | RMSE          | RMSE%          | StDev         | %Stdev         | Mean GPS      | Mean MM5      | n              |
|---------------------------|---------------|----------------|---------------|----------------|---------------|----------------|---------------|---------------|----------------|
| ANP1                      | 0.9487        | -0.2232        | 0.3742        | 16.0228        | 0.3126        | 13.3862        | 2.3354        | 2.5586        | 13             |
| ARP3                      | 0.4591        | -0.3424        | 0.6468        | 17.0123        | 0.5611        | 14.7571        | 3.8021        | 4.1445        | 23             |
| AZCN                      | 0.7873        | -0.1299        | 0.4523        | 25.4572        | 0.4475        | 25.1845        | 1.7769        | 1.9068        | 16             |
| BARH                      | 0.86          | 0.2868         | 0.952         | 32.2194        | 1.0149        | 34.3492        | 2.9546        | 2.6678        | 5              |
| BARN                      | 0.8119        | 0.2241         | 0.5612        | 23.1629        | 0.5261        | 21.713         | 2.423         | 2.1989        | 23             |
| BIL1                      | 0.8185        | -0.2129        | 0.3635        | 19.6366        | 0.3043        | 16.4391        | 1.8513        | 2.0641        | 16             |
| BLKV                      | 0.9561        | -0.0772        | 0.3246        | 10.8786        | 0.3272        | 10.9656        | 2.9842        | 3.0614        | 14             |
| BLMM                      | 0.8779        | 0.1862         | 0.7359        | 24.168         | 0.7353        | 24.1481        | 3.0451        | 2.8588        | 16             |
| BLRW                      | 0.8856        | -0.367         | 0.6077        | 20.9624        | 0.5231        | 18.0455        | 2.899         | 3.266         | 7              |
| CCV3                      | 0.7           | -0.0217        | 0.6172        | 12.6527        | 0.6307        | 12.929         | 4.8781        | 4.8998        | 23             |
| CHAI                      | 0.8348        | -0.0407        | 0.7067        | 17.5548        | 0.7221        | 17.9381        | 4.0257        | 4.0664        | 22             |
| CHO1                      | 0.8128        | -0.5086        | 0.6411        | 39.1941        | 0.4031        | 24.6444        | 1.6356        | 2.1442        | 16             |
| CLK1                      | 0.7295        | -0.2488        | 0.5185        | 20.1932        | 0.4651        | 18.1142        | 2.5676        | 2.8164        | 23             |
| CNWM                      | 0.8867        | -0.0625        | 0.5668        | 19.4981        | 0.5807        | 19.9756        | 2.9068        | 2.9693        | 17             |
| COVX                      | 0.9018        | -0.4469        | 0.7546        | 33.7637        | 0.666         | 29.8008        | 2.235         | 2.682         | 6              |
| DQUA                      | 0.8457        | -0.0343        | 0.6251        | 16.7812        | 0.6395        | 17.1697        | 3.7247        | 3.759         | 21             |
| DRV1                      | 0.9475        | -0.0498        | 0.464         | 12.2417        | 0.4787        | 12.6303        | 3.7901        | 3.8399        | 14             |
| DSRC                      | 0.9101        | 0.2101         | 0.3082        | 16.0871        | 0.2329        | 12.1563        | 1.9156        | 1.7056        | 16             |
| ENGI                      | 0.8921        | -0.0238        | 0.4218        | 9.1867         | 0.4306        | 9.3782         | 4.5914        | 4.6153        | 23             |
| FBYN                      | 0.9232        | -0.0714        | 0.3828        | 11.5577        | 0.3846        | 11.6099        | 3.3123        | 3.3837        | 23             |
| FST1                      | 0.5075        | -0.2511        | 0.7298        | 45.4884        | 0.7077        | 44.1119        | 1.6044        | 1.8555        | 16             |
| GAL1                      | 0.6742        | -0.2967        | 0.6085        | 14.4542        | 0.5432        | 12.9028        | 4.2097        | 4.5064        | 23             |
| GDAC                      | 0.8392        | -0.2257        | 0.5212        | 20.9489        | 0.4852        | 19.502         | 2.4881        | 2.7138        | 16             |
| GWEN                      | 0.8967        | -0.3287        | 0.3807        | 26.915         | 0.2075        | 14.6666        | 1.4146        | 1.7433        | 7              |
| HAG1                      | 0.9893        | -0.1233        | 0.1641        | 8.8557         | 0.1141        | 6.1577         | 1.853         | 1.9763        | 10             |
| HBRK                      | 0.9071        | -0.0511        | 0.3982        | 13.6413        | 0.4078        | 13.9723        | 2.9188        | 2.9698        | 16             |
| HDF1                      | 0.8717        | 0.1867         | 0.448         | 17.4484        | 0.4169        | 16.2352        | 2.5678        | 2.3812        | 22             |
| HKLO                      | 0.8573        | -0.2212        | 0.6161        | 18.0565        | 0.5885        | 17.2494        | 3.4119        | 3.6331        | 22             |
| HTV1                      | 0.9637        | -0.1875        | 0.4353        | 15.483         | 0.4042        | 14.3784        | 2.8115        | 2.999         | 18             |
| HVLK                      | 0.8664        | -0.0933        | 0.4403        | 14.9982        | 0.4478        | 15.2561        | 2.9354        | 3.0287        | 13             |
| JTNT                      | 0.8019        | 0.0933         | 0.4673        | 14.2691        | 0.4682        | 14.2961        | 3.2747        | 3.1814        | 23             |
| KYW1                      | 0.6774        | -0.0747        | 0.5194        | 10.6541        | 0.5256        | 10.7805        | 4.8753        | 4.9499        | 23             |
| LMNO                      | 0.9675        | -0.0721        | 0.2706        | 8.1947         | 0.27          | 8.1755         | 3.3027        | 3.3748        | 15             |
| LTHM                      | 0.6319        | 0.0203         | 0.5109        | 19.481         | 0.5457        | 20.8096        | 2.6225        | 2.6022        | 8              |
| MBWW                      | 0.0924        | 0.2227         | 0.4548        | 18.8097        | 0.4283        | 17.714         | 2.4179        | 2.1951        | 7              |
| MC01                      | 0.8464        | 0.1215         | 0.4392        | 21.2047        | 0.432         | 20.8567        | 2.0714        | 1.9499        | 22             |
| MCN1                      | 0.9031        | 0.2248         | 0.5818        | 14.593         | 0.5486        | 13.7615        | 3.9866        | 3.7617        | 23             |
| MOB1                      | 0.847         | 0.0759         | 0.5305        | 11.0382        | 0.5368        | 11.1701        | 4.806         | 4.7301        | 23             |
| MOR1                      | 0.8685        | 0.1375         | 0.7835        | 25.8429        | 0.7886        | 26.0138        | 3.0317        | 2.8942        | 23             |
| MRRN                      | 0.9444        | -0.1765        | 0.3458        | 13.349         | 0.304         | 11.7372        | 2.5901        | 2.7666        | 23             |
| NDBC                      | 0.8774        | -0.0378        | 0.4386        | 9.5606         | 0.4468        | 9.7391         | 4.5879        | 4.6257        | 23             |
| NDS1                      | 0.8663        | -0.0949        | 0.5522        | 16.9636        | 0.5562        | 17.087         | 3.2551        | 3.35          | 23             |
| NLGN                      | 0.8606        | -0.1385        | 0.4861        | 15.9103        | 0.4764        | 15.5932        | 3.0554        | 3.194         | 23             |
| OKOM                      | 0.9138        | 0.1486         | 0.4701        | 12.4706        | 0.4583        | 12.1556        | 3.7699        | 3.6214        | 19             |
| PATT                      | 0.7735        | -0.1092        | 0.4685        | 11.3997        | 0.4728        | 11.504         | 4.11          | 4.2192        | 14             |
| PLS1                      | 0.6322        | -0.0956        | 0.4477        | 25.6466        | 0.4724        | 27.0623        | 1.7456        | 1.8412        | 7              |
| PLTC                      | 0.9262        | -0.1075        | 0.2743        | 13.6273        | 0.2606        | 12.9481        | 2.0125        | 2.12          | 16             |
| PNB1                      | 0.9469        | -0.2384        | 0.4044        | 17.9327        | 0.3374        | 14.9608        | 2.2551        | 2.4935        | 16             |
| PRCO                      | 0.8372        | 0.0681         | 0.5706        | 16.7032        | 0.5829        | 17.0645        | 3.4161        | 3.348         | 18             |
| RWDN                      | 0.9245        | -0.041         | 0.3094        | 10.2188        | 0.3143        | 10.3789        | 3.0279        | 3.0689        | 21             |
| SAV1                      | 0.8319        | 0.218          | 0.7138        | 17.3286        | 0.695         | 16.8717        | 4.1193        | 3.9014        | 23             |
| SEAW                      | 0.4226        | -0.1038        | 0.3512        | 16.2336        | 0.3625        | 16.7514        | 2.1637        | 2.2675        | 7              |
| SHK1                      | 0.8896        | -0.01          | 0.5915        | 20.3565        | 0.6047        | 20.8111        | 2.9057        | 2.9156        | 23             |
| SIO3                      | 0.5987        | -0.9514        | 1.1674        | 53.9522        | 0.6987        | 32.2913        | 2.1637        | 3.1151        | 16             |
| SLAI                      | 0.4376        | -0.2154        | 0.8069        | 32.6661        | 0.8399        | 34.0032        | 2.47          | 2.6854        | 7              |
| SPN1                      | 0.5706        | -0.1145        | 0.3427        | 20.9878        | 0.3488        | 21.3654        | 1.6327        | 1.7473        | 7              |
| SUM1                      | 0.9132        | 0.157          | 0.3162        | 11.5515        | 0.2806        | 10.2511        | 2.737         | 2.58          | 23             |
| SYCN                      | 0.8394        | -0.0778        | 0.4771        | 21.4801        | 0.4843        | 21.8067        | 2.2209        | 2.2988        | 18             |
| TCUN                      | 0.8902        | 0.0829         | 0.3385        | 12.8406        | 0.3359        | 12.7423        | 2.6364        | 2.5534        | 22             |
| VCIO                      | 0.8812        | 0.0055         | 0.417         | 13.4435        | 0.4263        | 13.7445        | 3.1017        | 3.0963        | 23             |
| WDLM                      | 0.746         | -0.2196        | 0.5602        | 21.8283        | 0.527         | 20.533         | 2.5664        | 2.786         | 23             |
| WHN1                      | 0.8808        | -0.0218        | 0.4202        | 16.0802        | 0.4291        | 16.4194        | 2.6132        | 2.635         | 23             |
| WLCI                      | 0.7736        | -0.2769        | 0.6397        | 28.2083        | 0.6002        | 26.4665        | 2.2678        | 2.5447        | 13             |
| WNCI                      | 0.8456        | 0.1026         | 0.5633        | 19.6502        | 0.5709        | 19.9161        | 2.8666        | 2.764         | 17             |
| WNFL                      | 0.7853        | 0.1133         | 0.6214        | 15.1181        | 0.6277        | 15.272         | 4.1102        | 3.9969        | 19             |
| WSMN                      | 0.6562        | 0.1778         | 0.4245        | 14.363         | 0.4063        | 13.7474        | 2.9553        | 2.7775        | 10             |
| <b>Means</b>              | <b>0.8070</b> | <b>-0.0720</b> | <b>0.5128</b> | <b>18.7648</b> | <b>0.4875</b> | <b>17.5238</b> | <b>2.9336</b> | <b>3.0056</b> | <b>17.3333</b> |
| <b>Means of n &gt; 10</b> | <b>0.8381</b> | <b>-0.0645</b> |               | <b>17.6927</b> |               | <b>16.4643</b> |               |               | <b>19.2143</b> |

## Appendix C: Location-Specific Statistics

Table C-1-7. CONUS Statistics: 06 UTC Initialization, 24H Forecast

| ID                        | Correlation   | Bias           | RMSE          | RMSE%          | StDev         | %Stdev         | Mean GPS      | Mean MM5      | n              |
|---------------------------|---------------|----------------|---------------|----------------|---------------|----------------|---------------|---------------|----------------|
| ANP1                      | 0.9418        | -0.073         | 0.2945        | 12.7945        | 0.2969        | 12.9014        | 2.3015        | 2.3745        | 13             |
| ARP3                      | 0.4452        | -0.3053        | 0.6083        | 15.5779        | 0.5379        | 13.7766        | 3.9047        | 4.21          | 23             |
| AZCN                      | 0.7543        | -0.1162        | 0.4981        | 27.3457        | 0.5013        | 27.5243        | 1.8213        | 1.9375        | 15             |
| BARH                      | 0.8535        | 0.0204         | 0.9595        | 34.2791        | 1.0725        | 38.3166        | 2.799         | 2.7786        | 5              |
| BARN                      | 0.9172        | 0.2154         | 0.3928        | 16.9757        | 0.3359        | 14.5144        | 2.314         | 2.0985        | 23             |
| BIL1                      | 0.7753        | -0.2055        | 0.363         | 19.3157        | 0.3091        | 16.4444        | 1.8794        | 2.0849        | 16             |
| BLKV                      | 0.9576        | 0.0541         | 0.3017        | 9.7844         | 0.3081        | 9.989          | 3.084         | 3.0299        | 14             |
| BLMM                      | 0.8948        | 0.2319         | 0.7288        | 23.3451        | 0.7136        | 22.8573        | 3.1218        | 2.8899        | 16             |
| BLRW                      | 0.9552        | -0.3965        | 0.5176        | 17.6597        | 0.3594        | 12.2607        | 2.931         | 3.3275        | 7              |
| CCV3                      | 0.7577        | 0.008          | 0.5426        | 11.1426        | 0.5547        | 11.3918        | 4.8695        | 4.8616        | 23             |
| CHA1                      | 0.8381        | -0.0365        | 0.6565        | 16.5721        | 0.6709        | 16.9359        | 3.9615        | 3.9979        | 22             |
| CHO1                      | 0.8224        | -0.4755        | 0.6112        | 35.2421        | 0.3967        | 22.8725        | 1.7344        | 2.2098        | 16             |
| CLK1                      | 0.6936        | -0.2431        | 0.5287        | 20.7382        | 0.4801        | 18.8298        | 2.5494        | 2.7925        | 23             |
| CNWM                      | 0.904         | -0.012         | 0.51          | 17.3895        | 0.5239        | 17.8611        | 2.9329        | 2.9449        | 19             |
| COVX                      | 0.9869        | -0.4806        | 0.5856        | 25.6858        | 0.3741        | 16.409         | 2.28          | 2.7606        | 5              |
| DQUA                      | 0.8353        | -0.0165        | 0.5979        | 16.2173        | 0.6111        | 16.5754        | 3.6867        | 3.7032        | 23             |
| DRV1                      | 0.9252        | 0.027          | 0.5078        | 13.3218        | 0.5263        | 13.805         | 3.8121        | 3.785         | 14             |
| DSRC                      | 0.8641        | 0.1479         | 0.3167        | 17.8108        | 0.2892        | 16.2663        | 1.7781        | 1.6302        | 16             |
| ENG1                      | 0.915         | -0.0963        | 0.3834        | 8.4369         | 0.3794        | 8.3499         | 4.544         | 4.6403        | 23             |
| FBYN                      | 0.8821        | -0.2231        | 0.5147        | 15.9575        | 0.4742        | 14.703         | 3.2253        | 3.4485        | 23             |
| FST1                      | 0.5795        | -0.2966        | 0.688         | 46.3942        | 0.6411        | 43.2331        | 1.483         | 1.7796        | 16             |
| GAL1                      | 0.5813        | -0.2984        | 0.6534        | 15.7297        | 0.5944        | 14.3078        | 4.154         | 4.4525        | 23             |
| GDAC                      | 0.8171        | -0.2633        | 0.5377        | 22.0258        | 0.4842        | 19.8332        | 2.4413        | 2.7046        | 16             |
| GWEN                      | 0.706         | -0.3296        | 0.5025        | 32.9191        | 0.4156        | 27.2235        | 1.5265        | 1.8561        | 6              |
| HAG1                      | 0.9765        | -0.0345        | 0.2404        | 10.9632        | 0.2495        | 11.3793        | 2.1927        | 2.2272        | 11             |
| HBRK                      | 0.8337        | -0.0693        | 0.4719        | 16.0642        | 0.4831        | 16.4478        | 2.9373        | 3.0066        | 15             |
| HDF1                      | 0.8546        | 0.2228         | 0.4976        | 19.0325        | 0.4559        | 17.4384        | 2.6143        | 2.3916        | 21             |
| HKLO                      | 0.8284        | -0.3083        | 0.7221        | 21.6961        | 0.6683        | 20.0805        | 3.3283        | 3.6366        | 22             |
| HTV1                      | 0.923         | -0.1116        | 0.5466        | 19.4557        | 0.5506        | 19.5983        | 2.8094        | 2.921         | 18             |
| HVLK                      | 0.8874        | -0.1596        | 0.4435        | 15.1563        | 0.4307        | 14.719         | 2.9262        | 3.0857        | 13             |
| JTNT                      | 0.7376        | 0.1826         | 0.5221        | 15.8737        | 0.5001        | 15.2056        | 3.2892        | 3.1066        | 23             |
| KYWI                      | 0.5931        | -0.0116        | 0.5884        | 12.1213        | 0.6015        | 12.3913        | 4.8543        | 4.8659        | 23             |
| LMNO                      | 0.9659        | -0.026         | 0.269         | 8.2438         | 0.2778        | 8.5149         | 3.2629        | 3.2889        | 14             |
| LTHM                      | 0.4474        | -0.0728        | 0.6259        | 25.0104        | 0.6646        | 26.5556        | 2.5025        | 2.5753        | 8              |
| MBWW                      | 0.8751        | 0.2244         | 0.3           | 12.3337        | 0.215         | 8.8386         | 2.4321        | 2.2077        | 7              |
| MC01                      | 0.8645        | 0.1245         | 0.395         | 19.0399        | 0.3845        | 18.5378        | 2.0743        | 1.9498        | 20             |
| MCN1                      | 0.9109        | 0.2678         | 0.5966        | 15.0377        | 0.545         | 13.7389        | 3.9671        | 3.6993        | 23             |
| MOB1                      | 0.8876        | 0.2363         | 0.5072        | 10.5076        | 0.4589        | 9.5064         | 4.8272        | 4.5909        | 23             |
| MOR1                      | 0.8632        | 0.0916         | 0.7171        | 24.541         | 0.7272        | 24.8868        | 2.922         | 2.8304        | 23             |
| MRRN                      | 0.9029        | -0.29          | 0.5004        | 19.7677        | 0.417         | 16.4731        | 2.5316        | 2.8216        | 23             |
| NDBC                      | 0.8643        | -0.0271        | 0.4656        | 10.216         | 0.4753        | 10.4279        | 4.558         | 4.5851        | 23             |
| NDS1                      | 0.8505        | -0.1213        | 0.5741        | 17.6239        | 0.5738        | 17.6135        | 3.2578        | 3.3791        | 23             |
| NLGN                      | 0.8146        | -0.1201        | 0.5302        | 17.3554        | 0.528         | 17.2843        | 3.0548        | 3.1749        | 23             |
| OKOM                      | 0.8419        | 0.252          | 0.6681        | 17.5575        | 0.6357        | 16.7062        | 3.8051        | 3.5531        | 19             |
| PATT                      | 0.6088        | -0.0291        | 0.6786        | 16.6427        | 0.7036        | 17.2552        | 4.0777        | 4.1068        | 14             |
| PLS1                      | 0.7205        | -0.1502        | 0.4714        | 29.2868        | 0.4826        | 29.9843        | 1.6094        | 1.7596        | 7              |
| PLTC                      | 0.8372        | -0.1735        | 0.3663        | 19.5234        | 0.3332        | 17.7592        | 1.8763        | 2.0497        | 16             |
| PNB1                      | 0.9443        | -0.3524        | 0.5097        | 22.9217        | 0.3803        | 17.1031        | 2.2237        | 2.5761        | 16             |
| PRCO                      | 0.7331        | 0.0876         | 0.657         | 19.3187        | 0.6657        | 19.5764        | 3.4007        | 3.3131        | 23             |
| RWDN                      | 0.8574        | -0.1418        | 0.4633        | 15.6303        | 0.4514        | 15.2308        | 2.964         | 3.1058        | 22             |
| SAV1                      | 0.8979        | 0.2796         | 0.5787        | 13.9197        | 0.518         | 12.4605        | 4.1574        | 3.8778        | 23             |
| SEAW                      | 0.5466        | 0.0152         | 0.2291        | 10.3029        | 0.2469        | 11.104         | 2.2234        | 2.2083        | 7              |
| SHK1                      | 0.9338        | 0.0701         | 0.5665        | 19.8775        | 0.5753        | 20.1888        | 2.8498        | 2.7797        | 22             |
| SIO3                      | 0.5626        | -0.824         | 1.0684        | 47.5779        | 0.7024        | 31.2793        | 2.2456        | 3.0696        | 16             |
| SLAI                      | 0.598         | -0.2458        | 0.5545        | 22.8729        | 0.5369        | 22.1457        | 2.4243        | 2.6701        | 7              |
| SPN1                      | 0.5464        | -0.1848        | 0.4           | 25.8988        | 0.3831        | 24.8102        | 1.5443        | 1.729         | 7              |
| SUM1                      | 0.9155        | 0.1577         | 0.3146        | 11.3747        | 0.2784        | 10.0651        | 2.7661        | 2.6085        | 23             |
| SYCN                      | 0.811         | -0.0217        | 0.4985        | 22.0568        | 0.5133        | 22.7141        | 2.2599        | 2.2816        | 17             |
| TCUN                      | 0.881         | 0.0258         | 0.3223        | 11.9123        | 0.3288        | 12.1535        | 2.7056        | 2.6798        | 22             |
| VCIO                      | 0.8542        | 0.0502         | 0.4583        | 14.9663        | 0.4668        | 15.2435        | 3.062         | 3.0118        | 21             |
| WDLM                      | 0.6584        | -0.2377        | 0.5912        | 24.1153        | 0.5535        | 22.5766        | 2.4517        | 2.6894        | 23             |
| WHN1                      | 0.9149        | -0.0921        | 0.3714        | 14.554         | 0.3678        | 14.4158        | 2.5517        | 2.6438        | 23             |
| WLCI                      | 0.8371        | -0.3241        | 0.669         | 29.934         | 0.6092        | 27.2576        | 2.2351        | 2.5591        | 13             |
| WNCI                      | 0.7983        | -0.013         | 0.5574        | 20.8785        | 0.5734        | 21.4779        | 2.6698        | 2.6828        | 18             |
| WNFL                      | 0.9023        | 0.0194         | 0.4392        | 10.881         | 0.4508        | 11.1683        | 4.0366        | 4.0173        | 19             |
| WSMN                      | 0.6927        | 0.1523         | 0.3918        | 12.8893        | 0.3805        | 12.5174        | 3.0394        | 2.8871        | 10             |
| <b>Means</b>              | <b>0.8088</b> | <b>-0.0734</b> | <b>0.5173</b> | <b>19.0545</b> | <b>0.4878</b> | <b>17.7578</b> | <b>2.9190</b> | <b>2.9925</b> | <b>17.3333</b> |
| <b>Means of n &gt; 10</b> | <b>0.8240</b> | <b>-0.0580</b> |               | <b>18.2383</b> |               | <b>17.0422</b> |               |               | <b>19.2500</b> |

### Appendix C: Location-Specific Statistics

Table C-1-8. CONUS Statistics: 18 UTC Initialization, 06H Forecast

| ID                  | Correlation   | Bias           | RMSE          | RMSE%          | StDev         | %Stdev         | Mean GPS      | Mean MM5      | n              |
|---------------------|---------------|----------------|---------------|----------------|---------------|----------------|---------------|---------------|----------------|
| ANP1                | 0.9851        | -0.2339        | 0.3087        | 11.8692        | 0.2104        | 8.0883         | 2.6008        | 2.8348        | 12             |
| ARP3                | 0.5991        | -0.6407        | 0.8151        | 20.9456        | 0.5157        | 13.2521        | 3.8914        | 4.5321        | 22             |
| AZCN                | 0.9359        | -0.0457        | 0.2771        | 14.853         | 0.2828        | 15.1635        | 1.8653        | 1.9111        | 15             |
| BARH                | 0.6453        | 0.7944         | 1.6043        | 47.4772        | 1.6093        | 47.6277        | 3.379         | 2.5845        | 4              |
| BARN                | 0.927         | -0.0094        | 0.3486        | 14.4648        | 0.3563        | 14.7846        | 2.41          | 2.4194        | 23             |
| BIL1                | 0.7193        | -0.2086        | 0.3854        | 20.5491        | 0.334         | 17.8092        | 1.8753        | 2.0839        | 17             |
| BLKV                | 0.9513        | -0.4537        | 0.557         | 18.2777        | 0.3353        | 11.0024        | 3.0474        | 3.5011        | 14             |
| BLMM                | 0.9324        | -0.2873        | 0.6141        | 20.0238        | 0.5595        | 18.2417        | 3.0669        | 3.3542        | 17             |
| BLRW                | 0.8336        | -0.4084        | 0.7711        | 26.8577        | 0.7164        | 24.9549        | 2.8707        | 3.2791        | 6              |
| CCV3                | 0.8916        | -0.2556        | 0.4526        | 9.1249         | 0.382         | 7.7003         | 4.9605        | 5.2161        | 23             |
| CHA1                | 0.8535        | -0.4267        | 0.6505        | 15.4606        | 0.5044        | 11.9896        | 4.2072        | 4.6338        | 19             |
| CHO1                | 0.6998        | -0.1788        | 0.5413        | 32.1547        | 0.5267        | 31.2851        | 1.6835        | 1.8623        | 17             |
| CLK1                | 0.8909        | -0.1718        | 0.3427        | 12.675         | 0.3032        | 11.2141        | 2.704         | 2.8758        | 23             |
| CNWM                | 0.963         | -0.2433        | 0.4098        | 13.1005        | 0.3389        | 10.8319        | 3.1284        | 3.3716        | 19             |
| COVX                | 0.9929        | -0.2955        | 0.3405        | 12.6705        | 0.1953        | 7.2684         | 2.6875        | 2.983         | 4              |
| DQUA                | 0.9354        | -0.4026        | 0.517         | 12.6832        | 0.3328        | 8.1638         | 4.0766        | 4.4792        | 20             |
| DRV1                | 0.9622        | -0.4324        | 0.5553        | 15.1765        | 0.3616        | 9.8818         | 3.6591        | 4.0915        | 14             |
| DSRC                | 0.8639        | 0.1528         | 0.3198        | 15.8729        | 0.2896        | 14.3728        | 2.0147        | 1.8619        | 17             |
| ENG1                | 0.9111        | -0.3063        | 0.5147        | 10.766         | 0.4229        | 8.8463         | 4.7804        | 5.0867        | 23             |
| FBYN                | 0.8787        | -0.1457        | 0.4997        | 15.335         | 0.4887        | 14.9988        | 3.2585        | 3.4042        | 23             |
| FST1                | 0.3986        | -0.0787        | 0.7434        | 43.4463        | 0.762         | 44.5317        | 1.7111        | 1.7898        | 17             |
| GAL1                | 0.7709        | -0.4067        | 0.5979        | 13.9345        | 0.4481        | 10.4442        | 4.2907        | 4.6973        | 23             |
| GDAC                | 0.927         | -0.4159        | 0.4956        | 20.553         | 0.2777        | 11.5176        | 2.4112        | 2.8271        | 17             |
| GWEN                | 0.6633        | -0.6225        | 0.6902        | 41.6838        | 0.3332        | 20.1236        | 1.6558        | 2.2783        | 5              |
| HAG1                | 0.916         | -0.3361        | 0.4954        | 25.3941        | 0.3837        | 19.6658        | 1.951         | 2.2871        | 10             |
| HBRK                | 0.8694        | -0.1327        | 0.4728        | 15.7133        | 0.4686        | 15.5759        | 3.0088        | 3.1415        | 16             |
| HDF1                | 0.7467        | -0.1531        | 0.5467        | 22.3559        | 0.5371        | 21.9661        | 2.4453        | 2.5984        | 22             |
| HKLO                | 0.9327        | -0.3246        | 0.5408        | 14.7022        | 0.4427        | 12.0356        | 3.6785        | 4.0031        | 22             |
| HTV1                | 0.939         | -0.3854        | 0.5806        | 19.6329        | 0.4477        | 15.1369        | 2.9574        | 3.3428        | 17             |
| HVLK                | 0.9168        | -0.3182        | 0.463         | 16.1003        | 0.349         | 12.1377        | 2.8757        | 3.1939        | 14             |
| JTNT                | 0.8228        | -0.0977        | 0.4368        | 12.6493        | 0.4358        | 12.619         | 3.4534        | 3.5511        | 22             |
| KYW1                | 0.7837        | -0.2225        | 0.5055        | 10.2905        | 0.4642        | 9.4483         | 4.9128        | 5.1352        | 23             |
| LMNO                | 0.9491        | -0.401         | 0.5053        | 15.045         | 0.3182        | 9.474          | 3.3587        | 3.7597        | 15             |
| LTHM                | 0.7562        | 0.0419         | 0.6098        | 19.6327        | 0.6504        | 20.9387        | 3.1063        | 3.0644        | 8              |
| MBWW                | 0.3581        | -0.3075        | 0.3669        | 16.5394        | 0.2192        | 9.8806         | 2.2182        | 2.5257        | 6              |
| MC01                | 0.8701        | -0.025         | 0.3474        | 16.7996        | 0.3543        | 17.1328        | 2.0679        | 2.0929        | 23             |
| MCN1                | 0.9553        | -0.1879        | 0.43          | 10.6462        | 0.3955        | 9.7917         | 4.039         | 4.2269        | 23             |
| MOB1                | 0.9318        | -0.1607        | 0.3849        | 7.8524         | 0.358         | 7.3031         | 4.9021        | 5.0628        | 22             |
| MOR1                | 0.9819        | -0.3402        | 0.428         | 15.4421        | 0.2658        | 9.5913         | 2.7714        | 3.1116        | 22             |
| MRRN                | 0.9301        | -0.3062        | 0.4549        | 18.1758        | 0.344         | 13.743         | 2.503         | 2.8092        | 23             |
| NDBC                | 0.9333        | -0.322         | 0.4732        | 9.9921         | 0.3546        | 7.487          | 4.7356        | 5.0575        | 23             |
| NDS1                | 0.8757        | -0.3967        | 0.6867        | 20.525         | 0.5731        | 17.1306        | 3.3455        | 3.7422        | 23             |
| NLGN                | 0.8998        | -0.2677        | 0.5003        | 16.4173        | 0.4321        | 14.1809        | 3.0473        | 3.315         | 23             |
| OKOM                | 0.9262        | -0.1635        | 0.4265        | 11.4279        | 0.4047        | 10.8441        | 3.7323        | 3.8958        | 19             |
| PATT                | 0.8892        | -0.4225        | 0.5162        | 12.0817        | 0.3078        | 7.2033         | 4.2725        | 4.695         | 14             |
| PLS1                | 0.2974        | -0.0738        | 0.4702        | 25.3113        | 0.5087        | 27.383         | 1.8577        | 1.9315        | 6              |
| PLTC                | 0.8454        | -0.0968        | 0.3478        | 16.4167        | 0.3467        | 16.3639        | 2.1186        | 2.2153        | 14             |
| PNB1                | 0.8402        | -0.1857        | 0.6208        | 26.0278        | 0.6106        | 25.6002        | 2.3852        | 2.571         | 17             |
| PRCO                | 0.9347        | -0.2447        | 0.5092        | 13.8133        | 0.4595        | 12.4653        | 3.686         | 3.9307        | 18             |
| RWDN                | 0.8961        | -0.2737        | 0.4644        | 15.5444        | 0.3845        | 12.869         | 2.9879        | 3.2615        | 21             |
| SAV1                | 0.9265        | -0.1613        | 0.4676        | 10.7912        | 0.4488        | 10.3568        | 4.3336        | 4.4949        | 23             |
| SEAW                | 0.6095        | -0.0407        | 0.2309        | 10.3933        | 0.249         | 11.2067        | 2.2217        | 2.2624        | 6              |
| SHK1                | 0.9882        | -0.2634        | 0.3411        | 11.4436        | 0.2217        | 7.4359         | 2.9809        | 3.2443        | 23             |
| SIO3                | 0.7017        | -0.6364        | 0.8402        | 36.1682        | 0.5654        | 24.3393        | 2.3229        | 2.9594        | 17             |
| SLAI                | 0.93          | -0.179         | 0.3633        | 13.735         | 0.3379        | 12.7767        | 2.645         | 2.824         | 8              |
| SPN1                | 0.6929        | -0.3136        | 0.5197        | 30.1421        | 0.4539        | 26.3276        | 1.7242        | 2.0378        | 6              |
| SUM1                | 0.9014        | -0.1354        | 0.3274        | 11.6341        | 0.3048        | 10.831         | 2.8145        | 2.9499        | 23             |
| SYCN                | 0.8682        | -0.1103        | 0.4262        | 19.4783        | 0.4229        | 19.3297        | 2.188         | 2.2983        | 19             |
| TCUN                | 0.9253        | -0.1806        | 0.328         | 12.5899        | 0.28          | 10.7462        | 2.6057        | 2.7863        | 23             |
| VCIO                | 0.8655        | -0.3872        | 0.6052        | 19.3206        | 0.4756        | 15.1832        | 3.1322        | 3.5194        | 23             |
| WDLM                | 0.8046        | -0.2246        | 0.5153        | 19.4945        | 0.4742        | 17.9398        | 2.6433        | 2.8679        | 23             |
| WHN1                | 0.9425        | -0.2461        | 0.3971        | 16.0733        | 0.3187        | 12.8988        | 2.4708        | 2.7169        | 23             |
| WLCI                | 0.7076        | -0.422         | 0.7531        | 31.0331        | 0.6474        | 26.6756        | 2.4269        | 2.8488        | 14             |
| WNC1                | 0.9307        | -0.122         | 0.423         | 13.8825        | 0.4161        | 13.6564        | 3.0467        | 3.1687        | 19             |
| WNFL                | 0.7852        | -0.3084        | 0.5373        | 12.7973        | 0.4521        | 10.7668        | 4.1986        | 4.507         | 19             |
| WSMN                | 0.8504        | -0.0982        | 0.2546        | 8.4173         | 0.2453        | 8.1108         | 3.0248        | 3.1231        | 12             |
| <b>Mean</b>         | <b>0.8418</b> | <b>-0.2372</b> | <b>0.5040</b> | <b>17.9073</b> | <b>0.4245</b> | <b>15.1613</b> | <b>3.0217</b> | <b>3.2589</b> | <b>17.2879</b> |
| <b>Mean n&gt;10</b> | <b>0.8711</b> | <b>-0.2545</b> | <b>0.5040</b> | <b>16.7399</b> | <b>0.4245</b> | <b>14.1456</b> | <b>3.0217</b> | <b>3.2589</b> | <b>19.3214</b> |

## Appendix C: Location-Specific Statistics

Table C-1-9. CONUS Statistics: 18 UTC Initialization, 09H Forecast

| ID                  | Correlation   | Bias           | RMSE          | RMSE%          | StDev         | %Stdev         | Mean GPS      | Mean MMS      | n              |
|---------------------|---------------|----------------|---------------|----------------|---------------|----------------|---------------|---------------|----------------|
| ANP1                | 0.9427        | -0.3875        | 0.5279        | 22.4854        | 0.372         | 15.846         | 2.3479        | 2.7354        | 14             |
| ARP3                | 0.5654        | -0.5785        | 0.7694        | 20.014         | 0.5187        | 13.4915        | 3.8445        | 4.423         | 23             |
| AZCN                | 0.8988        | -0.1652        | 0.3432        | 19.5218        | 0.3101        | 17.6376        | 1.7582        | 1.9235        | 17             |
| BARH                | 0.8751        | 0.3432         | 0.8771        | 31.7192        | 0.8842        | 31.9762        | 2.7653        | 2.4221        | 6              |
| BARN                | 0.8359        | 0.0741         | 0.4809        | 20.2633        | 0.4858        | 20.4715        | 2.3732        | 2.2991        | 23             |
| BIL1                | 0.8461        | -0.2011        | 0.3132        | 16.7624        | 0.2474        | 13.2447        | 1.8682        | 2.0693        | 17             |
| BLKV                | 0.9156        | -0.3872        | 0.5774        | 19.1156        | 0.4446        | 14.7175        | 3.0208        | 3.408         | 14             |
| BLMM                | 0.9541        | -0.3043        | 0.5222        | 16.8844        | 0.4374        | 14.1427        | 3.0925        | 3.3968        | 17             |
| BLRW                | 0.9748        | -0.6395        | 0.8295        | 30.1298        | 0.5788        | 21.0245        | 2.7532        | 3.3926        | 6              |
| CCV3                | 0.7874        | -0.2576        | 0.5869        | 11.9313        | 0.5392        | 10.9613        | 4.9192        | 5.1769        | 23             |
| CHA1                | 0.9254        | -0.3435        | 0.6007        | 15.3524        | 0.5044        | 12.8904        | 3.9129        | 4.2565        | 22             |
| CHO1                | 0.76          | -0.4138        | 0.6067        | 38.3125        | 0.4573        | 28.8775        | 1.5835        | 1.9974        | 17             |
| CLK1                | 0.8431        | -0.2701        | 0.4153        | 16.151         | 0.3226        | 12.5435        | 2.5715        | 2.8417        | 23             |
| CNWM                | 0.942         | -0.2701        | 0.5066        | 16.7765        | 0.4411        | 14.6055        | 3.0199        | 3.29          | 18             |
| COVX                | 0.911         | -0.4817        | 0.707         | 31.6347        | 0.567         | 25.3671        | 2.235         | 2.7167        | 6              |
| DQUA                | 0.9626        | -0.3407        | 0.4656        | 12.4008        | 0.3256        | 8.6726         | 3.7543        | 4.095         | 20             |
| DRV1                | 0.9847        | -0.3101        | 0.43          | 11.6505        | 0.3092        | 8.3769         | 3.6912        | 4.0013        | 14             |
| DSRC                | 0.8829        | 0.1419         | 0.2856        | 14.7504        | 0.2555        | 13.1946        | 1.9365        | 1.7945        | 17             |
| ENG1                | 0.9162        | -0.272         | 0.4616        | 9.9324         | 0.3813        | 8.2047         | 4.6477        | 4.9197        | 23             |
| FBYN                | 0.9065        | -0.1971        | 0.4736        | 14.7049        | 0.4403        | 13.6717        | 3.2208        | 3.4179        | 23             |
| FST1                | 0.5515        | -0.1234        | 0.6374        | 39.7999        | 0.6446        | 40.2489        | 1.6015        | 1.7249        | 17             |
| GAL1                | 0.8207        | -0.356         | 0.5272        | 12.4189        | 0.3976        | 9.3665         | 4.245         | 4.601         | 23             |
| GDAC                | 0.7867        | -0.2133        | 0.5637        | 22.4358        | 0.5378        | 21.4061        | 2.5124        | 2.7257        | 17             |
| GWEN                | 0.7289        | -0.5756        | 0.6238        | 41.3183        | 0.2636        | 17.4607        | 1.5098        | 2.0854        | 6              |
| HAG1                | 0.9904        | -0.2985        | 0.3384        | 18.2614        | 0.1681        | 9.0696         | 1.853         | 2.1515        | 10             |
| HBRK                | 0.8611        | -0.0947        | 0.4583        | 15.6151        | 0.4622        | 15.7483        | 2.9347        | 3.0294        | 17             |
| HDF1                | 0.8901        | -0.0406        | 0.3833        | 15.303         | 0.3901        | 15.575         | 2.5045        | 2.5451        | 22             |
| HKLO                | 0.8886        | -0.4677        | 0.7095        | 20.5652        | 0.5467        | 15.8463        | 3.45          | 3.9176        | 21             |
| HTV1                | 0.9225        | -0.4386        | 0.6304        | 23.1409        | 0.466         | 17.1049        | 2.7241        | 3.1627        | 18             |
| HVLK                | 0.9178        | -0.2245        | 0.4025        | 13.6178        | 0.3467        | 11.7293        | 2.9557        | 3.1802        | 14             |
| JTNT                | 0.8104        | -0.1676        | 0.4715        | 14.1319        | 0.4506        | 13.5055        | 3.3361        | 3.5037        | 23             |
| KYW1                | 0.704         | -0.1915        | 0.5523        | 11.4574        | 0.5297        | 10.9881        | 4.8207        | 5.0122        | 23             |
| LMNO                | 0.9189        | -0.2495        | 0.4637        | 14.0663        | 0.4036        | 12.2451        | 3.2963        | 3.5457        | 16             |
| LTHM                | 0.6165        | -0.1365        | 0.5198        | 19.6323        | 0.532         | 20.0921        | 2.6478        | 2.7843        | 9              |
| MBWW                | 0.126         | 0.1558         | 0.3633        | 15.0645        | 0.3595        | 14.9073        | 2.4115        | 2.2557        | 6              |
| MC01                | 0.8147        | 0.031          | 0.4328        | 20.9577        | 0.4413        | 21.3739        | 2.0649        | 2.0339        | 23             |
| MCN1                | 0.9281        | -0.1919        | 0.5075        | 12.8277        | 0.4804        | 12.1425        | 3.9566        | 4.1484        | 23             |
| MOB1                | 0.8609        | -0.1322        | 0.5186        | 10.8035        | 0.5127        | 10.6813        | 4.8002        | 4.9324        | 23             |
| MOR1                | 0.9827        | -0.2087        | 0.3506        | 11.9053        | 0.2881        | 9.7814         | 2.945         | 3.1537        | 23             |
| MRRN                | 0.9182        | -0.2602        | 0.4383        | 17.5225        | 0.3606        | 14.4158        | 2.5012        | 2.7615        | 23             |
| NDBC                | 0.9041        | -0.1953        | 0.4319        | 9.3122         | 0.3938        | 8.4918         | 4.6377        | 4.833         | 23             |
| NDS1                | 0.8789        | -0.3394        | 0.6278        | 19.0649        | 0.54          | 16.3991        | 3.2928        | 3.6322        | 23             |
| NLGN                | 0.9318        | -0.316         | 0.4939        | 16.4955        | 0.3881        | 12.9625        | 2.9939        | 3.3099        | 23             |
| OKOM                | 0.8744        | -0.2149        | 0.6092        | 16.5029        | 0.5857        | 15.8653        | 3.6915        | 3.9064        | 19             |
| PATT                | 0.7589        | -0.4235        | 0.6397        | 15.5095        | 0.4975        | 12.0614        | 4.1244        | 4.5479        | 14             |
| PLS1                | 0.601         | -0.1452        | 0.2879        | 16.2728        | 0.2724        | 15.3937        | 1.7695        | 1.9147        | 6              |
| PLTC                | 0.8794        | -0.1947        | 0.3579        | 17.7346        | 0.3096        | 15.3383        | 2.0182        | 2.213         | 17             |
| PNB1                | 0.9357        | -0.3091        | 0.4741        | 21.3169        | 0.3705        | 16.6585        | 2.2239        | 2.5331        | 17             |
| PRCO                | 0.9319        | -0.3095        | 0.5189        | 14.7516        | 0.4285        | 12.1827        | 3.5173        | 3.8268        | 18             |
| RWDN                | 0.9321        | -0.2256        | 0.3767        | 12.7453        | 0.3092        | 10.4594        | 2.9558        | 3.1814        | 21             |
| SAV1                | 0.9553        | -0.2269        | 0.4279        | 10.467         | 0.3709        | 9.0742         | 4.0879        | 4.3147        | 23             |
| SEAW                | 0.4883        | -0.1799        | 0.35          | 16.4485        | 0.3288        | 15.454         | 2.1277        | 2.3076        | 6              |
| SHK1                | 0.9807        | -0.2739        | 0.3831        | 13.4998        | 0.2739        | 9.6509         | 2.8378        | 3.1117        | 23             |
| SIO3                | 0.5763        | -0.7686        | 0.9756        | 44.549         | 0.6194        | 28.2813        | 2.19          | 2.9586        | 17             |
| SLAI                | 0.942         | -0.0947        | 0.2762        | 10.8332        | 0.2774        | 10.8802        | 2.55          | 2.6447        | 8              |
| SPN1                | 0.5928        | -0.3522        | 0.5396        | 32.6858        | 0.4479        | 27.1283        | 1.651         | 2.0032        | 6              |
| SUM1                | 0.9137        | -0.1099        | 0.2981        | 10.7251        | 0.2833        | 10.1939        | 2.7791        | 2.889         | 23             |
| SYCN                | 0.8239        | -0.117         | 0.4945        | 22.242         | 0.4936        | 22.2029        | 2.2231        | 2.34          | 19             |
| TCUN                | 0.9338        | 0.0057         | 0.249         | 9.3014         | 0.2548        | 9.5178         | 2.6772        | 2.6716        | 22             |
| VCIO                | 0.8566        | -0.2357        | 0.513         | 16.3943        | 0.4658        | 14.8879        | 3.1289        | 3.3646        | 23             |
| WDLM                | 0.8165        | -0.2078        | 0.4745        | 18.4913        | 0.4362        | 16.9971        | 2.5663        | 2.7741        | 23             |
| WHN1                | 0.8189        | -0.2264        | 0.5929        | 23.4111        | 0.5603        | 22.1233        | 2.5325        | 2.7589        | 23             |
| WLCI                | 0.8265        | -0.5261        | 0.7751        | 32.369         | 0.5907        | 24.6686        | 2.3945        | 2.9206        | 14             |
| WNCI                | 0.9405        | -0.245         | 0.4543        | 15.2071        | 0.3937        | 13.1772        | 2.9874        | 3.2324        | 18             |
| WNFL                | 0.6339        | -0.3288        | 0.6345        | 15.5332        | 0.5575        | 13.6484        | 4.0848        | 4.4136        | 19             |
| WSMN                | 0.583         | -0.1192        | 0.3776        | 12.7108        | 0.3758        | 12.6491        | 2.9706        | 3.0899        | 11             |
| <b>Means</b>        | <b>0.8330</b> | <b>-0.2443</b> | <b>0.5047</b> | <b>18.5744</b> | <b>0.4277</b> | <b>15.6054</b> | <b>2.9303</b> | <b>3.1746</b> | <b>17.5606</b> |
| <b>Mean n&gt;10</b> | <b>0.8593</b> | <b>-0.2503</b> |               | <b>17.5031</b> |               | <b>14.8263</b> |               |               | <b>19.5357</b> |

## Appendix C: Location-Specific Statistics

Table C-1-10. CONUS Statistics: 18 UTC Initialization, 12H Forecast

| ID                  | Correlation   | Bias           | RMSE          | RMSE%          | StDev         | %Stdev         | Mean GPS      | Mean MM5      | n              |
|---------------------|---------------|----------------|---------------|----------------|---------------|----------------|---------------|---------------|----------------|
| ANP1                | 0.934         | -0.263         | 0.4045        | 17.1687        | 0.3199        | 13.5781        | 2.3562        | 2.6191        | 13             |
| ARP3                | 0.5306        | -0.3823        | 0.6345        | 15.9499        | 0.5183        | 13.0298        | 3.978         | 4.3603        | 22             |
| AZCN                | 0.9039        | -0.1567        | 0.3551        | 19.8531        | 0.3298        | 18.4405        | 1.7887        | 1.9454        | 15             |
| BARH                | 0.8782        | 0.2981         | 0.8111        | 30.9774        | 0.8264        | 31.5591        | 2.6185        | 2.3204        | 6              |
| BARN                | 0.9587        | 0.1032         | 0.2544        | 11.1238        | 0.238         | 10.4068        | 2.2873        | 2.1841        | 22             |
| BIL1                | 0.744         | -0.2611        | 0.3849        | 20.9413        | 0.2921        | 15.8895        | 1.8381        | 2.0993        | 16             |
| BLKV                | 0.8788        | -0.3309        | 0.6107        | 19.8165        | 0.5326        | 17.2835        | 3.0816        | 3.4126        | 14             |
| BLMM                | 0.9758        | -0.1427        | 0.3552        | 10.8815        | 0.3359        | 10.2914        | 3.2643        | 3.407         | 16             |
| BLRW                | 0.9369        | -0.1823        | 0.4314        | 14.9046        | 0.4284        | 14.7981        | 2.8947        | 3.077         | 6              |
| CCV3                | 0.8706        | -0.1953        | 0.4393        | 9.0063         | 0.4028        | 8.2574         | 4.8779        | 5.0732        | 22             |
| CHA1                | 0.9337        | -0.2469        | 0.4954        | 12.6445        | 0.44          | 11.2328        | 3.9175        | 4.1644        | 21             |
| CHO1                | 0.7309        | -0.4419        | 0.6403        | 39.1596        | 0.4785        | 29.2645        | 1.635         | 2.0769        | 16             |
| CLK1                | 0.8322        | -0.2991        | 0.4581        | 17.9221        | 0.3551        | 13.8934        | 2.5561        | 2.8552        | 22             |
| CNWM                | 0.9367        | -0.2146        | 0.4696        | 15.1802        | 0.4291        | 13.872         | 3.0935        | 3.3082        | 19             |
| COVX                | 0.9992        | -0.4733        | 0.4766        | 18.9876        | 0.0648        | 2.5812         | 2.51          | 2.9833        | 4              |
| DQUA                | 0.9424        | -0.4047        | 0.5427        | 14.0612        | 0.37          | 9.5876         | 3.8593        | 4.264         | 22             |
| DRV1                | 0.9642        | -0.2146        | 0.4597        | 12.5402        | 0.4218        | 11.5084        | 3.6654        | 3.88          | 14             |
| DSRC                | 0.8978        | 0.1713         | 0.2992        | 16.2736        | 0.2534        | 13.7796        | 1.8387        | 1.6674        | 16             |
| ENG1                | 0.9116        | -0.1644        | 0.4146        | 8.9766         | 0.3896        | 8.4348         | 4.6187        | 4.7831        | 22             |
| FBYN                | 0.9247        | -0.2484        | 0.4497        | 14.0795        | 0.3837        | 12.0129        | 3.1937        | 3.4421        | 22             |
| FST1                | 0.5914        | -0.1965        | 0.6509        | 44.2279        | 0.6409        | 43.5472        | 1.4716        | 1.6681        | 16             |
| GAL1                | 0.7702        | -0.342         | 0.5612        | 13.3591        | 0.4554        | 10.8408        | 4.201         | 4.5431        | 22             |
| GDAC                | 0.6637        | -0.1773        | 0.5923        | 23.5493        | 0.5836        | 23.2058        | 2.515         | 2.6923        | 16             |
| GWEN                | 0.7796        | -0.4059        | 0.4675        | 28.3071        | 0.2592        | 15.6987        | 1.6514        | 2.0573        | 5              |
| HAG1                | 0.9723        | -0.1487        | 0.3063        | 13.8651        | 0.2822        | 12.777         | 2.209         | 2.3577        | 10             |
| HBRK                | 0.8259        | 0.0198         | 0.4522        | 15.0538        | 0.4676        | 15.5671        | 3.004         | 2.9842        | 15             |
| HDF1                | 0.9146        | 0.0844         | 0.3634        | 13.9299        | 0.3626        | 13.9013        | 2.6087        | 2.5243        | 20             |
| HKLO                | 0.9297        | -0.5469        | 0.6838        | 19.8371        | 0.4211        | 12.2157        | 3.4471        | 3.994         | 20             |
| HTV1                | 0.942         | -0.3811        | 0.5297        | 19.826         | 0.3793        | 14.194         | 2.672         | 3.0531        | 17             |
| HVLK                | 0.883         | -0.1779        | 0.4551        | 15.531         | 0.4359        | 14.878         | 2.93          | 3.1079        | 13             |
| JTNT                | 0.7366        | -0.1424        | 0.559         | 16.6935        | 0.5533        | 16.5229        | 3.3487        | 3.491         | 22             |
| KYW1                | 0.5101        | -0.1694        | 0.7279        | 15.1283        | 0.7246        | 15.0592        | 4.8115        | 4.9808        | 22             |
| LMNO                | 0.8586        | -0.0958        | 0.502         | 14.8709        | 0.5114        | 15.1488        | 3.3757        | 3.4715        | 14             |
| LTHM                | 0.4212        | -0.315         | 0.7552        | 30.4517        | 0.728         | 29.3555        | 2.48          | 2.795         | 9              |
| MBWW                | 0.4764        | 0.001          | 0.2373        | 9.8129         | 0.26          | 10.7494        | 2.4187        | 2.4176        | 6              |
| MC01                | 0.8689        | 0.0809         | 0.3722        | 17.9583        | 0.3728        | 17.9848        | 2.0727        | 1.9918        | 20             |
| MCN1                | 0.9356        | -0.0295        | 0.459         | 11.5784        | 0.4688        | 11.8263        | 3.9641        | 3.9936        | 22             |
| MOB1                | 0.8228        | -0.0699        | 0.6017        | 12.3981        | 0.6117        | 12.604         | 4.8534        | 4.9232        | 22             |
| MOR1                | 0.9802        | -0.2137        | 0.3488        | 12.1374        | 0.2822        | 9.8187         | 2.8737        | 3.0874        | 22             |
| MRRN                | 0.8634        | -0.3099        | 0.5727        | 23.1721        | 0.4929        | 19.9444        | 2.4715        | 2.7814        | 22             |
| NDBC                | 0.8578        | -0.0976        | 0.4914        | 10.6742        | 0.4929        | 10.7077        | 4.6035        | 4.7011        | 22             |
| NDS1                | 0.8368        | -0.2013        | 0.5917        | 17.7487        | 0.5695        | 17.0828        | 3.334         | 3.5354        | 22             |
| NLGN                | 0.8911        | -0.2532        | 0.5544        | 18.4762        | 0.5048        | 16.8242        | 3.0005        | 3.2537        | 22             |
| OKOM                | 0.8663        | -0.1821        | 0.6377        | 17.1527        | 0.6288        | 16.9146        | 3.7176        | 3.8998        | 18             |
| PATT                | 0.8937        | -0.4486        | 0.5848        | 14.158         | 0.3894        | 9.4267         | 4.1306        | 4.5792        | 14             |
| PLS1                | 0.5191        | -0.142         | 0.3914        | 23.764         | 0.3995        | 24.259         | 1.6468        | 1.7888        | 6              |
| PLTC                | 0.8917        | -0.1873        | 0.3231        | 16.7153        | 0.272         | 14.0689        | 1.9331        | 2.1204        | 16             |
| PNB1                | 0.8867        | -0.2819        | 0.5967        | 27.019         | 0.5432        | 24.5956        | 2.2086        | 2.4904        | 16             |
| PRCO                | 0.8862        | -0.2692        | 0.51          | 14.5798        | 0.4434        | 12.6752        | 3.4983        | 3.7675        | 22             |
| RWDN                | 0.9555        | -0.2116        | 0.3409        | 11.6164        | 0.2739        | 9.333          | 2.9345        | 3.1461        | 21             |
| SAV1                | 0.9567        | 0.1145         | 0.3496        | 8.4417         | 0.3381        | 8.1641         | 4.1419        | 4.0274        | 22             |
| SEAW                | 0.7608        | -0.0661        | 0.1675        | 7.5688         | 0.1686        | 7.6187         | 2.2132        | 2.2792        | 6              |
| SHK1                | 0.959         | -0.2291        | 0.465         | 16.5938        | 0.4147        | 14.7966        | 2.8024        | 3.0315        | 21             |
| SIO3                | 0.46          | -0.622         | 0.8454        | 36.1288        | 0.5914        | 25.2732        | 2.34          | 2.962         | 16             |
| SLAI                | 0.8344        | -0.0784        | 0.3658        | 14.9679        | 0.382         | 15.63          | 2.4437        | 2.5221        | 8              |
| SPN1                | 0.5268        | -0.4307        | 0.6057        | 38.5949        | 0.4666        | 29.729         | 1.5695        | 2.0002        | 6              |
| SUM1                | 0.9041        | 0.0031         | 0.2902        | 10.2834        | 0.2971        | 10.5248        | 2.8224        | 2.8193        | 22             |
| SYCN                | 0.8267        | -0.129         | 0.5372        | 23.6977        | 0.5375        | 23.7119        | 2.2669        | 2.396         | 17             |
| TCUN                | 0.8606        | -0.0756        | 0.3814        | 14.0222        | 0.3827        | 14.0678        | 2.7202        | 2.7957        | 22             |
| VCIO                | 0.8576        | -0.0781        | 0.4685        | 14.9295        | 0.474         | 15.1034        | 3.1384        | 3.2165        | 20             |
| WDLM                | 0.8302        | -0.3167        | 0.4876        | 19.785         | 0.3795        | 15.3985        | 2.4645        | 2.7811        | 22             |
| WHN1                | 0.8981        | -0.1756        | 0.4193        | 17.0343        | 0.3897        | 15.8334        | 2.4615        | 2.637         | 22             |
| WLCI                | 0.8686        | -0.5276        | 0.8016        | 33.4359        | 0.628         | 26.1977        | 2.3973        | 2.925         | 13             |
| WNCI                | 0.8712        | -0.267         | 0.5962        | 20.9033        | 0.5486        | 19.2327        | 2.8523        | 3.1192        | 22             |
| WNFL                | 0.8593        | -0.2789        | 0.4824        | 11.9799        | 0.405         | 10.0581        | 4.0266        | 4.3055        | 18             |
| WSMN                | 0.6118        | -0.1444        | 0.37          | 12.5819        | 0.3591        | 12.2113        | 2.941         | 3.0854        | 10             |
| <b>Means</b>        | <b>0.8303</b> | <b>-0.1994</b> | <b>0.4885</b> | <b>17.9544</b> | <b>0.4301</b> | <b>15.6815</b> | <b>2.9373</b> | <b>3.1367</b> | <b>16.7727</b> |
| <b>Mean n&gt;10</b> | <b>0.8512</b> | <b>-0.2030</b> | <b>0.4885</b> | <b>17.2617</b> | <b>0.4301</b> | <b>15.2322</b> | <b>2.9373</b> | <b>3.1367</b> | <b>18.6607</b> |

## Appendix C: Location-Specific Statistics

Table C-1-11. CONUS Statistics: 18 UTC Initialization, 15H Forecast

| ID                  | Correlation   | Bias           | RMSE          | RMSE%          | StDev         | %Stdev         | Mean GPS      | Mean MM5      | n              |
|---------------------|---------------|----------------|---------------|----------------|---------------|----------------|---------------|---------------|----------------|
| ANP1                | 0.8929        | -0.1973        | 0.4499        | 19.1206        | 0.4208        | 17.885         | 2.3531        | 2.5504        | 13             |
| ARP3                | 0.5726        | -0.3087        | 0.607         | 14.7319        | 0.5349        | 12.9828        | 4.12          | 4.4287        | 22             |
| AZCN                | 0.87          | -0.1429        | 0.3512        | 18.9156        | 0.3321        | 17.8846        | 1.8567        | 1.9996        | 15             |
| BARH                | 0.8173        | 0.3267         | 0.924         | 35.5226        | 0.9664        | 37.1505        | 2.6012        | 2.2745        | 5              |
| BARN                | 0.9299        | 0.102          | 0.3043        | 13.8076        | 0.2934        | 13.3146        | 2.2039        | 2.1018        | 22             |
| BIL1                | 0.7803        | -0.2333        | 0.3561        | 19.5303        | 0.2778        | 15.2365        | 1.8231        | 2.0564        | 16             |
| BLKV                | 0.8773        | -0.3414        | 0.6461        | 20.859         | 0.5692        | 18.3774        | 3.0974        | 3.4388        | 14             |
| BLMM                | 0.9412        | -0.1343        | 0.4899        | 15.5485        | 0.4866        | 15.4431        | 3.1508        | 3.2851        | 16             |
| BLRW                | 0.9449        | -0.0049        | 0.4444        | 15.4546        | 0.4868        | 16.9286        | 2.8758        | 2.8807        | 6              |
| CCV3                | 0.8053        | -0.1615        | 0.5288        | 11.0039        | 0.5154        | 10.7248        | 4.8057        | 4.9672        | 22             |
| CHA1                | 0.8325        | -0.3245        | 0.723         | 17.6477        | 0.6639        | 16.2031        | 4.0971        | 4.4216        | 19             |
| CHO1                | 0.7476        | -0.3832        | 0.5686        | 32.2174        | 0.4339        | 24.5825        | 1.765         | 2.1482        | 16             |
| CLK1                | 0.8611        | -0.2494        | 0.404         | 15.6889        | 0.3253        | 12.6326        | 2.5753        | 2.8247        | 22             |
| CNWM                | 0.9195        | -0.1071        | 0.4931        | 16.316         | 0.4953        | 16.3885        | 3.0221        | 3.1291        | 18             |
| COVX                | 0.9711        | -0.52          | 0.6063        | 28.4846        | 0.3369        | 15.8256        | 2.1286        | 2.6485        | 7              |
| DQUA                | 0.8896        | -0.3626        | 0.6357        | 16.5898        | 0.5344        | 13.9467        | 3.8318        | 4.1944        | 22             |
| DRV1                | 0.9046        | -0.0089        | 0.6524        | 17.2364        | 0.677         | 17.8854        | 3.7853        | 3.7942        | 14             |
| DSRC                | 0.9022        | 0.1704         | 0.2973        | 16.4268        | 0.2517        | 13.9037        | 1.81          | 1.6396        | 16             |
| ENG1                | 0.9175        | -0.1022        | 0.427         | 9.0503         | 0.4243        | 8.9939         | 4.7177        | 4.8199        | 22             |
| FBYN                | 0.9307        | -0.1594        | 0.3911        | 12.1272        | 0.3656        | 11.3352        | 3.225         | 3.3844        | 22             |
| FST1                | 0.6055        | -0.1979        | 0.6111        | 43.5519        | 0.5972        | 42.5569        | 1.4032        | 1.6011        | 16             |
| GAL1                | 0.7485        | -0.3717        | 0.606         | 14.4059        | 0.4899        | 11.6463        | 4.2068        | 4.5785        | 22             |
| GDAC                | 0.6502        | -0.1077        | 0.5873        | 23.616         | 0.5963        | 23.9771        | 2.4869        | 2.5945        | 16             |
| GWEN                | 0.6154        | -0.2429        | 0.418         | 24.0963        | 0.3803        | 21.9234        | 1.7346        | 1.9775        | 5              |
| HAG1                | 0.9725        | -0.1252        | 0.2675        | 12.0749        | 0.2492        | 11.2484        | 2.215         | 2.3402        | 10             |
| HBRK                | 0.761         | -0.1923        | 0.6657        | 22.9299        | 0.6597        | 22.7225        | 2.9033        | 3.0957        | 15             |
| HDF1                | 0.8829        | 0.0673         | 0.4288        | 16.8564        | 0.4339        | 17.0583        | 2.5439        | 2.4765        | 21             |
| HKLO                | 0.919         | -0.4051        | 0.5825        | 16.4893        | 0.4294        | 12.1568        | 3.5325        | 3.9375        | 20             |
| HTV1                | 0.9002        | -0.3561        | 0.5782        | 21.9497        | 0.4696        | 17.8263        | 2.6344        | 2.9904        | 17             |
| HVLK                | 0.9231        | -0.284         | 0.4206        | 14.8657        | 0.3229        | 11.412         | 2.8292        | 3.1132        | 13             |
| JTNT                | 0.7228        | -0.0854        | 0.595         | 17.4913        | 0.6027        | 17.7177        | 3.402         | 3.4873        | 22             |
| KYW1                | 0.5142        | -0.1839        | 0.7199        | 15.022         | 0.7124        | 14.8655        | 4.7922        | 4.9761        | 22             |
| LMNO                | 0.8781        | -0.2141        | 0.4803        | 14.8258        | 0.4461        | 13.7727        | 3.2393        | 3.4533        | 14             |
| LTHM                | 0.4786        | 0.0396         | 0.5993        | 23.5539        | 0.6343        | 24.928         | 2.5444        | 2.5048        | 9              |
| MBWW                | 0.6808        | 0.0827         | 0.1937        | 8.3899         | 0.1918        | 8.3108         | 2.3082        | 2.2255        | 6              |
| MC01                | 0.858         | 0.1541         | 0.3536        | 17.1618        | 0.3265        | 15.8468        | 2.0602        | 1.906         | 20             |
| MCN1                | 0.9524        | -0.0776        | 0.3993        | 10.2533        | 0.4009        | 10.2943        | 3.8945        | 3.9721        | 22             |
| MOB1                | 0.8777        | -0.0589        | 0.4855        | 9.9814         | 0.4933        | 10.1408        | 4.8644        | 4.9233        | 22             |
| MOR1                | 0.9626        | -0.2215        | 0.452         | 16.5851        | 0.4033        | 14.7969        | 2.7256        | 2.9471        | 22             |
| MRRN                | 0.9372        | -0.1821        | 0.4096        | 15.9846        | 0.376         | 14.6719        | 2.5625        | 2.7446        | 21             |
| NDBC                | 0.9166        | -0.0391        | 0.4173        | 9.0039         | 0.4253        | 9.1752         | 4.6351        | 4.6742        | 22             |
| NDS1                | 0.8456        | -0.1851        | 0.5726        | 17.1143        | 0.5546        | 16.576         | 3.3456        | 3.5308        | 22             |
| NLGN                | 0.9256        | -0.2811        | 0.54          | 18.396         | 0.4719        | 16.077         | 2.9353        | 3.2164        | 22             |
| OKOM                | 0.9283        | -0.0391        | 0.4293        | 11.2196        | 0.4399        | 11.4968        | 3.8261        | 3.8653        | 18             |
| PATT                | 0.901         | -0.445         | 0.5644        | 13.4612        | 0.3602        | 8.591          | 4.1926        | 4.6376        | 14             |
| PLS1                | 0.561         | -0.1207        | 0.4659        | 28.0359        | 0.4929        | 29.6636        | 1.6617        | 1.7823        | 6              |
| PLTC                | 0.9283        | -0.1727        | 0.2787        | 14.1702        | 0.2264        | 11.5096        | 1.9667        | 2.1394        | 15             |
| PNB1                | 0.9251        | -0.1871        | 0.4036        | 18.8676        | 0.3693        | 17.2666        | 2.1389        | 2.326         | 16             |
| PRCO                | 0.8233        | -0.1652        | 0.5469        | 15.2707        | 0.5336        | 14.9001        | 3.5811        | 3.7463        | 22             |
| RWDN                | 0.8755        | -0.2637        | 0.4503        | 16.4184        | 0.3744        | 13.6527        | 2.7424        | 3.0062        | 20             |
| SAV1                | 0.8893        | -0.032         | 0.5628        | 14.2381        | 0.5751        | 14.5496        | 3.9529        | 3.9849        | 22             |
| SEAW                | 0.6077        | -0.0468        | 0.2167        | 9.7338         | 0.2318        | 10.4107        | 2.2267        | 2.2735        | 6              |
| SHK1                | 0.9793        | -0.2267        | 0.38          | 13.8829        | 0.3125        | 11.4163        | 2.7372        | 2.9639        | 21             |
| SIO3                | 0.4279        | -0.5297        | 0.827         | 34.2689        | 0.6559        | 27.1797        | 2.4131        | 2.9428        | 16             |
| SLAI                | 0.8752        | 0.1197         | 0.3277        | 12.7709        | 0.3262        | 12.7099        | 2.5663        | 2.4466        | 8              |
| SPN1                | 0.532         | -0.4846        | 0.6237        | 39.0739        | 0.4301        | 26.9464        | 1.5962        | 2.0808        | 6              |
| SUM1                | 0.9326        | 0.0169         | 0.2455        | 8.5712         | 0.2506        | 8.7521         | 2.8638        | 2.8469        | 22             |
| SYCN                | 0.8489        | -0.1987        | 0.5296        | 24.3177        | 0.5052        | 23.1942        | 2.1779        | 2.3767        | 18             |
| TCUN                | 0.9244        | -0.0368        | 0.2536        | 9.4971         | 0.2571        | 9.6285         | 2.6698        | 2.7066        | 21             |
| VCIO                | 0.8858        | -0.1256        | 0.4248        | 13.3321        | 0.4158        | 13.0501        | 3.1861        | 3.3118        | 21             |
| WDLM                | 0.7965        | -0.328         | 0.5091        | 20.6208        | 0.3985        | 16.1414        | 2.4689        | 2.7969        | 22             |
| WHN1                | 0.883         | -0.2376        | 0.4506        | 18.6296        | 0.3918        | 16.201         | 2.4186        | 2.6562        | 22             |
| WLC1                | 0.9697        | -0.3485        | 0.4463        | 17.8603        | 0.2901        | 11.611         | 2.4988        | 2.8474        | 13             |
| WNC1                | 0.8136        | -0.2062        | 0.6077        | 22.6075        | 0.5904        | 21.9637        | 2.6883        | 2.8945        | 16             |
| WNFL                | 0.7977        | -0.1384        | 0.5229        | 12.5491        | 0.5189        | 12.4522        | 4.167         | 4.3054        | 18             |
| WSMN                | 0.8821        | -0.0739        | 0.1814        | 5.9164         | 0.1746        | 5.6955         | 3.0655        | 3.1394        | 10             |
| <b>Means</b>        | <b>0.8307</b> | <b>-0.1649</b> | <b>0.4838</b> | <b>17.6696</b> | <b>0.4421</b> | <b>16.0047</b> | <b>2.9311</b> | <b>3.0959</b> | <b>16.7121</b> |
| <b>Mean n&gt;10</b> | <b>0.8525</b> | <b>-0.1791</b> |               | <b>16.8049</b> |               | <b>15.2056</b> |               |               | <b>18.5536</b> |

## Appendix C: Location-Specific Statistics

Table C-1-12. CONUS Statistics: 18 UTC Initialization, 18H Forecast

| ID                  | Correlation   | Bias           | RMSE          | RMSE%          | StDev         | %Stdev         | Mean GPS      | Mean MMS      | n              |
|---------------------|---------------|----------------|---------------|----------------|---------------|----------------|---------------|---------------|----------------|
| ANP1                | 0.9225        | -0.1573        | 0.4672        | 19.8917        | 0.4666        | 19.8666        | 2.3489        | 2.5062        | 9              |
| ARP3                | 0.4334        | -0.4161        | 0.7368        | 18.2031        | 0.6257        | 15.4584        | 4.0475        | 4.4636        | 18             |
| AZCN                | 0.9217        | -0.1583        | 0.3038        | 17.1882        | 0.2708        | 15.3233        | 1.7675        | 1.9258        | 12             |
| BARH                | 0.8           | 0.0697         | 0.5802        | 17.8104        | 0.7055        | 21.6554        | 3.2577        | 3.188         | 3              |
| BARN                | 0.9227        | 0.1418         | 0.369         | 15.3468        | 0.3512        | 14.605         | 2.4045        | 2.2627        | 17             |
| BIL1                | 0.647         | -0.2484        | 0.3923        | 22.2813        | 0.3172        | 18.012         | 1.7608        | 2.0093        | 12             |
| BLKV                | 0.9051        | -0.2683        | 0.5317        | 15.9722        | 0.4815        | 14.4625        | 3.329         | 3.5973        | 11             |
| BLMM                | 0.9812        | -0.3813        | 0.4665        | 17.4081        | 0.2807        | 10.4746        | 2.68          | 3.0613        | 12             |
| BLRW                | 0.9624        | -0.427         | 0.6207        | 25.48          | 0.4934        | 20.2555        | 2.436         | 2.863         | 6              |
| CCV3                | 0.8551        | -0.1602        | 0.4065        | 8.1774         | 0.3844        | 7.7333         | 4.9712        | 5.1314        | 18             |
| CHA1                | 0.809         | 0.0831         | 0.5975        | 13.932         | 0.6111        | 14.2491        | 4.2886        | 4.2055        | 16             |
| CHO1                | 0.7399        | -0.321         | 0.5281        | 28.0533        | 0.438         | 23.2659        | 1.8825        | 2.2035        | 12             |
| CLK1                | 0.8761        | -0.2562        | 0.3813        | 15.3061        | 0.2906        | 11.6652        | 2.4913        | 2.7475        | 18             |
| CNWM                | 0.9731        | -0.4857        | 0.5585        | 22.7279        | 0.2879        | 11.7171        | 2.4574        | 2.9432        | 12             |
| COVX                | 0.9386        | -0.765         | 0.8343        | 44.9784        | 0.3647        | 19.6625        | 1.855         | 2.62          | 6              |
| DQUA                | 0.9431        | -0.4056        | 0.579         | 15.8154        | 0.4252        | 11.6147        | 3.6611        | 4.0666        | 18             |
| DRV1                | 0.844         | -0.1975        | 0.65          | 17.8596        | 0.6495        | 17.8457        | 3.6396        | 3.8371        | 11             |
| DSRC                | 0.8435        | 0.1345         | 0.3366        | 20.118         | 0.3223        | 19.2614        | 1.6733        | 1.5388        | 12             |
| ENGI                | 0.8794        | 0.0552         | 0.4379        | 9.4306         | 0.447         | 9.6267         | 4.6431        | 4.5879        | 18             |
| FBYN                | 0.8238        | -0.1384        | 0.5276        | 16.8775        | 0.5239        | 16.7586        | 3.1259        | 3.2643        | 18             |
| FST1                | 0.8206        | -0.252         | 0.51          | 35.6346        | 0.4631        | 32.3582        | 1.4312        | 1.6833        | 12             |
| GAL1                | 0.5455        | -0.5696        | 0.8377        | 20.5561        | 0.632         | 15.5103        | 4.075         | 4.6446        | 18             |
| GDAC                | 0.874         | -0.2033        | 0.4012        | 18.1733        | 0.3612        | 16.3643        | 2.2075        | 2.4108        | 12             |
| GWEN                | 0.8189        | -0.3964        | 0.4445        | 32.4568        | 0.2249        | 16.4194        | 1.3696        | 1.766         | 5              |
| HAG1                | 0.9954        | -0.1291        | 0.1871        | 8.7444         | 0.1463        | 6.8387         | 2.14          | 2.2691        | 7              |
| HBRK                | 0.9674        | -0.2561        | 0.3493        | 12.6301        | 0.2504        | 9.0545         | 2.766         | 3.0221        | 10             |
| HDF1                | 0.8664        | 0.1558         | 0.4691        | 16.8315        | 0.457         | 16.3967        | 2.7871        | 2.6313        | 16             |
| HK10                | 0.9049        | -0.4115        | 0.6362        | 19.1202        | 0.5022        | 15.0932        | 3.3274        | 3.7389        | 15             |
| HTV1                | 0.8592        | -0.1939        | 0.5909        | 20.8296        | 0.5765        | 20.3215        | 2.8369        | 3.0308        | 16             |
| HVLK                | 0.8775        | -0.1119        | 0.3934        | 14.5063        | 0.3976        | 14.66          | 2.712         | 2.8238        | 10             |
| JTNT                | 0.7188        | -0.1664        | 0.5894        | 17.7343        | 0.5818        | 17.5061        | 3.3234        | 3.4898        | 18             |
| KYW1                | 0.6898        | -0.0873        | 0.5621        | 11.5341        | 0.5724        | 11.7447        | 4.8734        | 4.9607        | 17             |
| LMNO                | 0.8846        | -0.1792        | 0.5079        | 16.8038        | 0.4963        | 16.4217        | 3.0225        | 3.2017        | 12             |
| LTHM                | 0.7827        | 0.0893         | 0.2408        | 10.3122        | 0.245         | 10.4909        | 2.335         | 2.2457        | 6              |
| MBWW                | 0.684         | 0.1754         | 0.2777        | 11.9932        | 0.2359        | 10.1854        | 2.3157        | 2.1402        | 6              |
| MC01                | 0.9449        | 0.1502         | 0.2893        | 13.3196        | 0.2548        | 11.7348        | 2.1716        | 2.0215        | 17             |
| MCN1                | 0.9243        | 0.0072         | 0.5221        | 12.5219        | 0.5372        | 12.8837        | 4.1692        | 4.162         | 18             |
| MOB1                | 0.8673        | 0.1905         | 0.5227        | 10.4953        | 0.5009        | 10.0565        | 4.9804        | 4.7898        | 18             |
| MOR1                | 0.9475        | -0.2209        | 0.5035        | 18.3439        | 0.4664        | 16.9917        | 2.745         | 2.9659        | 17             |
| MRRN                | 0.9157        | -0.3423        | 0.5057        | 20.1496        | 0.3836        | 15.2867        | 2.5096        | 2.852         | 17             |
| NDBC                | 0.8877        | 0.0603         | 0.426         | 9.1165         | 0.434         | 9.2863         | 4.6731        | 4.6127        | 18             |
| NDS1                | 0.9371        | -0.2416        | 0.436         | 14.1032        | 0.3735        | 12.0809        | 3.0917        | 3.3333        | 18             |
| NLGN                | 0.8208        | -0.2296        | 0.6553        | 23.1763        | 0.6316        | 22.3372        | 2.8276        | 3.0571        | 18             |
| OKOM                | 0.8676        | -0.1209        | 0.5559        | 14.3783        | 0.5617        | 14.527         | 3.8665        | 3.9873        | 15             |
| PATT                | 0.9261        | -0.2956        | 0.4064        | 9.4066         | 0.2914        | 6.7437         | 4.3205        | 4.6161        | 12             |
| PLS1                | 0.3829        | -0.0874        | 0.4795        | 28.9058        | 0.5165        | 31.1349        | 1.659         | 1.7463        | 6              |
| PLTC                | 0.9324        | -0.184         | 0.2997        | 16.7923        | 0.2471        | 13.8436        | 1.785         | 1.969         | 12             |
| PNB1                | 0.9414        | -0.0498        | 0.3285        | 15.058         | 0.3406        | 15.6102        | 2.1818        | 2.2317        | 11             |
| PRCO                | 0.8673        | -0.1665        | 0.5261        | 15.1936        | 0.5136        | 14.8309        | 3.4629        | 3.6294        | 18             |
| RWDN                | 0.8061        | -0.2614        | 0.5405        | 20.1927        | 0.4886        | 18.2537        | 2.6767        | 2.9382        | 16             |
| SAV1                | 0.8067        | 0.1098         | 0.6948        | 16.5666        | 0.7059        | 16.8327        | 4.1939        | 4.0841        | 18             |
| SEAW                | 0.7429        | -0.1969        | 0.235         | 10.611         | 0.1404        | 6.3414         | 2.2143        | 2.4112        | 6              |
| SHK1                | 0.9747        | -0.0585        | 0.3437        | 12.2973        | 0.3491        | 12.4906        | 2.7951        | 2.8536        | 17             |
| SIO3                | 0.5406        | -0.4493        | 0.8595        | 35.9486        | 0.7653        | 32.009         | 2.3908        | 2.8401        | 12             |
| SLAI                | 0.8299        | 0.0695         | 0.3352        | 15.2842        | 0.3592        | 16.3787        | 2.1933        | 2.1238        | 6              |
| SPN1                | 0.9391        | -0.4608        | 0.4751        | 32.2276        | 0.1268        | 8.6034         | 1.4743        | 1.9352        | 6              |
| SUM1                | 0.8693        | 0.0254         | 0.3366        | 12.3977        | 0.3453        | 12.7209        | 2.7147        | 2.6893        | 18             |
| SYCN                | 0.9387        | 0.078          | 0.2332        | 9.8055         | 0.2305        | 9.6921         | 2.3786        | 2.3006        | 11             |
| TCUN                | 0.8449        | -0.013         | 0.2774        | 10.7525        | 0.2862        | 11.093         | 2.5797        | 2.5926        | 16             |
| VCIO                | 0.8763        | -0.2406        | 0.4793        | 16.124         | 0.4266        | 14.3504        | 2.9727        | 3.2132        | 18             |
| WDLM                | 0.775         | -0.4346        | 0.5501        | 23.2776        | 0.3477        | 14.7124        | 2.3634        | 2.798         | 17             |
| WHN1                | 0.8874        | -0.1891        | 0.4167        | 17.1552        | 0.3821        | 15.7315        | 2.4291        | 2.6182        | 18             |
| WLC1                | 0.9584        | -0.3231        | 0.5159        | 22.0953        | 0.4265        | 18.2699        | 2.3347        | 2.6577        | 9              |
| WNCI                | 0.9445        | -0.3201        | 0.4447        | 18.7887        | 0.3224        | 13.6204        | 2.3668        | 2.6869        | 12             |
| WNFL                | 0.8411        | -0.2097        | 0.519         | 12.4336        | 0.4914        | 11.7728        | 4.1741        | 4.3837        | 15             |
| WSMN                | 0.9301        | 0.0859         | 0.1739        | 5.5493         | 0.1604        | 5.1178         | 3.1346        | 3.0486        | 9              |
| <b>Means</b>        | <b>0.8482</b> | <b>-0.1690</b> | <b>0.4726</b> | <b>17.6240</b> | <b>0.4134</b> | <b>14.9730</b> | <b>2.8799</b> | <b>3.0490</b> | <b>13.3030</b> |
| <b>Mean n&gt;10</b> | <b>0.8518</b> | <b>-0.1674</b> |               | <b>16.8624</b> |               | <b>14.9423</b> |               |               | <b>15.1538</b> |

## Appendix C: Location-Specific Statistics

Table C-1-13. CONUS Statistics: 18 UTC Initialization, 21H Forecast

| ID                  | Correlation   | Bias           | RMSE          | RMSE%          | StDev         | %Stdev         | Mean GPS      | Mean MM5      | n              |
|---------------------|---------------|----------------|---------------|----------------|---------------|----------------|---------------|---------------|----------------|
| ANP1                | 0.8198        | -0.1178        | 0.5103        | 23.916         | 0.5308        | 24.8769        | 2.1337        | 2.2515        | 8              |
| ARP3                | 0.6877        | -0.3751        | 0.6614        | 16.0933        | 0.5605        | 13.6387        | 4.1097        | 4.4848        | 18             |
| AZCN                | 0.9313        | -0.0226        | 0.2347        | 12.4399        | 0.245         | 12.9863        | 1.8864        | 1.909         | 11             |
| BARH                | 0.606         | -0.4046        | 0.7169        | 23.9877        | 0.7248        | 24.252         | 2.9887        | 3.3933        | 3              |
| BARN                | 0.9029        | 0.0854         | 0.3965        | 15.5482        | 0.3984        | 15.6237        | 2.5502        | 2.4648        | 18             |
| BIL1                | 0.7993        | -0.2576        | 0.3634        | 19.6868        | 0.2702        | 14.6379        | 1.846         | 2.1036        | 10             |
| BLKV                | 0.9085        | -0.1875        | 0.4262        | 13.3629        | 0.3998        | 12.5338        | 3.1897        | 3.3773        | 12             |
| BLMM                | 0.9691        | -0.1842        | 0.3426        | 13.1785        | 0.303         | 11.6552        | 2.5997        | 2.7839        | 11             |
| BLRW                | 0.9397        | -0.2035        | 0.5602        | 21.7031        | 0.5638        | 21.8411        | 2.5814        | 2.7849        | 7              |
| CCV3                | 0.8592        | 0.0585         | 0.4367        | 8.6575         | 0.4453        | 8.8281         | 5.0443        | 4.9857        | 18             |
| CHA1                | 0.7673        | 0.0796         | 0.6911        | 15.8259        | 0.7091        | 16.2361        | 4.3672        | 4.2876        | 16             |
| CHO1                | 0.7143        | -0.324         | 0.6123        | 32.2622        | 0.5477        | 28.8554        | 1.898         | 2.222         | 10             |
| CLK1                | 0.7893        | -0.1945        | 0.3814        | 14.6991        | 0.3376        | 13.0106        | 2.5947        | 2.7892        | 18             |
| CNWM                | 0.9213        | -0.1176        | 0.53          | 18.532         | 0.5364        | 18.7526        | 2.8601        | 2.9777        | 14             |
| COVX                | 0.5019        | -0.8423        | 0.9396        | 55.0738        | 0.4655        | 27.2874        | 1.706         | 2.5483        | 5              |
| DQUA                | 0.9588        | -0.2876        | 0.4389        | 11.7972        | 0.3412        | 9.1703         | 3.7206        | 4.0082        | 18             |
| DRV1                | 0.8465        | -0.3421        | 0.7127        | 19.8413        | 0.6531        | 18.1799        | 3.5922        | 3.9343        | 12             |
| DSRC                | 0.8699        | 0.2008         | 0.3435        | 19.627         | 0.2923        | 16.7016        | 1.75          | 1.5492        | 11             |
| ENG1                | 0.8913        | 0.2321         | 0.4885        | 10.2612        | 0.4423        | 9.2911         | 4.7608        | 4.5287        | 18             |
| FBYN                | 0.8982        | -0.1012        | 0.4118        | 12.7432        | 0.4107        | 12.7104        | 3.2315        | 3.3327        | 18             |
| FST1                | 0.881         | -0.3573        | 0.4654        | 32.2764        | 0.3128        | 21.6936        | 1.4419        | 1.7992        | 11             |
| GAL1                | 0.357         | -0.5005        | 0.9208        | 21.9648        | 0.7953        | 18.9717        | 4.1921        | 4.6925        | 18             |
| GDAC                | 0.8439        | -0.1181        | 0.4158        | 17.8161        | 0.4181        | 17.9164        | 2.3336        | 2.4517        | 11             |
| GWEN                | 0.8752        | -0.3313        | 0.3757        | 25.0631        | 0.1941        | 12.9497        | 1.4992        | 1.8305        | 6              |
| HAG1                | 0.973         | -0.0443        | 0.1191        | 6.4366         | 0.1211        | 6.5453         | 1.85          | 1.8943        | 6              |
| HBRK                | 0.976         | -0.1982        | 0.2861        | 10.1483        | 0.2175        | 7.7143         | 2.819         | 3.0172        | 10             |
| HDF1                | 0.8855        | 0.2396         | 0.4533        | 15.8097        | 0.3966        | 13.833         | 2.8669        | 2.6273        | 17             |
| HKLO                | 0.8819        | -0.2727        | 0.5467        | 16.0145        | 0.4894        | 14.3356        | 3.4139        | 3.6866        | 16             |
| HTV1                | 0.9225        | 0.0344         | 0.4554        | 14.5438        | 0.4712        | 15.0496        | 3.1312        | 3.0968        | 14             |
| HVLK                | 0.7749        | -0.1885        | 0.4539        | 16.1772        | 0.4353        | 15.5125        | 2.806         | 2.9945        | 10             |
| JTNT                | 0.6499        | -0.0936        | 0.605         | 18.4204        | 0.6151        | 18.7264        | 3.2844        | 3.378         | 18             |
| KYW1                | 0.7373        | -0.2109        | 0.5663        | 11.7167        | 0.5408        | 11.1888        | 4.8331        | 5.044         | 18             |
| LMNO                | 0.9246        | -0.2215        | 0.4587        | 14.8852        | 0.4213        | 13.6716        | 3.0818        | 3.3033        | 11             |
| LTHM                | 0.8821        | 0.4435         | 0.7011        | 27.845         | 0.6072        | 24.113         | 2.518         | 2.0745        | 5              |
| MBWW                | 0.3605        | 0.1372         | 0.3315        | 14.6015        | 0.326         | 14.357         | 2.2706        | 2.1333        | 7              |
| MC01                | 0.9415        | 0.277          | 0.376         | 16.468         | 0.262         | 11.4764        | 2.2832        | 2.0062        | 17             |
| MCN1                | 0.9303        | 0.184          | 0.5434        | 12.8263        | 0.5262        | 12.4185        | 4.237         | 4.053         | 18             |
| MOB1                | 0.8786        | 0.2675         | 0.5324        | 10.7426        | 0.4736        | 9.5574         | 4.9557        | 4.6882        | 18             |
| MOR1                | 0.9491        | -0.0392        | 0.4321        | 15.2218        | 0.4428        | 15.5986        | 2.8387        | 2.8779        | 18             |
| MRRN                | 0.9258        | -0.1279        | 0.3526        | 12.8702        | 0.3381        | 12.341         | 2.7398        | 2.8678        | 18             |
| NDBC                | 0.9136        | 0.0195         | 0.3606        | 7.6732         | 0.3706        | 7.8841         | 4.7001        | 4.6806        | 18             |
| NDS1                | 0.9206        | -0.2739        | 0.4943        | 15.6049        | 0.4234        | 13.3666        | 3.1673        | 3.4412        | 18             |
| NLGN                | 0.7499        | -0.355         | 0.8093        | 27.2513        | 0.7484        | 25.2001        | 2.9698        | 3.3247        | 18             |
| OKOM                | 0.8652        | 0.0444         | 0.5141        | 12.7746        | 0.5302        | 13.1735        | 4.0247        | 3.9803        | 15             |
| PATT                | 0.9269        | -0.2743        | 0.3971        | 9.3198         | 0.2999        | 7.0384         | 4.2612        | 4.5355        | 12             |
| PLS1                | 0.7042        | -0.2258        | 0.3957        | 24.8991        | 0.356         | 22.3996        | 1.5893        | 1.8151        | 6              |
| PLTC                | 0.9247        | -0.1187        | 0.249         | 13.4857        | 0.2295        | 12.4325        | 1.8464        | 1.9651        | 11             |
| PNB1                | 0.8948        | -0.0148        | 0.465         | 19.8746        | 0.4875        | 20.834         | 2.3399        | 2.3547        | 11             |
| PRCO                | 0.9179        | -0.1603        | 0.4022        | 11.7843        | 0.3796        | 11.1209        | 3.4131        | 3.5734        | 18             |
| RWDN                | 0.707         | -0.2463        | 0.5876        | 20.5096        | 0.5489        | 19.161         | 2.8649        | 3.1112        | 18             |
| SAV1                | 0.9202        | 0.0103         | 0.4206        | 10.0191        | 0.4327        | 10.3065        | 4.1982        | 4.1879        | 18             |
| SEAW                | 0.7582        | -0.1657        | 0.231         | 10.1767        | 0.1739        | 7.658          | 2.2703        | 2.436         | 7              |
| SHK1                | 0.9598        | -0.0244        | 0.3885        | 13.6867        | 0.399         | 14.0556        | 2.8384        | 2.8628        | 18             |
| SIO3                | 0.3897        | -0.4803        | 1.0456        | 45.0882        | 0.9741        | 42.0051        | 2.3191        | 2.7994        | 11             |
| SLAI                | 0.8869        | -0.0811        | 0.2411        | 12.2268        | 0.2539        | 12.8743        | 1.972         | 2.0531        | 5              |
| SPN1                | 0.9114        | -0.5025        | 0.523         | 37.2485        | 0.1586        | 11.2996        | 1.404         | 1.9065        | 6              |
| SUM1                | 0.8504        | 0.0544         | 0.3322        | 12.4147        | 0.3378        | 12.624         | 2.6759        | 2.6215        | 17             |
| SYCN                | 0.9106        | 0.0142         | 0.2587        | 11.0594        | 0.2698        | 11.5338        | 2.3393        | 2.3251        | 12             |
| TCUN                | 0.8596        | 0.0573         | 0.2869        | 11.3797        | 0.2898        | 11.4933        | 2.5211        | 2.4638        | 17             |
| VCIO                | 0.8029        | -0.2367        | 0.5229        | 17.7553        | 0.4807        | 16.3205        | 2.9453        | 3.1819        | 17             |
| WDLM                | 0.7782        | -0.3826        | 0.5549        | 22.6202        | 0.4137        | 16.8612        | 2.4533        | 2.8358        | 18             |
| WHN1                | 0.8769        | -0.0842        | 0.4014        | 15.2163        | 0.4039        | 15.3087        | 2.6381        | 2.7223        | 18             |
| WLCI                | 0.8713        | -0.2193        | 0.4425        | 19.7902        | 0.4052        | 18.1199        | 2.236         | 2.4553        | 10             |
| WNCI                | 0.9361        | -0.1658        | 0.3744        | 15.4822        | 0.3506        | 14.4986        | 2.4182        | 2.5841        | 12             |
| WNFL                | 0.8605        | -0.1093        | 0.4507        | 10.825         | 0.4525        | 10.8705        | 4.1631        | 4.2723        | 15             |
| WSMN                | 0.8617        | 0.2111         | 0.302         | 9.4101         | 0.2309        | 7.1947         | 3.2095        | 2.9984        | 8              |
|                     |               |                |               |                |               |                |               |               |                |
|                     |               |                |               |                |               |                |               |               |                |
| <b>Means</b>        | <b>0.8347</b> | <b>-0.1233</b> | <b>0.4703</b> | <b>17.4040</b> | <b>0.4240</b> | <b>15.2223</b> | <b>2.9180</b> | <b>3.0412</b> | <b>13.2879</b> |
| <b>Mean n&gt;10</b> | <b>0.8493</b> | <b>-0.1134</b> |               | <b>16.1523</b> |               | <b>14.8495</b> |               |               | <b>15.0566</b> |



# Appendix C: Location-Specific Statistics

Table C-1-14. CONUS Statistics: 18 UTC Initialization, 24H Forecast

| ID        | Correlation   | Bias           | RMSE          | RMSE%          | StDev         | %Stdev         | Mean GPS      | Mean MM5      | n              |
|-----------|---------------|----------------|---------------|----------------|---------------|----------------|---------------|---------------|----------------|
| ANP1      | 0.8132        | 0.0323         | 0.5534        | 23.1325        | 0.5907        | 24.6876        | 2.3925        | 2.3602        | 8              |
| ARP3      | 0.7256        | -0.3206        | 0.6           | 14.6748        | 0.5238        | 12.8112        | 4.0886        | 4.4092        | 16             |
| AZCN      | 0.9427        | 0.0217         | 0.2317        | 12.4715        | 0.2432        | 13.0885        | 1.858         | 1.8363        | 10             |
| BARH      | 0.3096        | -0.398         | 0.6024        | 18.7015        | 0.5539        | 17.1943        | 3.2213        | 3.6193        | 3              |
| BARN      | 0.9084        | 0.1719         | 0.4136        | 15.6765        | 0.3877        | 14.6965        | 2.6383        | 2.4664        | 17             |
| BIL1      | 0.8426        | -0.2218        | 0.326         | 16.5183        | 0.2533        | 12.8366        | 1.9733        | 2.1952        | 9              |
| BLKV      | 0.9009        | -0.2004        | 0.4198        | 13.67          | 0.3869        | 12.5983        | 3.0708        | 3.2712        | 11             |
| BLMM      | 0.9351        | -0.1321        | 0.5209        | 19.7203        | 0.5285        | 20.0068        | 2.6414        | 2.7734        | 11             |
| BLRW      | 0.9599        | 0.1026         | 0.6252        | 21.4327        | 0.6755        | 23.1603        | 2.9168        | 2.8143        | 6              |
| CCV3      | 0.8477        | 0.0287         | 0.4882        | 9.744          | 0.5033        | 10.0462        | 5.0102        | 4.9815        | 16             |
| CHA1      | 0.8373        | 0.0316         | 0.5324        | 11.9957        | 0.5515        | 12.4265        | 4.4384        | 4.4068        | 14             |
| CHO1      | 0.7957        | -0.2343        | 0.479         | 23.4796        | 0.4431        | 21.7207        | 2.04          | 2.2743        | 9              |
| CLK1      | 0.8378        | -0.073         | 0.3371        | 12.4771        | 0.3399        | 12.5805        | 2.7017        | 2.7748        | 16             |
| CNWM      | 0.9293        | 0.0791         | 0.4384        | 14.7855        | 0.4475        | 15.0917        | 2.9651        | 2.8859        | 14             |
| COVX      | 0.6564        | -0.8522        | 0.9065        | 61.5827        | 0.3454        | 23.4668        | 1.472         | 2.3242        | 5              |
| DQUA      | 0.943         | -0.0821        | 0.3754        | 9.4692         | 0.3801        | 9.5889         | 3.9644        | 4.0464        | 14             |
| DRV1      | 0.9529        | -0.1991        | 0.4881        | 12.7192        | 0.4697        | 12.2413        | 3.8373        | 4.0364        | 10             |
| DSRC      | 0.9042        | 0.2229         | 0.3224        | 17.3773        | 0.2443        | 13.1678        | 1.8555        | 1.6325        | 11             |
| ENG1      | 0.8968        | 0.312          | 0.5423        | 11.3104        | 0.4581        | 9.5545         | 4.7948        | 4.4827        | 16             |
| FBYN      | 0.7934        | -0.1404        | 0.5802        | 18.5108        | 0.5802        | 18.5133        | 3.1342        | 3.2746        | 17             |
| FST1      | 0.9048        | -0.2521        | 0.3727        | 23.1835        | 0.2893        | 17.9956        | 1.6074        | 1.8595        | 10             |
| GAL1      | 0.7036        | -0.2321        | 0.5463        | 12.863         | 0.5108        | 12.0267        | 4.2471        | 4.4792        | 16             |
| GDAC      | 0.9199        | -0.1463        | 0.3172        | 13.4942        | 0.2952        | 12.5584        | 2.3509        | 2.4972        | 11             |
| GWEN      | 0.6517        | -0.3791        | 0.5079        | 34.0274        | 0.3779        | 25.3206        | 1.4926        | 1.8717        | 5              |
| HAG1      | 0.9367        | -0.1046        | 0.2247        | 11.7971        | 0.2179        | 11.4395        | 1.905         | 2.0096        | 6              |
| HBRK      | 0.9537        | -0.0572        | 0.2754        | 9.657          | 0.284         | 9.9579         | 2.852         | 2.9091        | 10             |
| HDF1      | 0.9099        | 0.2703         | 0.4379        | 16.0061        | 0.3559        | 13.0075        | 2.736         | 2.4657        | 16             |
| HKLO      | 0.8827        | -0.0468        | 0.4292        | 12.2675        | 0.4406        | 12.5945        | 3.4984        | 3.5452        | 16             |
| HTV1      | 0.8907        | 0.3279         | 0.7311        | 20.6946        | 0.6825        | 19.3194        | 3.5327        | 3.2048        | 12             |
| HVLK      | 0.7542        | -0.1491        | 0.4412        | 15.481         | 0.4377        | 15.3578        | 2.85          | 2.9991        | 10             |
| JTNT      | 0.7076        | -0.0332        | 0.5168        | 15.4786        | 0.5316        | 15.922         | 3.3385        | 3.3718        | 17             |
| KYW1      | 0.7096        | -0.2379        | 0.5822        | 12.0407        | 0.5488        | 11.3496        | 4.8352        | 5.0731        | 16             |
| LMNO      | 0.8836        | -0.2137        | 0.5129        | 16.9213        | 0.4915        | 16.2146        | 3.031         | 3.2447        | 10             |
| LTHM      | 0.9961        | 0.2442         | 0.4392        | 17.4002        | 0.4081        | 16.1688        | 2.524         | 2.2798        | 5              |
| MBWW      | 0.7118        | 0.0154         | 0.1882        | 8.6437         | 0.2055        | 9.4371         | 2.1778        | 2.1625        | 6              |
| MC01      | 0.8996        | 0.2213         | 0.35          | 16.1245        | 0.28          | 12.9           | 2.1705        | 1.9492        | 16             |
| MCN1      | 0.9296        | 0.1086         | 0.5433        | 13.2502        | 0.5498        | 13.4085        | 4.1001        | 3.9915        | 16             |
| MOB1      | 0.8728        | 0.2491         | 0.5555        | 11.4749        | 0.5127        | 10.5924        | 4.8407        | 4.5916        | 16             |
| MOR1      | 0.9399        | 0.0214         | 0.4517        | 16.1451        | 0.466         | 16.6558        | 2.798         | 2.7766        | 16             |
| MRRN      | 0.9164        | -0.137         | 0.3587        | 13.2201        | 0.3417        | 12.594         | 2.713         | 2.85          | 17             |
| NDBC      | 0.8755        | 0.1965         | 0.5413        | 11.2829        | 0.5199        | 10.8368        | 4.7975        | 4.601         | 17             |
| NDS1      | 0.8981        | -0.1437        | 0.4637        | 14.6347        | 0.4544        | 14.3423        | 3.1682        | 3.3119        | 17             |
| NLGN      | 0.8893        | -0.1633        | 0.4625        | 14.8316        | 0.446         | 14.3028        | 3.1183        | 3.2816        | 17             |
| OKOM      | 0.8148        | 0.1789         | 0.6182        | 15.8011        | 0.6125        | 15.6561        | 3.9121        | 3.7332        | 15             |
| PATT      | 0.9429        | -0.2206        | 0.3506        | 8.0717         | 0.2858        | 6.5798         | 4.3432        | 4.5638        | 11             |
| PLS1      | 0.8434        | -0.1819        | 0.2839        | 18.339         | 0.2438        | 15.7455        | 1.5482        | 1.7301        | 5              |
| PLTC      | 0.9395        | -0.1951        | 0.2481        | 14.5824        | 0.1626        | 9.5558         | 1.7011        | 1.8962        | 9              |
| PNB1      | 0.8913        | -0.2955        | 0.5235        | 24.8566        | 0.4555        | 21.6289        | 2.106         | 2.4015        | 10             |
| PRCO      | 0.9186        | -0.0093        | 0.3625        | 10.4113        | 0.3736        | 10.7282        | 3.4821        | 3.4915        | 17             |
| RWDN      | 0.7414        | -0.2361        | 0.5008        | 17.4554        | 0.4552        | 15.8672        | 2.8688        | 3.1049        | 17             |
| SAV1      | 0.8384        | 0.1501         | 0.65          | 14.6398        | 0.6531        | 14.7112        | 4.4397        | 4.2896        | 16             |
| SEAW      | 0.6535        | -0.1135        | 0.2631        | 11.4429        | 0.2601        | 11.3095        | 2.2997        | 2.4132        | 6              |
| SHK1      | 0.9264        | -0.0558        | 0.5046        | 18.3305        | 0.518         | 18.8156        | 2.7529        | 2.8087        | 16             |
| SIO3      | 0.3974        | -0.4666        | 1.0137        | 41.968         | 0.9439        | 39.0768        | 2.4155        | 2.882         | 11             |
| SLA1      | 0.5537        | -0.0595        | 0.3509        | 16.1864        | 0.3867        | 17.8353        | 2.168         | 2.2275        | 5              |
| SPN1      | 0.8976        | -0.3012        | 0.3605        | 21.9419        | 0.2214        | 13.4783        | 1.643         | 1.9442        | 5              |
| SUM1      | 0.7631        | 0.2733         | 0.4855        | 17.1125        | 0.4154        | 14.6396        | 2.8373        | 2.5639        | 15             |
| SYCN      | 0.8523        | 0.2455         | 0.454         | 18.5988        | 0.4006        | 16.4081        | 2.4413        | 2.1957        | 11             |
| TCUN      | 0.8408        | 0.1396         | 0.3302        | 12.7064        | 0.3091        | 11.8927        | 2.5989        | 2.4593        | 16             |
| VCIO      | 0.8009        | -0.1658        | 0.5064        | 16.7033        | 0.4932        | 16.2686        | 3.0315        | 3.1972        | 17             |
| WDLM      | 0.6773        | -0.282         | 0.5294        | 20.7808        | 0.4628        | 18.1632        | 2.5477        | 2.8298        | 16             |
| WHN1      | 0.8337        | -0.1245        | 0.4544        | 17.3543        | 0.4513        | 17.2378        | 2.6183        | 2.7427        | 16             |
| WLCI      | 0.7789        | -0.121         | 0.4047        | 16.6451        | 0.4096        | 16.8471        | 2.4314        | 2.5525        | 9              |
| WNCI      | 0.9512        | -0.1227        | 0.3488        | 13.7696        | 0.3411        | 13.4623        | 2.5334        | 2.6561        | 12             |
| WNFL      | 0.8788        | -0.0291        | 0.3929        | 9.5258         | 0.4055        | 9.833          | 4.1243        | 4.1534        | 15             |
| WSMN      | 0.8134        | 0.1568         | 0.3202        | 10.1585        | 0.2985        | 9.4688         | 3.1524        | 2.9956        | 8              |
| Means     | <b>0.8336</b> | <b>-0.0656</b> | <b>0.4589</b> | <b>16.6326</b> | <b>0.4260</b> | <b>14.9847</b> | <b>2.9651</b> | <b>3.0307</b> | <b>12.2576</b> |
| Mean n>10 | <b>0.8544</b> | <b>-0.0351</b> |               | <b>15.3416</b> |               | <b>14.4759</b> |               |               | <b>14.2857</b> |

## Appendix C: Location-Specific Statistics

Table C-2-1. Alaska Statistics: 00 UTC Initialization, 06H Forecast

| ID           | Correlation   | Bias          | RMSE          | RMSE%          | StDev         | %Stdev        | Mean GPS      | Mean MM5      | n              |
|--------------|---------------|---------------|---------------|----------------|---------------|---------------|---------------|---------------|----------------|
| CENA         | 0.8177        | -0.0159       | 0.2649        | 12.8416        | 0.2709        | 13.135        | 2.0626        | 2.0785        | 21             |
| CLGO         | 0.9775        | -0.0707       | 0.1308        | 6.0873         | 0.1137        | 5.2905        | 2.1489        | 2.2195        | 16             |
| TLKA         | 0.9248        | 0.1793        | 0.2527        | 10.5           | 0.1828        | 7.5928        | 2.407         | 2.2277        | 20             |
| GNAA         | 0.8369        | 0.2439        | 0.3125        | 14.4388        | 0.2001        | 9.2464        | 2.164         | 1.9201        | 21             |
|              |               |               |               |                |               |               |               |               |                |
| <b>Means</b> | <b>0.8892</b> | <b>0.0842</b> | <b>0.2402</b> | <b>10.9669</b> | <b>0.1919</b> | <b>8.8162</b> | <b>2.1956</b> | <b>2.1115</b> | <b>19.5000</b> |

Table C-2-2. Alaska Statistics: 00 UTC Initialization, 09H Forecast

| ID           | Correlation | Bias         | RMSE        | RMSE%        | StDev       | %Stdev       | Mean GPS    | Mean MM5    | n              |
|--------------|-------------|--------------|-------------|--------------|-------------|--------------|-------------|-------------|----------------|
| CENA         | 0.85        | -0.05        | 0.25        | 12.59        | 0.25        | 12.58        | 2.00        | 2.06        | 22             |
| CLGO         | 0.72        | -0.27        | 0.48        | 24.38        | 0.41        | 20.69        | 1.97        | 2.24        | 17             |
| TLKA         | 0.64        | -0.07        | 0.39        | 17.97        | 0.39        | 18.05        | 2.18        | 2.26        | 22             |
| GNAA         | 0.29        | -0.04        | 0.40        | 20.78        | 0.41        | 21.15        | 1.94        | 1.98        | 22             |
|              |             |              |             |              |             |              |             |             |                |
| <b>Means</b> | <b>0.62</b> | <b>-0.11</b> | <b>0.38</b> | <b>18.93</b> | <b>0.37</b> | <b>18.12</b> | <b>2.02</b> | <b>2.13</b> | <b>20.7500</b> |

Table C-2-3. Alaska Statistics: 00 UTC Initialization, 12H Forecast

| ID           | Correlation | Bias         | RMSE        | RMSE%        | StDev       | %Stdev       | Mean GPS    | Mean MM5    | n              |
|--------------|-------------|--------------|-------------|--------------|-------------|--------------|-------------|-------------|----------------|
| CENA         | 0.87        | -0.01        | 0.20        | 10.28        | 0.21        | 10.50        | 1.98        | 2.00        | 22             |
| CLGO         | 0.87        | -0.25        | 0.35        | 18.09        | 0.26        | 13.16        | 1.95        | 2.20        | 18             |
| TLKA         | 0.71        | -0.12        | 0.36        | 16.34        | 0.34        | 15.67        | 2.18        | 2.30        | 23             |
| GNAA         | 0.55        | -0.01        | 0.31        | 16.22        | 0.32        | 16.58        | 1.94        | 1.95        | 23             |
|              |             |              |             |              |             |              |             |             |                |
| <b>Means</b> | <b>0.75</b> | <b>-0.10</b> | <b>0.31</b> | <b>15.23</b> | <b>0.28</b> | <b>13.98</b> | <b>2.01</b> | <b>2.11</b> | <b>21.5000</b> |

Table C-2-4. Alaska Statistics: 00 UTC Initialization, 15H Forecast

| ID           | Correlation | Bias        | RMSE        | RMSE%        | StDev       | %Stdev       | Mean GPS    | Mean MM5    | n              |
|--------------|-------------|-------------|-------------|--------------|-------------|--------------|-------------|-------------|----------------|
| CENA         | 0.87        | 0.07        | 0.21        | 10.18        | 0.21        | 9.93         | 2.07        | 2.00        | 19             |
| CLGO         | 0.72        | -0.10       | 0.39        | 19.72        | 0.39        | 19.73        | 1.99        | 2.09        | 16             |
| TLKA         | 0.83        | -0.03       | 0.27        | 11.88        | 0.27        | 12.12        | 2.26        | 2.29        | 21             |
| GNAA         | 0.67        | 0.07        | 0.29        | 14.78        | 0.29        | 14.72        | 1.99        | 1.92        | 21             |
|              |             |             |             |              |             |              |             |             |                |
| <b>Means</b> | <b>0.77</b> | <b>0.00</b> | <b>0.29</b> | <b>14.14</b> | <b>0.29</b> | <b>14.12</b> | <b>2.08</b> | <b>2.08</b> | <b>19.2500</b> |

## Appendix C: Location-Specific Statistics

Table C-2-5. Alaska Statistics: 00 UTC Initialization, 18H Forecast

| ID           | Correlation | Bias        | RMSE        | RMSE%        | StDev       | %Stdev       | Mean GPS    | Mean MM5    | n              |
|--------------|-------------|-------------|-------------|--------------|-------------|--------------|-------------|-------------|----------------|
| CENA         | 0.77        | 0.12        | 0.30        | 14.57        | 0.28        | 13.61        | 2.06        | 1.93        | 21             |
| CLGO         | 0.88        | -0.06       | 0.24        | 11.87        | 0.24        | 11.83        | 2.04        | 2.10        | 17             |
| TLKA         | 0.83        | 0.08        | 0.25        | 10.76        | 0.24        | 10.43        | 2.34        | 2.26        | 21             |
| GNAA         | 0.85        | 0.12        | 0.23        | 11.17        | 0.20        | 9.78         | 2.03        | 1.92        | 22             |
|              |             |             |             |              |             |              |             |             |                |
| <b>Means</b> | <b>0.83</b> | <b>0.07</b> | <b>0.26</b> | <b>12.09</b> | <b>0.24</b> | <b>11.41</b> | <b>2.12</b> | <b>2.05</b> | <b>20.2500</b> |

Table C-2-6. Alaska Statistics: 00 UTC Initialization, 21H Forecast

| ID           | Correlation | Bias        | RMSE        | RMSE%        | StDev       | %Stdev       | Mean GPS    | Mean MM5    | n              |
|--------------|-------------|-------------|-------------|--------------|-------------|--------------|-------------|-------------|----------------|
| CENA         | 0.64        | 0.11        | 0.37        | 18.15        | 0.37        | 17.79        | 2.06        | 1.95        | 23             |
| CLGO         | 0.50        | -0.15       | 0.57        | 29.98        | 0.57        | 29.92        | 1.92        | 2.07        | 15             |
| TLKA         | 0.59        | 0.16        | 0.45        | 18.57        | 0.43        | 17.72        | 2.43        | 2.27        | 23             |
| GNAA         | 0.67        | 0.03        | 0.34        | 17.57        | 0.35        | 17.87        | 1.96        | 1.92        | 23             |
|              |             |             |             |              |             |              |             |             |                |
| <b>Means</b> | <b>0.60</b> | <b>0.04</b> | <b>0.44</b> | <b>21.07</b> | <b>0.43</b> | <b>20.83</b> | <b>2.09</b> | <b>2.05</b> | <b>21.0000</b> |

Table C-2-7. Alaska Statistics: 00 UTC Initialization, 24H Forecast

| ID           | Correlation | Bias        | RMSE        | RMSE%        | StDev       | %Stdev      | Mean GPS    | Mean MM5    | n              |
|--------------|-------------|-------------|-------------|--------------|-------------|-------------|-------------|-------------|----------------|
| CENA         | 0.81        | 0.26        | 0.36        | 16.09        | 0.26        | 11.50       | 2.23        | 1.98        | 19             |
| CLGO         | 0.95        | 0.02        | 0.17        | 7.61         | 0.17        | 7.82        | 2.18        | 2.17        | 16             |
| TLKA         | 0.84        | 0.27        | 0.35        | 13.76        | 0.23        | 8.90        | 2.53        | 2.26        | 19             |
| GNAA         | 0.86        | 0.22        | 0.27        | 12.45        | 0.16        | 7.52        | 2.14        | 1.92        | 20             |
|              |             |             |             |              |             |             |             |             |                |
| <b>Means</b> | <b>0.86</b> | <b>0.19</b> | <b>0.28</b> | <b>12.48</b> | <b>0.20</b> | <b>8.94</b> | <b>2.27</b> | <b>2.08</b> | <b>18.5000</b> |

Table C-2-8. Alaska Statistics: 12 UTC Initialization, 06H Forecast

| ID           | Correlation   | Bias          | RMSE          | RMSE%          | StDev         | %Stdev         | Mean GPS      | Mean MM5      | n              |
|--------------|---------------|---------------|---------------|----------------|---------------|----------------|---------------|---------------|----------------|
| CENA         | 0.8397        | 0.0961        | 0.2566        | 12.3606        | 0.2442        | 11.7589        | 2.0764        | 1.9802        | 20             |
| CLGO         | 0.8883        | 0.0495        | 0.2246        | 11.0112        | 0.2258        | 11.0704        | 2.0394        | 1.9898        | 17             |
| TLKA         | 0.8719        | 0.2444        | 0.337         | 14.4228        | 0.2382        | 10.1915        | 2.3368        | 2.0924        | 20             |
| GNAA         | 0.9203        | 0.2888        | 0.323         | 15.9488        | 0.1483        | 7.3224         | 2.0253        | 1.7365        | 21             |
|              |               |               |               |                |               |                |               |               |                |
| <b>Means</b> | <b>0.8801</b> | <b>0.1697</b> | <b>0.2853</b> | <b>13.4359</b> | <b>0.2141</b> | <b>10.0858</b> | <b>2.1195</b> | <b>1.9497</b> | <b>19.5000</b> |

## Appendix C: Location-Specific Statistics

Table C-2-8. Alaska Statistics: 12 UTC Initialization, 09H Forecast

| ID           | Correlation   | Bias          | RMSE          | RMSE%          | StDev         | %Stdev         | Mean GPS      | Mean MM5      | n              |
|--------------|---------------|---------------|---------------|----------------|---------------|----------------|---------------|---------------|----------------|
| CENA         | 0.787         | 0.115         | 0.3041        | 14.6185        | 0.2882        | 13.8517        | 2.0803        | 1.9653        | 22             |
| CLGO         | 0.6069        | -0.0891       | 0.5115        | 26.6866        | 0.5214        | 27.2013        | 1.9168        | 2.0059        | 15             |
| TLKA         | 0.6803        | 0.2793        | 0.4847        | 20.0708        | 0.4055        | 16.7904        | 2.415         | 2.1357        | 22             |
| GNAA         | 0.6954        | 0.1042        | 0.3525        | 18.1591        | 0.3446        | 17.7553        | 1.9411        | 1.8369        | 22             |
|              |               |               |               |                |               |                |               |               |                |
| <b>Means</b> | <b>0.6924</b> | <b>0.1024</b> | <b>0.4132</b> | <b>19.8838</b> | <b>0.3899</b> | <b>18.8997</b> | <b>2.0883</b> | <b>1.9860</b> | <b>20.2500</b> |

Table C-2-9. Alaska Statistics: 12 UTC Initialization, 12H Forecast

| ID           | Correlation   | Bias          | RMSE          | RMSE%          | StDev         | %Stdev        | Mean GPS      | Mean MM5      | n              |
|--------------|---------------|---------------|---------------|----------------|---------------|---------------|---------------|---------------|----------------|
| CENA         | 0.8136        | 0.2657        | 0.3698        | 16.779         | 0.2639        | 11.9745       | 2.204         | 1.9383        | 20             |
| CLGO         | 0.9357        | 0.0693        | 0.1913        | 8.9577         | 0.1838        | 8.6059        | 2.136         | 2.0667        | 17             |
| TLKA         | 0.9114        | 0.3115        | 0.368         | 14.8229        | 0.201         | 8.0958        | 2.4827        | 2.1711        | 20             |
| GNAA         | 0.8733        | 0.241         | 0.2989        | 14.0964        | 0.1812        | 8.5431        | 2.1206        | 1.8796        | 21             |
|              |               |               |               |                |               |               |               |               |                |
| <b>Means</b> | <b>0.8835</b> | <b>0.2219</b> | <b>0.3070</b> | <b>13.6640</b> | <b>0.2075</b> | <b>9.3048</b> | <b>2.2358</b> | <b>2.0139</b> | <b>19.5000</b> |

Table C-2-11. Alaska Statistics: 12 UTC Initialization, 18H Forecast

| ID           | Correlation   | Bias          | RMSE          | RMSE%          | StDev         | %Stdev         | Mean GPS      | Mean MM5      | n              |
|--------------|---------------|---------------|---------------|----------------|---------------|----------------|---------------|---------------|----------------|
| CENA         | 0.8613        | 0.1478        | 0.2669        | 12.728         | 0.2278        | 10.8611        | 2.0973        | 1.9495        | 21             |
| CLGO         | 0.8962        | 0.0068        | 0.2293        | 10.9638        | 0.2368        | 11.3184        | 2.0919        | 2.0851        | 16             |
| TLKA         | 0.9501        | 0.1691        | 0.226         | 9.278          | 0.1537        | 6.3099         | 2.436         | 2.2669        | 21             |
| GNAA         | 0.7475        | 0.2401        | 0.3445        | 16.0953        | 0.2532        | 11.8271        | 2.1404        | 1.9003        | 21             |
|              |               |               |               |                |               |                |               |               |                |
| <b>Means</b> | <b>0.8638</b> | <b>0.1410</b> | <b>0.2667</b> | <b>12.2663</b> | <b>0.2179</b> | <b>10.0791</b> | <b>2.1914</b> | <b>2.0505</b> | <b>19.7500</b> |

Table C-2-12. Alaska Statistics: 12 UTC Initialization, 21H Forecast

| ID           | Correlation   | Bias           | RMSE          | RMSE%          | StDev         | %Stdev         | Mean GPS      | Mean MM5      | n              |
|--------------|---------------|----------------|---------------|----------------|---------------|----------------|---------------|---------------|----------------|
| CENA         | 0.7476        | 0.01           | 0.3132        | 15.8365        | 0.3212        | 16.2397        | 1.9777        | 1.9677        | 20             |
| CLGO         | 0.8168        | -0.0976        | 0.3314        | 16.5285        | 0.3278        | 16.3491        | 2.005         | 2.1026        | 15             |
| TLKA         | 0.7791        | -0.0386        | 0.2962        | 13.5837        | 0.3013        | 13.8175        | 2.1802        | 2.2189        | 20             |
| GNAA         | 0.5849        | 0.0497         | 0.3077        | 15.746         | 0.3116        | 15.9428        | 1.9543        | 1.9046        | 20             |
|              |               |                |               |                |               |                |               |               |                |
| <b>Means</b> | <b>0.7321</b> | <b>-0.0191</b> | <b>0.3121</b> | <b>15.4237</b> | <b>0.3155</b> | <b>15.5873</b> | <b>2.0293</b> | <b>2.0485</b> | <b>18.7500</b> |

### Appendix C: Location-Specific Statistics

Table C-2-13. Alaska Statistics: 12 UTC Initialization, 24H Forecast

| <b>ID</b>    | <b>Correlation</b> | <b>Bias</b>    | <b>RMSE</b>   | <b>RMSE%</b>   | <b>StDev</b>  | <b>%Stdev</b>  | <b>Mean GPS</b> | <b>Mean MM5</b> | <b>n</b>       |
|--------------|--------------------|----------------|---------------|----------------|---------------|----------------|-----------------|-----------------|----------------|
| CENA         | 0.7801             | 0.0833         | 0.2891        | 14.5326        | 0.2836        | 14.2592        | 1.9891          | 1.9058          | 21             |
| CLGO         | 0.8635             | -0.1306        | 0.2909        | 14.9584        | 0.2685        | 13.8042        | 1.9449          | 2.0756          | 16             |
| TLKA         | 0.8187             | -0.0482        | 0.2662        | 12.1899        | 0.2683        | 12.2845        | 2.1841          | 2.2323          | 21             |
| GNAA         | 0.6308             | 0.0223         | 0.2992        | 15.294         | 0.3057        | 15.6281        | 1.956           | 1.9338          | 21             |
|              |                    |                |               |                |               |                |                 |                 |                |
| <b>Means</b> | <b>0.7733</b>      | <b>-0.0183</b> | <b>0.2864</b> | <b>14.2437</b> | <b>0.2815</b> | <b>13.9940</b> | <b>2.0185</b>   | <b>2.0369</b>   | <b>19.7500</b> |

## **Vita**

Captain Patricia A. Vollmer graduated from Lake Taylor High School in Norfolk, Virginia in June 1991. She entered undergraduate studies at The Pennsylvania State University in University Park, Pennsylvania where she earned her Bachelor's Degree in Meteorology and was commissioned through the Reserve Officer Training Corps in May 1995.

Her first duty assignment was with the 21<sup>st</sup> Air Support Operations Squadron, Fort Polk, Louisiana and included staff weather officer duties supporting both the Joint Readiness Training Center and 2d Armored Cavalry Regiment. While assigned to Fort Polk, she deployed to Tuzla Air Base, Bosnia-Herzegovina in 1997 in support of Operation JOINT GUARD. In 1998, Captain Vollmer was assigned to the 607<sup>th</sup> Weather Squadron, Yongsan Army Garrison, Seoul, Republic of Korea. There, she was staff weather officer to the 17<sup>th</sup> Aviation Brigade. Also, while with the 607<sup>th</sup> Weather Squadron, she had the opportunity to serve as the combined Plans and Programs officer, in support of joint and multi-national weather operations in the Korean theater of operations. She entered the Graduate School of Engineering and Management, Air Force Institute of Technology in August 2000. Upon graduation, Captain Vollmer's next duty assignment will be with the Air Force Technical Applications Center at Patrick AFB, Florida.

| <b>REPORT DOCUMENTATION PAGE</b>  |                    |  |                                   | <i>Form Approved<br/>OMB No. 074-0188</i>                             |   |
|---|--------------------|--|-----------------------------------|---|---|
| <p>The public reporting burden for this collection of information is estimated to average 1 hour per response, including the time for reviewing instructions, searching existing data sources, gathering and maintaining the data needed, and completing and reviewing the collection of information. Send comments regarding this burden estimate or any other aspect of the collection of information, including suggestions for reducing this burden to Department of Defense, Washington Headquarters Services, Directorate for Information Operations and Reports (0704-0188), 1215 Jefferson Davis Highway, Suite 1204, Arlington, VA 22202-4302. Respondents should be aware that notwithstanding any other provision of law, no person shall be subject to a penalty for failing to comply with a collection of information if it does not display a currently valid OMB control number.</p> <p><b>PLEASE DO NOT RETURN YOUR FORM TO THE ABOVE ADDRESS.</b></p>   |                    |  |                                   |   |   |
| <b>1. REPORT DATE (DD-MM-YYYY)</b><br>26-03-2002  |                    | <b>2. REPORT TYPE</b><br>Master's Thesis |                                   | <b>3. DATES COVERED (From - To)</b><br>Jun 2001 - Mar 2002            |   |
| <b>4. TITLE AND SUBTITLE</b><br>GPS-DERIVED PRECIPITABLE WATER COMPARED WITH THE AIR FORCE WEATHER AGENCY'S MM5 MODEL OUTPUT  |                    |  |                                   | <b>5a. CONTRACT NUMBER</b>  |   |
|   |                    |  |                                   | <b>5b. GRANT NUMBER</b>   |   |
|   |                    |  |                                   | <b>5c. PROGRAM ELEMENT NUMBER</b>                                     |   |
| <b>6. AUTHOR(S)</b><br>Vollmer, Patricia A., Captain, USAF  |                    |  |                                   | <b>5d. PROJECT NUMBER</b>   |   |
|   |                    |  |                                   | <b>5e. TASK NUMBER</b>  |   |
|   |                    |  |                                   | <b>5f. WORK UNIT NUMBER</b>   |   |
| <b>7. PERFORMING ORGANIZATION NAMES(S) AND ADDRESS(S)</b><br>Air Force Institute of Technology<br>Graduate School of Engineering and Management (AFIT/EN)<br>2950 P Street, Building 640<br>WPAFB OH 45433-7765   |                    |  |                                   | <b>8. PERFORMING ORGANIZATION REPORT NUMBER</b><br>AFIT/GM/ENP/02M-11 |   |
| <b>9. SPONSORING/MONITORING AGENCY NAME(S) AND ADDRESS(ES)</b><br>AFWA/DNXT<br>Attn: Bruce Telfeyan<br>301 Peacekeeper Dr.<br>Offutt AFB, NE<br>DSN: 271-1690<br>e-mail: bruce.telfeyan@afwa.af.mil   |                    |  |                                   | <b>10. SPONSOR/MONITOR'S ACRONYM(S)</b>                               |   |
|   |                    |  |                                   | <b>11. SPONSOR/MONITOR'S REPORT NUMBER(S)</b>                         |   |
| <b>12. DISTRIBUTION/AVAILABILITY STATEMENT</b><br>APPROVED FOR PUBLIC RELEASE; DISTRIBUTION UNLIMITED.  |                    |  |                                   |   |   |
| <b>13. SUPPLEMENTARY NOTES</b>  |                    |  |                                   |   |   |
| <b>14. ABSTRACT</b><br>Current moisture initialization sources lack the spatial and temporal resolution required for mesoscale moisture forecast accuracy critical for military operations. The Global Positioning System (GPS) satellite constellation provides an opportunity to extract accurate moisture observations based on the refraction of the GPS signal through the troposphere. GPS-derived precipitable water (PW) from two different research areas was independently compared with the Air Force Weather Agency's (AFWA's) MM5 PW model output. Results were concurrent with similar studies comparing GPS-derived PW with numerical weather models. The mean correlation in CONUS was 92.5%, while in Alaska it was 72.8%. Mean model biases were -1.22 mm in CONUS and 0.69 mm in Alaska, where a negative bias signifies the model having higher PWs. Mean RMSEs were 4.36 mm in CONUS and 2.76 mm in Alaska.<br>The GPS network's superior temporal resolution captured the diurnal variations in PW, while the model consistently failed to take such variations into account as its forecast progressed. This seems it could be the largest source of error between the two data sets. A number of non-meteorological error sources exist that could impact use of GPS-derived PW in operational applications, such as terrain differences between the GPS receiver sites and the model interpolated heights. These error sources need to be further addressed prior to operational assimilation of this data into military weather models. |                    |  |                                   |   |   |
| <b>15. SUBJECT TERMS</b><br>Meteorology, Global Positioning System, Numerical Methods and Procedures, Satellites, Atmospheric Moisture Content  |                    |  |                                   |   |   |
| <b>16. SECURITY CLASSIFICATION OF:</b>  |                    |  | <b>17. LIMITATION OF ABSTRACT</b> | <b>18. NUMBER OF PAGES</b>  | <b>19a. NAME OF RESPONSIBLE PERSON</b>  |
| <b>a. REPORT</b>  | <b>b. ABSTRACT</b> | <b>c. THIS PAGE</b>                      |                                   |   | Gary R. Huffines, Maj, USAF (AFIT/ENP)  |
| U   | U                  | U  | UU                                | 108   | <b>19b. TELEPHONE NUMBER (Include area code)</b><br>(937) 255-3636, x4511; e-mail: gary.huffines@afit.edu |